UNIVERSITÀ DEGLI STUDI DI PADOVA

Sede Amministrativa: Università degli Studi di Padova

DIPARTIMENTO DI GEOSCIENZE

SCUOLA DI DOTTORATO DI RICERCA

IN SCIENZE DELLA TERRA

CICLO XXIV

Candidato: ALESSANDRO GUASTONI

LCT (LITHIUM, CESIUM, TANTALUM) AND NYF (NIOBIUM, YTTRIUM, FLUORINE) PEGMATITES IN THE CENTRAL ALPS. PROXIES OF EXHUMATION HISTORY OF THE ALPINE NAPPE STACK IN THE LEPONTINE DOME

Direttore della Scuola: Ch.mo Prof. Gilberto Artioli

Supervisori: Ch.mo Prof. Gilberto Artioli, Ch.mo Prof. Giorgio Pennacchioni

"Io, Galileo Galilei portato di persona a giudizio e inginocchiato innanzi a voi, Eminentissimi e Reverendissimi Cardinali".…".professai e credetti che il Sole è il centro dell'Universo ed è immobile, e che la Terra non è il centro ed è mobile, io son pronto a togliere dalle menti delle Vostre Eminenze e di ogni Cattolico Cristiano, questo grave sospetto giustamente nutrito contro di me, perciò con cuore sincero e fede non finta, io abiuro, maledico, e detesto i detti errori e le dette eresie contrari alla detta Santa Chiesa"……

Convento di Minerva, Rome june 22th 1633:

Acknowledgements

It is a long list of parents, friends, and people I am indebted to thank and who supported me during these three years I dedicated to work on my Ph.D. thesis. First of all my mom Esther and my dad Giancarlo who asked themselves several times why I was still studying at 46 years old! Mariangela who was always close to me and helped me during last month to organize the amount of data I was via via producing.

Then we can follow to thank my tutors Prof. Gilberto Artioli and Prof. Giorgio Pennacchioni; Ph.D. student Riccardo Pozzobon who was so involved in my work and he helped me (or he did for me) to draw most of the figures; my friends Angelo Stroppini and Pierluigi Grammatica, who shared with me beautiful mineralogical excursions in the Alps; Dr. Federico Pezzotta, Curator of the Museum of Natural History of Milan, for the facilities to utilize SEM; Dr Pietro Vignola of CNR of Milan for the study of triplite; Dr. Matteo Parisatto of Dept of Geoscience of the University of Padova for microtomography analysis of perthites; Prof Richard Spiess of the Dept of Geoscience of the University of Padova involved in the EBSD analysis; Raul Carampin of CNR of Padova for WDS analysis; Dr. Micaela Longo who helped me to draw bulk rock diagrams; Prof. Fabrizio Nestola of Dept of Geoscience of University of Padova, Prof. Francesco Demartin of Dept. of Chemistry of University of Milan, and Dr. Uwe Kolitsch of Museum of natural History of Vienna for analysis by single crystal X-ray diffraction; Prof. Gianmario Molin, Director of CAM (Centro di Ateneo per i Musei di Padova) who gave me the opportunity to reach my Ph.D. goal; Matteo Chinellato and Roberto Appiani for the beautiful images of minerals of Alpine pegmatites.

Summary

The E-W-trending Southern Steep Belt (SSB) of the Western-Central Alps hosts a major Tertiary pegmatitic field which extends for more than 80 km along the belt axis, from Centovalli Line in the west, to Chiavenna valley and throughout the Oligocene Masino-Bregaglia intrusive massif to the east. The pegmatitic field extends for a thickness of few kilometers north of the Insubric line. Pegmatites intrude both the boundary of Alpine nappes involved in greenschist to amphibolites facies "Lepontine" metamorphism and the Masino-Bregaglia intrusion. Most pegmatites (>95%) consist of simply K-feldspar and subordinate quartz + muscovite (defined as "barren" pegmatites), but a few dykes show a more complex mineralogy including Sn-Nb-Ta-Y-REE-U oxides, Y-REE phosphates, Mn-Fe-phosphates, Ti-Zr-silicates, Be-Y-REE-silicates, almandine-spessartine garnets, and schorl-dravite-fluorelbaite tourmaline group minerals.

A series of 11 pegmatites were selected for detailed mineralogical, geochemical, structural and textural analysis. Crystal-chemistry studies were performed on accessory phases including Nb-Ta-Y-REE oxides, tourmaline group minerals and phosphates. Major and trace elements geochemistry of pegmatite bulk rock, rock-forming and accessory minerals (on the basis of several proxies as Al/Ga; K/Rb; K/Ba; K/Cs; Nb/Ta; Ba/Rb; Rb/Sr; Y/Ce; LREE/HREE; Zr/Hf) allowed distinction of different geochemical and mineralogical pegmatite populations ranging from NYF (niobium yttrium, fluorine), LCT (lithium, cesium, tantalum) pegmatites or mixed LCT-NYF signatures Actually, LCT pegmatites of Central Alps never reached a high degree of geochemical evolution. The most evolved pegmatites crop-out at Codera valley and are characterized by elbaite, Mn-phosphates, pink-beryl and Cs-feldspars. In the Vigezzo valley, NYF and LCT populations are hosted within leucocratic orthogneiss belonging to Pioda di Crana and Camughera-Moncucco units and to ultramafic rocks of Antrona-Zermatt Sass units. In this latter case the pegmatites show incipient albitization. In the Mesolcina valley, LCT and mixed LCT-NYF miarolitic pegmatites crosscut amphibolites and migmatitic gneiss. In the Codera valley LCT and NYF pegmatites are hosted by tonalites ("serizzo") and granodiorites (ghiandone), respectively.

Pegmatitic textures are well developed: large K-feldspar (comb structures), layering of K-feldspar+albite+quartz and garnets developed at the bottom of the dikes, quartz and garnet graphic textures, massive albite (Ab 90–95 wt%) with a fine- to medium-grained texture, white and amazonitic K-feldspar, albite (*clevelandite*), fluorite, green (*emeralds*) and pinkish (*morganite)* beryls, smoky and colorless quartz at the core zone, pluridecimetric K-feldspar and blades of muscovite, secondary cavities and primary miarolitic pockets have been respectively observed. Structural data of pegmatitic dikes give NNW-SSE to N-S direction, 60°- 80° dip and crosscut the layering and foliation of the hosting rocks.

Plots of the geochemical diagrams indicate granite-granodiorite of Masino-Bregaglia, San Fedelino two mica granite and microgranitic dikes within Masino-Bregaglia have geochemical characters to allow them candidate as potential sources of the LCT-NYF pegmatites in the Central Alps. It must be also considered Masino-Bregaglia intrusion extends his tail toward west for more than 50 kilometers. Due to very pronounced easterly axial plunge of up to 25° formed during and after the emplacement, increasingly deeper levels of Masino Bregaglia tonalites (Iorio tonalite) and granodiorite (Melirolo augengneiss) are exposed

westwards with an history of crystallization defining an early interval of 33.0 to 26 Ma. These structural data raise the possibility that pegmatites inherit a vertical chemical zonation from a zoned magmatic source represented in this case by Masino-Bregaglia intrusion and San Fedelino two-mica granite stocks.

It may be hypothesized small granitic stocks (similar in composition to San Fedelino two mica granite) or apophysis and small dikes outcrop along Central Alps with composition similar to granodiorite porphyritic dike outcrop at Loana valley, Vigezzo were the feeder of pegmatitic liquids able to escape from small satellite granite-granodiorite bodies.

LCT pegmatites contain beryl and Be-bearing minerals as accessory minerals whereas NYF pegmatite have sensible enrichments of niobium- tantalum- yttrium- rare-earths-uranium oxides, phosphates and silicate minerals. Anatectic migmatite melts invoked as potential sources to generate LCT and NYF pegmatites find some unanswered problems as explained in the Chapter 9. In any case an anatectic orgin for barren pegmatites would be feasible taking into consideration that the P-T contour map isograds during the peak metamorphism of Thermal Lepontine Dome reached amphibolites grade metamorphism and were able to produce leucosome granitic melts following a mechanism discussed by Burry et al., (2005) and Berger et al., (2008)

Chapter 1

Chapter 2

LCT (LITHIUM, CESIUM, TANTALUM) AND NYF (NIOBIUM, YTTRIUM, FLUORINE) PEGMATITES IN THE CENTRAL ALPS. PROXIES OF EXHUMATION HISTORY OF THE ALPINE NAPPE STACK IN THE LEPONTINE DOME

CHAPTER 1

Meaning, history, economic importance, classification and genetic inferences of pegmatites

1.1 What are pegmatites?

The term pegmatite refers to the presence of skeletal quartz and perthitic microcline which define an intergrowth called graphic granite, because the intimate association of these two minerals resemble an ancient cuneiform writing "…*composée 'essentiellement de felspath lamellaire et de quarz…*" (Haüy, 1801; Brongniart, 1813). Graphic granite is a texture feature which may distinguish pegmatites having rock-forming silicate minerals as major components. The principal components of pegmatites are SiO_2, $KAlSi_3O_8$ and $NaAlSi_3O_8$ and possess the composition of igneous granitic rocks (Jahns and Tuttle, 1963). The vast majority of pegmatites have the compositions near the ternary diagram (albite-K-feldspar-quartz) of hydrous haplogranite minima at 100-300 MPa (Tuttle and Bowen, 1958).

Pegmatites are igneous magmatic rocks but their characteristic textures and mineralogical assemblage are those that distinguish pegmatites from other igneous rocks. The textural and mineralogical features that allows to identify and classify a pegmatite in the field can be summarized as follows:

- Coarse to giant grain-size of single rock forming or accessory minerals (Fig. 1.1)
- Quartz, plagioclase, and microcline tend to segregate in nearly monomineralic zones
- Development of quartz+K-feldspar intergrowth graphic texture (Fig 1.2)
- Development of garnet, tourmaline graphic texture with quartz; phosphates graphic texture with albite

- Abrupt change in the grain-size of minerals: branching of giant K-feldspar “comb texture” developing from the rim toward the core of the pegmatite
- Development of rhytmic layering composed by alternance of monomineralic phases (e.g. quartz-feldspars-garnets)
- Preferred orientation of large monomineralic assemblages (e.g. microcline, tourmaline, beryl, lithium aluminosilicates, and phosphates) which define a “comb texture” developed perpendicular to the pegmatite contact, with individual crystals expand toward the center of the dike
- Concentric zoning, or shell zoning, of pegmatites with variable texture and mineralogy where it may be distinguished border, wall, intermediate and core zones
- Core zone of pegmatites characterized by abundance of quartz and accessory mineral projecting toward the core centre (e.g. beryl, spodumene, topaz, tourmaline)
- Development of miarolitic cavities and pocket zones, defined as primary cavities, which result from trapping bubbles of an exsolved gas phase inside the parent pegmatite body
- Skeletal or branching crystal habits are typically developed in tourmalines, microcline, phosphates and Sn-Nb-Ta-Y-REE-U oxides
- Micas and albite var. "*cleavelandite*" to form spherical or radial aggregates
- Zonation and variations within individual mineral phases characterized by sharp variation in the chemical composition (e.g. tourmaline, mica)
- Replacement or pseudomorphism of secondary minerals after primary pegmatite minerals by circulation of late stage hydrothermal fluids (e.g lepidolite or muscovite after tourmaline; secondary phosphates after primary phosphates; zeolites after silicates; beryllium silicates like bavenite, bertrandite, bityite, helvite, milarite, phenakite after beryl)

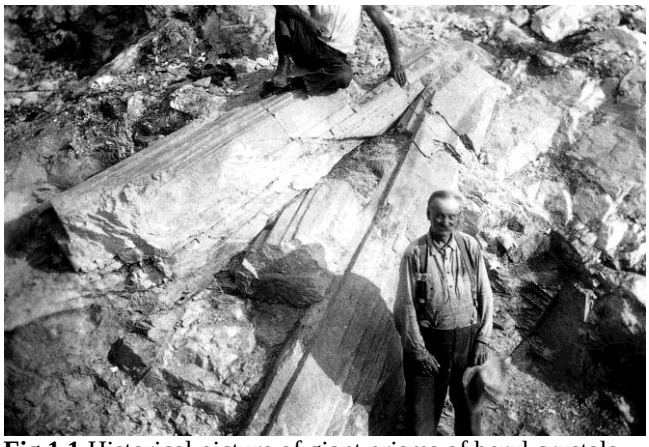

Fig 1.1 Historical picture of giant prisms of beryl crystals from pegmatite in Maine, U.S.A.

Fig 1.2 Develop of graphic pegmatite texture with variable grain size at Pulsifer quarry, Maine, USA.

The above mentioned textures are typical of pegmatites of granitic derivation (Černý and Ercit, 2005; London 2006) but this does not imply all these structures can be observed in a single pegmatitic dike or within a pegmatite field, because they develop in different families of pegmatites. Typical pegmatite texture, defined as coarse grained rock can be observed in all igneous rocks in composition. For example in ultramafic rocks which develop komatitic textures or mafic rocks which develop a coarse grained gabbroic pegmatite texture.

Scarce information available in literature in terms of texture, mineralogy, geochemistry, about peralkaline group of magmatic intrusive rocks imply that pegmatites, belonging to agpaitic rocks, do not fall, in sensu stricto of the term, into the granitic pegmatites. For such reason hyperalkaline and alkaline pegmatites do not enter in any of pegmatites classification utilized by the community of pegmatologists (Wise, 1999; Černý and Ercit, 2005). The reason is derived by the lackness of a systematic description of agpaitic textures and the above mentioned scarce information about these rocks, even if often these pegmatites show a marked NYF (niobium, yttrium, fluorine) geochemical character. Generally peralkaline pegmatites do not evidence layered aplitic structures, graphic intergrowth or skeletal crystal habit, which represents the trademark to identify and define a granitic pegmatite.

Another category of pegmatites, those contaminated by metasomatic reactions with the country rocks (e.g. desilicated pegmatites and albitized pegmatites) do not find a place as metasomatic pegmatites in the modern classification of pegmatites (Černý and Ercit, 2005). As it will be discussed later on the albitized pegmatites of Alpe Rosso-Pizzo Marcio, Vigezzo valley, have been classified and included into a specific category of the LCT pegmatites, even if these show pervasive albitization processes produced by metasomatic reactions with the ultramafic hosting rocks (Guastoni et al., 2008).

The vast majority of granitic pegmatites occur within granitic, sensu lato, bodies. These pegmatites can be defined syngenetic because they are clearly genetically related to the granitic source and associated to plutons emplaced in subvolcanic, shallow, or at deeper depth of intrusion. The pegmatites formed at subvolcanic and shallow depth (2-3 km or more) tend to form dike with granophyric or coarse grained

margins, miarolitic cavities with ovoid form within the hosting granite (e.g. Cuasso al Monte and Baveno in the Southern Alps). The transition from equigranular texture of the granite and the pools of miarolitic pegmatites is generally abrupt. Pegmatites generated at deeper depth (4-6 km of depth) show a more gradual grain transition from the hosting granite and the pegmatite itself. Aplitic and layered textures are common along the rim portions and generally these pegmatites lack of miarolitic cavities. Deeper seated pegmatites (6-10 km of depth and more) are generally unzoned or weakly zoned structures are observable. They develop quartz core zones, that in many cases occupy the volume of miarolitic pockets which result filled by vitreous, smoky masses of quartz.

Pegmatites may form pods within the granite or coalesce upward and segregate toward the roof of the parent pluton. They intrude in form of dikes into the surrounding rocks and emanate from the carapace of the pluton, in this case are defined epigenetic pegmatites. Immediate around the pluton swarms of pegmatites and aplites widespread and they tend to cross-cut and form reticulated structures, often developing hydrothermalized aureola within the surrounding rocks.

According to London (1992, 1996, 2005, 2008, 2009) pegmatites are silicate liquids, granitic in composition, with high contents in fluids (H_2O), semi-volatiles and volatiles elements (boron, fluorine, phosphorous). High concentrations of B, F, and P in silicate melts can enhance H_2O solubility to the point of complete miscibility leading to a supercritical transition from silicate melt to aqueous fluid. The vast majority of granitic pegmatites have compositions near the hydrous haplogranite minima. Flux content (water and volatiles) of even the most geochemical fractionated pegmatites is not more than a few weight percent in the whole-rock composition. London defines thems as flux-rich hydrosilicate melts; the melts that form granitic pegmatites are H_2O-bearing or H_2O-saturated haplogranitic liquids, with the addition of 1–2 wt% total of B, P, and F.

1.2 Historical perspective to the study of pegmatites

First observations in favour of the plutonic nature of granites and against the origin of granites by dry fusion or sedimentary origin were made by Élie de Beaumont in his publication « Note sur les emanations volcaniques et metalliferes » (1847). This author alludes to the presence of cavities, with fluid, and observed that an "*aura*" surrounding granite partakes some of the characters of the granite including pegmatite, graphic granite and greisen. In the same period, Theodor Scheerer (1847), one of the leading proponents of the aqueo-igneous-fusion, thought that at the time of final granite solidification water would be released from the melt. He envisioned that a wet, hydrous granitic fluid would be sufficiently fluid to penetrate the foliation planes of schists. Brögger was the first petrologist to recognize the formation of pegmatites in successive stages proposing both igneous and hydrothermal processes to generate pegmatites (Brögger, 1890).

Later on Waring (1905), describing tourmaline-bearing pegmatites from Pala, San Diego County. stated: "*…later a more aqueous magma was forced up through the reopened cavities and formed the upper portions of the vein.*."

In 1913 Mäkinen studied the pegmatitic dike of Tammela, Finland, and identified two distinct periods of crystallization; one at temperatures above 575°C and the second at lower temperatures. In 1915 a very modern idea of pegmatite crystallization processes was expressed by Galpin: "*After a pegmatite dike has partly or wholly formed, later magmatic solutions may come up along its walls through any cracks or openings which for various reasons may have developed in it"...."In certain cases it seems that there are reactions between the later solutions and minerals in the pre-deposited rocks".* In 1923 Fersman published a paper where he described the nepheline-syenite pegmatites of the Kola peninsula identifying four distinct intrusive phases which he respectively named epimagmatic, pegmatitic, pneumatolytic and hydrothermal. In 1925 several authors including Cook (on a molybdenite deposit), Müllbauer (on Bavarian phosphate pegmatites), Hess (on the history of pegmatites), Schaller and Landes (on the pegmatites of Pala, California), published the results of five independent studies related to the evolution of hydrothermal solutions of magmatic origin, which defined responsible for the late stage mineralizations.

Fersman (1931) and Lindgren (1937) observed in field a continuum transition from pegmatites to hydrothermal conditions occurring in granitic systems. These authors developed more or less at the same time an idea by which elaborated the temperature versus volatile concentration diagram, envisaging a continuum of crystallization processes from magmatic stage to hydrothermal stage.

Landes (1933) pointed out that pegmatites are a by-product of large bodies of intrusive magmas. The water and other "*fugitive elements*" , as Landes stated, become concentrated in the residual magma, a part of which may escape and form pegmatites. Because of its content of volatiles, the freezing point is lower and coarser crystals will form. Simple pegmatites are formed by magmatic minerals and complex pegmatites owe their character to further mineralization by hydrothermal solutions, which dissolve older minerals and precipitate new ones.

During the world war II, publications, studies, and field explorations on pegmatites were oriented to discover strategic minerals like beryl, tantalum oxides and sheet micas. This exploration work produced detailed mapping and regional studies. Systematic field studies by the United State Geological Survey (USGS) recognized and mapped several pegmatite districts like those in New England, South Dakota, Colorado, New Mexico.

Cameron et al., (1949) defined the internal zonation within pegmatites and evidenced pegmatites as result of fractional crystallization using the Bowen's (1928) series as model of fractional crystallization from silicate melts. The actions of an aqueous vapour associated to pegmatites (in the sense of liquid, gas or supercritical fluids) was indicated to contribute to form miarolitic cavities, replacement metasomatic pegmatite bodies and wallrock alterations.

In the fifties the studies made by Jahns (1953, 1955) on pegmatites introduced the concept of internal evolution of pegmatites controlled by aqueous fluids. These authors developed a petrological model for pegmatites which emphasizes the role of water as a dissolved constituent in silicate melts. This idea implies that fluid inclusions can be also of primary origin and the crystallization of pegmatites can be lowered at a supercritical state, below 550°C. Jahns (1953) summarized his views on the origins of giant texture crystals

in pegmatites in line with the idea previously expressed by Cameron et al. (1949), stating that "…*Suffice it to say here that the typical pegmatitic magma that yielded these enormous crystals must have been rich in hyperfusible constituents and probably had very low viscosity"…"Temperatures almost certainly were below 600°C, and the confining pressures were sufficiently great to prevent major escape of volatile constituents during the period of giant-crystal growth."* Jahns's term "hyperfusible constituents" refers to those components of evolved granitic systems that act as fluxes to reduce the solidus temperatures of silicate melts, that decrease viscosity as well, and enhance the miscibility of insoluble phases. These new ideas opened the collaboration to experimental petrology studies on granitic pegmatites with Tuttle and Burnham (Jahns and Tuttle, 1963; Jahns and Burnham, 1969). The experimental results of the studies performed by Jahns-Burnham define a model on the evolution and crystallization of pegmatites with lowering temperatures and evolving silicate melts which can be very summarized with three major steps:

First step: crystallization from hydrous silicate melt develop phaneritic textures, in granite or pegmatite

Second step: crystallization concomitantly from silicate melt and exsolved supercritical aqueous fluid yield giant pegmatite texture along with finer-grained to aplitic textures.

Third step: crystallization in absence of silicate melt, yield a wide variety of late-stage minerals and textures including pocket minerals and miarolitic cavities.

Jahns appears to have understood the growth of giant crystals from granitic melt at subsolidus temperatures requires high rates of diffusion of normally slow-moving components, such as Si and Al. For such reason Jahns called upon the fluxing effects of B, P, and F, in addition to H_2O, to reduce viscosity sufficiently to speed up diffusion in the short time of crystallization. The geochemical behaviour of fluxing components were already recognized by Wyllie and Tuttle (1964). The experimental application and the effects of fluorine, boron phosphorous on pegmatite crystallization processes will be the topic argument of investigation from early 1980's by David London.

Fenn published his studies on crystallization processes of alkali feldspars and graphic quartz-feldspar intergrowth (1977; 1986) in pegmatites. This author observed the growth rates and nucleation densities in alkali feldspars decrease as the initial H_2O content of the melt is increased. He concluded that graphic texture in pegmatite are a product of crystal growth from very viscous silicate melts undersaturated in H_2O.

The 80's and 90's were addressed by the pegmatite studies of Petr Černý, David London and other authors.

Černý works were mainly dedicated to mineral-chemistry, geochemistry and classification of pegmatites. London focused his studies to the experimental petrology of pegmatites. The contributes of Černý will be discussed in the chapter on classification of pegmatites focused to the development on the anatomy, the internal structural features, and the geochemical evolution of pegmatite provinces developed on regional scale (Černý 1991a; 1991b).

London studies were first addressed to fluid inclusions and calibration of lithium aluminosilicates at the Tanco pegmatite in Manitoba (London and Burt, 1982; London 1984). Later he applied to experimental petrology of pegmatites using the Macusani glass as starting material, a water, volatile-rich natural peraluminous rhyolite obsidian, he used to reproduce textural characters of pegmatites under H_2O-

undersaturated conditions (London et al., 1988; London et al., 1989). London obtained from his experimental studies with macusanite, and the addition of B, P, F, an increase of silicate-melt-aqueous vapour miscibility. Boron and phosphorous, but not F, help to increase H_2O solubility in melt to approximately 9-10 wt% H_2O at hypercritical fluid temperature and very low confining pressure at 200-300 MPa. The experiments with Macusani glass (macusanite) at 200 MPa yielded mineralogical fabrics and zonation that very resemble those observed in zoned granitic pegmatites (typically peraluminous, Li-Be-Ta-rich pegmatites). The mineralogical fabrics and zonation texture with inward crystallization are characterized by:

(1) fine-grained sodic feldspar-quartz border zones;

(2) fringe of very coarse-grained graphic quartz-feldspar intergrowths that flair radially toward melt and terminate with nearly monophase K-feldspar;

(3) core of very coarse-grained, nearly monomineralic quartz or virgilite ($LiAlSi_5O_{12}$) and mica;

(4) late-stage, fine-grained albite+mica intergrowths obtained from alkaline, Na-rich interstitial melt at hypercritical H_2O saturation. (London, 1986a; London et al., 1988; London et al., 1989).

Since early 90's several other authors (Chakoumakos and Lumpkin, 1990; Webber et al., 1999; Morgan and London, 1999) developed studies on cooling of epigenetic pegmatites intruding surrounding rocks. These authors, calculating the temperature of silicate liquids of pegmatites within injecting rocks at the time of emplacement, stated pegmatite dikes cooled down in few months, weeks or days, either a pegmatite dike had developed giant crystal textures or other textures like miarolitic pockets.

London (2009) presented his schematic model to explain the most common textural domains observed in granitic pegmatites. This model, which represents the result of his experimental studies on petrology of pegmatites, has three major arguments which can be summarized as follows:

(1) crystallization proceeds from melts whose temperatures are significantly (tens to hundreds of degrees Celsius) below their liquidus temperatures

(2) bulk compositions and viscosities of pegmatite forming liquids are close to the haplogranite system with the addition of fluxing components of H_2O, B, P, and F

(3) significant increases in the flux content promote the formation of giant crystals and other pegmatite textures through a reduction in melt viscosity that greatly enhances the diffusivity of Si and Al.

1.3 Economic importance of pegmatites

In the pegmatites volume published by London (2008) Petr Černý wrote the preface where he summarized very well the significance of why studying pegmatites with this sentence: " *Even the simplest pegmatite bodies, if large enough, serve as sources of feldspars and micas for the ceramic industry. More evolved, complex pegmatites can carry, in their sum as well as individually, other industrial minerals such as refractory lithium aluminosilicates, and a broad spectrum of accessory phases of a multitude of rare elements, most of them with advanced high-technology applications: lithium, cesium, beryllium, tantalum"…"Enormous markets thrive on pegmatite-generated gemstock and collectibles. To name a few,*

polychromatic tourmaline, topaz, and beryl from granitic pegmatites are among the best-looking, and possibly the most valuable specimens of any species of mineral from any environment, and the faceted stones of these and other minerals surpass the quality of most of their non-pegmatitic analogs".

Pegmatites are the main sources of industrial minerals such as feldspars widely used in glassmaking, ceramics, and to some extent as filler in paint, plastics, and rubber. Clear quartz from pegmatites, which contains very few impurities and few ppm of trace elements, is utilized in sophisticated electronic systems, such as polarized laser beams. Clear quartz-crystals are also used for prisms and lenses in optical instruments, prisms, optical filters, and timing devices. Micas, in particular muscovite, is the principal mineral used by the electrical industry in capacitors that are ideal for high frequency and radio frequency. Phlogopite mica remains stable at higher temperatures (to 900° C) is used in applications in which a combination of high-heat stability and electrical properties are required. Beryllium is produced by beryl (which contain about 4% of Be) and by bertrandite (which contain about 1% of Be). Beryllium metal is utilized in beryllium-copper alloys, beryllium oxide ceramics, and in a wide variety of products in aerospace, automotive, computer, defense, electronics, heavy machinery, home appliance, industrial component, telecommunications, medical, nuclear, oil and gas drilling, plastic molding (McNeil, 2005). Spodumene and petalite, for high contents in aluminum and lithium, are currently utilized in the production of refractory ceramics, glass, and primary aluminum. Niobium-Tantalum oxides (pyrochlore-microlite, columbite-tantalite, wodginite, and euxenite group minerals are the main producers of niobium-tantalum metals) find their the principal use for niobium as an additive in steelmaking, mostly in the manufacture of micro-alloyed steels. Niobium is used in high-strength low-alloy steels consumed by pipeline, automobile and construction industries. Tantalum is utilized to produce capacitors and superalloys. Most of the tantalum is consumed by the electronics industry, and goes into making capacitors, as electronic devices like cellular telephones (USGS, 2009). Tin is produced by cassiterite; large production of this metal come from pegmatites which find major uses as electrical solders, metal containers, can market, transportation, and construction.

Zirconium and hafnium are produced by zircon. Zirconium metal is used in corrosive environments, nuclear fuel cladding. Milled or ground zircon is utilized in refractory paints for coating the surfaces of molds. In the form of refractory bricks and blocks, zircon is used in furnaces for containing molten metals. Zirconia-silica-base refractories are also used in the manufacture of cubic zirconia, fiber optic connector components, refractory coatings, engineering ceramics and dental applications. The principal uses of hafnium are in high-temperature ceramics, nickel-base superalloys, nozzles for plasma arc metal cutting, and nuclear control rods.

Even if the abundance and the economic importance of rare-earth minerals in pegmatites such as allanites, euxenites and parisite-bastnasite group minerals is well recognized actually their utilize is limited by the major and economic importance offered by carbonatite deposits. Pegmatites will represent an economic potential in future exploitations taking into consideration the high demand of the market for rare earths. Rare earths find large use in pollution control catalysts, permanent magnets, and rechargeable batteries, cellular telephones, compact disk players, digital cameras, digital video disk players, laptop computers, fiber optics,

dental and surgical lasers, magnetic resonance imaging, medical contrast agents, medical isotopes, and emission tomography, X-ray detectors.

Pegmatites are the source-rock of coloured gemstones like polychrome tourmalines, topaz, coloured varieties of beryl such as aquamarine, emerald, morganite, amazonite a green variety of microcline, coloured spodumene crystals like kunzite and hiddenite, and an impressive number of collectable mineral species among oxides, phosphates and silicate minerals (London, 2008) which make the mineral market an attractive economic prospective for exploitation of minerals for collectors (Fig. 1.3). High demand for aesthetic gem-quality minerals for collecting during last ten years opened new opportunities to gem and mineral mines (Fig. 1.4). For example requests of polychrome tourmaline crystals for collectable has surpassed the market values of cut gemstones (Pezzotta,1999a)

Fig. 1.3 Exceptional tabular crystal of hambergite, a very rare beryllium borate from LCT pegmatite of Madagascar

Fig 1.4 Beautiful purple crystals of fluorapatite from LCT pegmatite at Pulsifer quarry, Maine, USA.

1.4 Classification of pegmatites: a brief history

The first classification of pegmaties was probably made by Landes (1933) applied to U.S. pegmatites. He introduced first fundamental criteria to use in classifying a pegmatite in the field by the shape, the size, the presence of cavities and the genetic relationship respect the parent intrusion. In the 60's and 70's various Russian geologist published their studies on pegmatites (Vlasov, 1961; Solodov, 1962; Solodov, 1971; Sokolov et al., 1975). These soviet authors addressed their studies to the pegmatite classification defining five types of granitic pegmatites based on zonal complexity and the distance from the source rock as follows:

(1) simple graphic granite pegmatite

(2) blocky microcline pegmatite

(3) fully differentiated pegmatite (unspecified)

(4) rare-metal Li-bearing pegmatite grading toward rare-element miarolitic pegmatite

(5) albite-spodumene or albite-lepidolite pegmatite.

Ginsburg et al. (1979) proposed pressure-temperature diagram with four classes including abyssal, muscovite, rare elements, and miarolitic pegmatites. Ginsburg (1984) summarized the P-T diagram and the four pegmatite classes as follows: " *They originate* (granitic pegmatites) *only under specific barometric conditions which impede the evacuation of the volatiles from magmatic melt. The minimal depth at which the development of the pegmatitic process is feasible, corresponds to 1.5-2 km, while the vertical span of pegmatites is estimated to be about 15 km. In the same regard, according to the geological location and correspondingly to the thermodynamic parameters, they can be classified into a number of formations (5), encountered within various structural storeys of the terrestrial crust and varying in mineralization. Four pegmatitic formations are distinguished: of small depths and pressures, commonly referred to as the crystal-*

bearing; of medium depths and pressures, referred to as the rare-metal; of high pressures, called micaceous, and of very high pressures, referred to as the ceramic.

Černý (1990; 1991a) inspired by Ginsburg and soviet authors revised the classification of pegmatites and to improve it introduced additional petrological, paragenetic and geochemical criteria. He maintained the four classes of pegmatites, abyssal, muscovite, rare-element and miarolitic, but introduced a new, separate geochemical concept for three petrogenetic families of pegmatites. He defined a LCT (lithium, cesium, tantalum) peraluminous (A/CNK>1) in bulk composition family of pegmatites, a NYF (niobium, yttrium, fluorine) metaluminous (A/CNK<1), subaluminous (A/CNK=1) and peralkaline (A/NK<1) in bulk composition family of pegmatites, and a mixed LCT-NYF family of pegmatites.

LCT pegmatite family include four types: beryl (with two subtypes, beryl-columbite and beryl-columbite-phosphate respectively), complex (with four subtypes, spodumene, petalite, lepidolite, amblygonite), albite-spodumene, and albite. NYF pegmatite family only included rare-earth type (with two subtypes, allanite-monazite and gadolinite respectively).

Rare element and miarolitic classes were related to syngenetic or epigenetic granitic pegmatite origin whereas abyssal and muscovite class of pegmatites were related to segregations of anatectic leucosome without any relationships to granites under a metamorphic regime of upper amphibolitic to granulitic facies.

Mike Wise (1999) introduced an expanded NYF classification of related pegmatites with NYF geochemistry of A-type granite plutons, post-tectonic to anorogenic plutons formed in continental or oceanic rift zones, based on aluminum saturation index. He defined three NYF pegmatite groups as: peralkaline, which include fayalite and amphibole pegmatite type (with aegirine-arfvedsonite, riebeckite, allanite subtype), metaluminous which include allanite pegmatite type (with allanite, euxenite, gadolinite subtype) and peraluminous which include beryl, phenakite, topaz, fluorite pegmatite type (with beryl, tourmaline, topaz subtype).

1.5 The classification of granitic pegmatites revisited

Ercit (2005) rewieved REE-bearing granitic pegmatites and collected additional data for the abyssal and muscovite-class of pegmatites that in previous classifications were poorly represented (Černý 1990; 1991a; Wise 1999). He defined a category of NYF pegmatites also among the abyssal (with two subdivisions into allanite-monazite-uraninite and Y-REE-Nb-oxide subtype), muscovite, muscovite-rare element classes in addition to those belonging to the rare-element and miarolitic classes. Černý and Ercit (2005) combining their previous classification on pegmatites (Černý 1991a; Ercit 2005), introduced a new petrogenetic classification. This classification represents the evolution of the ideas of previous pegmatite classifications and today represents the guide utilized by the pegmatologist community to classify pegmatites on regional scale. What Černý and Ercit have done is to maintain the structure of previous classifications. Pegmatites are divided into peraluminous, metaluminous and subaluminous with the exclusion of the peralkaline (agpaitic) pegmatites and those considered contaminated by reactions with country rocks (metasomatic) like albitized

pegmatites hosted in ultrabasic rocks and amphibolites (Martin Izard et al., 1995; Guastoni et al., 2008). The geological classes of granitic pegmatites and their geochemical-mineralogical subdivisions defined by the authors include five classes, ten subclasses, thirteen types, and seven subtypes. The classes fall in the P-T diagram of metamorphic facies which characterize the petrology of their host-rock. Pressure-temperature are referred to the peak metamorphism which occurred during pegmatite emplacement. In reality a real connection between the depth of pegmatite emplacement and the metamorphic grade of the host rock during their emplacement is deficient. This represents a strong limitation for pegmatite fields emplaced in active orogenic chains like the case of the pegmatites from Central Alps, argument of this study, discussed later on, where polymetamorphism develops at different crustal depth and at different age intervals.

Abyssal class pegmatites are hosted in the P–T range of the granulite facies extended to upper-amphibolite conditions (Bucher and Frey, 1994), but their host terranes are generally polymetamorphic (Grew et al., 2000). Four subclasses of abyssal pegmatites can be distinguished: they include AB-HREE (abyssal heavy rare-earths), AB-LREE (abyssal light rare-earths), AB-U (abyssal uranium), AB-B,Be (abyssal boron-beryllium).

Muscovite class pegmatites show conformable and deformed structures within host rocks at high-pressure amphibolite facies characterized by kyanite–sillimanite paragenesis of the Barrovian metamorphic facies-series. The pegmatites are typically barren, carrying feldspar of ceramic grade, quartz and industrial mica, which gave them the original name.

Muscovite–rare-element class pegmatites are mostly discordant respect to the metamorphic foliation of their host rocks, and occasionally show regional zonation respect to parental granites (Shmakin 1976; Ercit, 2005). They are hosted by moderate to high amphibolite facies 2-7 kbar, 650°C to 520°C. Two subclasses of pegmatites within the muscovite–rare-element class can be distinguished: they include MSREL-REE (muscovite rare-element rare-earths) with geochemical signature Be, Y, REE, Ti, U, Th, Nb-Ta and MSREL-Li (muscovite rare-element lithium) with geochemical signature Li, Be, Nb.

Černý (1990; 1991a) defined abyssal and muscovite class of pegmatites those related to segregations of anatectic leucosome without any relationships to granites in a metamorphic regime of upper amphibolitic to granulitic facies. Abyssal class are now redefined with a question mark by Černý and Ercit (2005) in terms that the protolith may be an anatectic leucosome or granitic in origin. Other authors suggest that some of the muscovite, in particular MSREL class pegmatites population derive from granitic parents (Shmakin 1976; Ginsburg et al., 1979).

Rare-element class pegmatites include two subclasses REL–REE (rare-element rare-earths) and REL–Li (rare-element lithium). REL–REE subclass is derived from post-to anorogenic metaluminous to peraluminous granites at variable crustal depths. The REL–REE subclass has HFSE (High field strength elements) enrichments, is emplaced at variable depth, but generally shallow. REL-REE subclass is subdivided into three types: allanite–monazite type, euxenite type both with negligible amounts to absence of Be (Wise 1999), and gadolinite type. The REL–REE pegmatites are impoverished in phosphorus and the contents of lithium, rubidium and cesium are low (Černý 1991; Brown 1999).

REL–Li subclass is emplaced in the low-pressure, from lower amphibolite to upper greenschist facies with andalusite-sillimanite and prex 2-4 kbar and differentiated from syn-to late-orogenic peraluminous granites. The REL–Li subclass constitutes the most diversified geochemical-mineralogical subclass and is subdivided into nine types. They include beryl type which include beryl–columbite subtype, beryl–columbite–phosphate subtype. The complex type which include spodumene subtype, petalite subtype, lepidolite subtype, elbaite subtype, amblygonite subtype. The albite–spodumene type and the albite type. These two last pegmatites types feature aplitic to saccharoidal albite dominant over quartz, and minor to accessory K-feldspar, spodumene or lepidolite.

Miarolitic class pegmatites include two subclasses, MI–REE (miarolitic rare-earths) and MI–Li (miarolitic lithium). The MI–REE subclass is syngenetic and mainly related to anorogenic granites that rise to shallow intrusive levels in the crust with exsolution of miarolitic cavities within parent granitic plutons. The miarolitic rare-earths subclass includes the topaz–beryl type and the gadolinite–fergusonite type like Baveno (Pezzotta et al., 1999) with Nb>Ta.

The MI–Li subclass is related to the same type of fertile granites that generate REL–Li-class pegmatites, and locally develops by gradual transition from the latter. Pressure reduction leads to exsolution of a vapour phase as in the MI–REE subclass, and promotes the formation of miarolitic cavities (London 1986). The subdivision of this subclass bears some similarity to the subdivision of the REL–Li subclass. The Mi-Li subclass includes the beryl–topaz type, the MI–spodumene type, the MI–petalite type, and the MI–lepidolite type.

1.6 Geochemical classification of pegmatites

Geochemical classification of pegmatites was first promoted by Černý (1990; 1991a) when he defined abbreviations for the two pegmatite families, respectively NYF (niobium, yttrium-REE, fluorine) and LCT (lithium, cesium, tantalum) to symbolize their chemical enrichments trends. It is important to emphasize that NYF or LCT geochemical signature does not necessarily mean that the elements characteristic of the other family are absent. For example minerals typical of NYF family like Y-Nb-Ta oxides, Y-REE phosphates, and Y-REE-silicates may be present in LCT pegmatites and elbaite, lepidolite may be carried by NYF pegmatities (Novák et al., 1999). Garnet pegmatite of Codera valley has mixed NYF-LCT characters and this will represent an interesting theme of Ph.D. discussion. Nevertheless, pegmatite populations with a combined signature do exist and they are assigned to the mixed NYF + LCT family.

NYF pegmatite family is marked by a Nb>Ta, Ti, Y, Sc, REE, Zr, U, Th, F enrichment. The parent granites are subaluminous, metaluminous peraluminous and peralkaline, A- to I-types and the degree of fractionation within the fertile granites is moderate (Simmons et al. 1987; Buck et al. 1999). Abundances of REE range for most LREE-enriched at 100 to 800 times chondritic, even if some exceptions. The NYF pegmatites comprise those that fall within the REL–REE and MI–REE subclasses and include syngenetic and epigenetic pegmatites.

LCT pegmatite family is progressively enriched in, Li, Rb, Cs, Be, Sn,Ta, Nb (with Ta>Nb), and also in B, P and F, with progressive fractionation of the melt and possibly distance from the source rock. The parent granites are mildly to peraluminous, S, I or mixed S + I type. REE abundances are low, with LREE at 100 to 10 times chondritic. LCT pegmatite populations include REL–Li and MI–Li subclasses. Most of LCT pegmatites have epigenetic character.

Mixed NYF + LCT family consists of pegmatites that display mixed geochemical and mineralogical characteristics. These characters can manifest as LCT accessory minerals and LCT trace-elements mixed within differentiated NYF pegmatites or LCT pegmatites formed during late stages of evolution of NYF pegmatite populations.

1.7 Generation of rare-element granitic pegmatites

Pegmatitic fields of the rare-element class are generated from deeper-seated and volatile-undersaturated parental granites and generally are associated to magmatic intrusive suites that lack of disseminated magmatic ores and aqueous fluid-transported mineralization (Černý, 1991c) Pegmatites related to granitic pegmatites are dominantly magmatic and largely volatile undersaturated (London et al., 1989). Disequilibrium crystallization and undercooling temperatures are the dominant crystallization processes which characterize pegmatites. The vast majority of pegmatites have the compositions near the ternary diagram (albite-K-feldspar-quartz) of hydrous haplogranite minima at 100-300 MPa (Tuttle and Bowen, 1958) but the undercooling temperatures and the addition of volatiles lead to extensive variations of initial pegmatite composition and in most cases cause complex internal zoning and extremely variable textural characters (London ,1987; London et al., 1988; London et al., 1989).

Classificative scheme of LCT and NYF granite families as defined by Černý and Ercit (2005) help to discriminate different sources for granitic pegmatites.

LCT granite include:

LCT I-type subaluminous (A/CNK=1) fertile granites of igneous protoliths, such as those generated by low-percentage anatexis of meta-igneous rocks of the basement (Wright and Haxel 1982). These granite will origin pegmatite poor in Cs, B, P, S

LCT S-type peraluminous (A/CNK>1) fertile granites of metasedimentary and metavolcanic protoliths (Černý and Brisbin, 1982a). These granite will origin pegmatite enriched in Cs, B, P, S. Peraluminous fertile granites display fractionation levels equal to those of evolved rare-element pegmatite liquid melts, with K/Rb as low as ~40, K/Cs ~250, Mg/Li ~ 1, Zr/Sn <1, Zr/Hf ~5, Nb/Ta ~0.03, Al/Ga ~750, and K/Ba as high as 24.000 ppm (Černý and Meintzer, 1988). However, many fertile granites are proven to have been derived by melting of mixed basement and supracrustal protoliths, and they show intermediate geochemical compositions (Walker et al. 1986).

NYF granite include:

NYF A-type anorogenic granites belong to bimodal gabbro-granite suites and are generated by partial melting of depleted lower crust generate subalkaline (A/NK =1) to metaluminous (A/CNK<1) NYF pegmatites (Simmons et al., 1987). These granites will generate topaz and fluorite-bearing pegmatites.

NYF I-type syn to late-orogenic granites generated by large anatexis of I-type tonalitic protoliths. These granite will generate topaz-bearing pegmatites (Buck et al., 1999; Kjellman et al., 1999). Petrological, isotopic and geochemical evidence suggest several possible modes of origin of the NYF-granite magmas. The sources could be from differentiation of mantle-derived basaltic magmas (Fowler and Doig, 1983); melting of middle or lower-crust depleted by a previous melting causing LCT granites to be mobilized but NYF granites to be conserved (Collins et al., 1982; Whalen et al., 1987; Černý, 1990, 1991a); melting of continental crust enriched in NYF elements by mantle-derived fluids following the model of bimodal gabbro–granite suites (Harris and Marriner 1980, Jackson et al., 1984; Martin and De Vito 2004).

London (2008), based on field and petrological studies, defines subvolcanic and shallow depth pegmatites as mostly related to A-type granites and generally belong to NYF pegmatite family. Deeply emplaced granite-pegmatite systems are generally peraluminous S-type and I-type granites with pegmatites characterized by the LCT chemical signature and with exceptions usually these pegmatites do not have miarolitic pockets.

Geology of Central Alps:
Tertiary plutonism, migmatites and Barrovian metamorphism

2.1 Introduction to the area of study

The Alps are the result of collision between the European continent and the Adriatic microplate. Alpine region, as defined, stretches from Nice to Vienna, across southeast France, northern Italy, Switzerland, Austria, northern Slovenia and parts of southern Germany. The molasses basins of southern Germany in the European plate and Po plain in the Adriatic plate border the chain belt to the north and south respectively. The main trend in the central Alps is WSW-ENE, the Alps in the west form a major arc, before merging into the NNW-SSE strike of the Apennines. (Wenk, 1953; Trümpy, 1960; Panza and Müller, 1978; Müller et al., 1980; Schmid et al., 1989).

The area of study is located in the Central-Western Alps, along the E-W-trending Southern Steep Belt (SSB) (Burry et al., 2005) of the Western-Central Alps. This area hosts a major Tertiary pegmatite field which extends for more than 90 km along the belt axis, from Centovalli Line in the west, to Chiavenna valley and throughout the Oligocene Masino-Bregaglia intrusive massif to the east (Fig. 2.1).

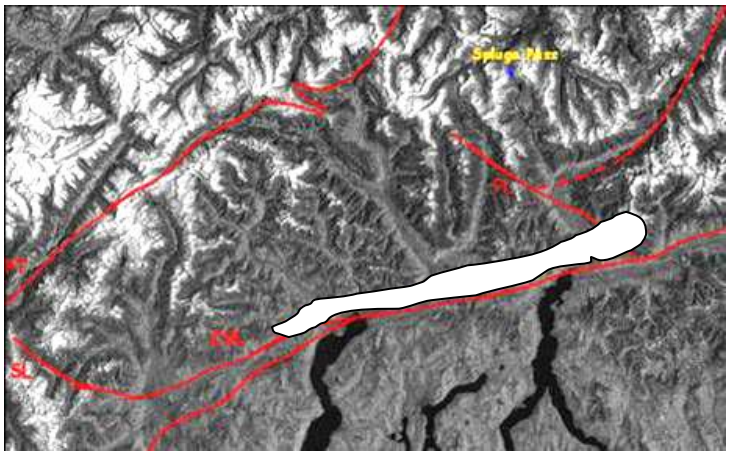

Fig. 2.1 Aerial view of Central Alps where pegmatite field is located (filled in white). Centovalli line (CVL), Simplon Line (SL), Forcola Line (FL) are outlined. Image redrawn and modified after Ghizzoni and Mazzoleni (2005).

The pegmatitic field extends for a thickness of few kilometers north of the Insubric line and toward west appears truncated by the the Simplon Line. This area hosts the South Penninic units (Frey et al., 1974) which are the structurally deepest rocks exposed in the Alps (Trümpy, 1960; Froitzheim et al., 1996) bordered to the south by the Insubric line (Periadriatic fault) that shortcuts the Lepontine Dome in the south. Penninic nappes consist of recumbent folds (Lugeon, 1901) composed by orthogneiss cores (Köppel et al., 1980) discontinuously mantled by schistose paragneiss envelope overlied by Mesozoic metasediments. Southern Steep Belt represents the root area of Penninic units characterized by steep oriented into subvertical and overturned orientation younger than the nappe stack itself (Heitzmann, 1987) (Fig 2.2).

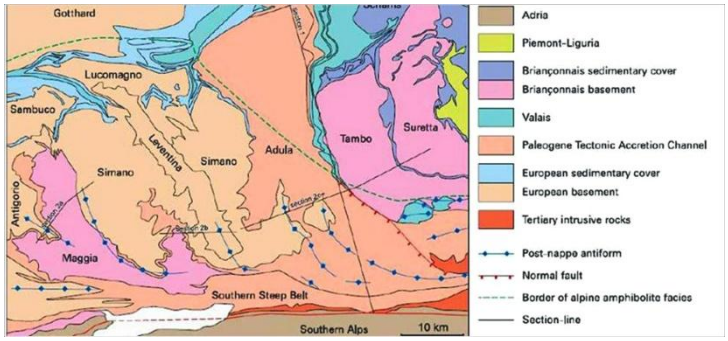

Fig. 2.2 Structural sketch of Penninic nappes and Southern Steep Belt along Central Alps. Pegmatites are hosted within different lithologies at different crustal-nappe levels.

Pegmatites intrude and cross cut in form of dykes the boundary of south Penninic Alpine nappes which are involved in poliphasic high-temperature greenschist to amphibolites facies. Pegmatites and aplites also intrude in form of dikes the tonalite-granodiorite rocks of Masino-Bregaglia intrusion and the S-type two mica (biotite and muscovite) San Fedelino leucogranite stock, which crop out adjacent to the southern-western portion of the Masino-Bregaglia massif (Fig. 2.3)

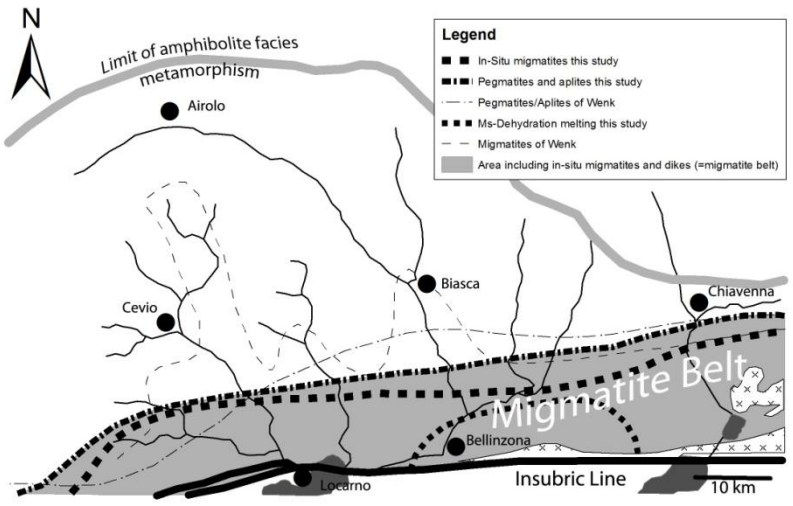

Fig 2.3 Pegmatite field extends for few kilometres north of Insubric Line and for more than 90 km along the belt axis within the SSB migmatite belt and Masino-Bregaglia intrusion. Redrawn after Burry et al., (2005)

Along the area of study above mentioned were selected three different zones each of them host pegmatites with peculiar geological, petrological, geochemical and mineralogical characters. The first area extends from the village of Domodossola in Ossola valley toward east along the Vigezzo valley where six pegmatite dikes were studied. The second area is localized in Mesolcina valley and Bodengo valley which include three more pegmatite dikes. The third area is localized in the Codera valley, in the earth of the Masino-Bregaglia massif, where two pegmatite dikes were studied.

2.2 Previous studies of the pegmatites along the Central Alps

It is undoubtedly that most of the studies of the pegmatite field which outcrops in the Central area of the Alps were devoted to describe the mineralogy, in particular the accessory or "exotic" minerals found in these pegmatites. First studies of rare accessory minerals found in these pegmatites were published by Spezia (1882) on beryl and by Strüver (1885) on columbite, both minerals occur in the pegmatites of Craveggia, in Vigezzo valley. Repossi (1906) published a paper on the minerals of San Fedelino pegmatites of Chiavenna valley, and Zambonini (1907, 1908) published two new minerals (strüverite and delorenzite) discovered in the pegmatites of Piano dei Lavonchi, Vigezzo valley. Taddei (1940) described the minerals which occur in several pegmatite dikes outcropping in Calanca and Mesolcina valley, Switzerland. Gramaccioli, (1958) reported an additional note on delorenzite from Craveggia, and Roggiani (1966) made the first description of the albitized pegmatite of Alpe Rosso, Vigezzo valley. Beautiful beryl aquamarine and garnet crystals associated with other uncommon minerals in the pegmatites in Codera valley were reported by Peco (1949) and by De Michele et al. (1970) (Fig. 2.4).

Fig. 2.4. Beryl var. aquamarine, crystal 4.5 centimetrs in length collected in the pegmatites of Codera valley. Collection of Museum of Natural History of Milan.

First contributions to the geological description of the pegmatite field of Central Alps were made by Preiswerk (1925) and Kündig (1926). Wenk (1970) was the first author who mapped and traced the limits of the pegmatite field along the Southern Steep Belt (see fig. 2.3). Bonsignore et al (1971) mapped the geology of Codera valley and mentioned the swarm of pegmatite dikes outcrop in the Codera valley. Rb/Sr isochrons and U-Pb age determinations from zircons in pegmatites hosted within Hercynian or older migmatites from Bodengo valley were published by Hänny et al. (1975) who determined an Alpine age, around 30 m.y., for the pegmatites from this area.

A temptative of classification of the pegmatites within the Masino-Bragaglia massif and around its contact aureola was made by Wenger and Armbruster (1991) using field observations of pegmatite textures and mineral data of columbites and micas. This temptative of classification was utilized to distinguish among undifferentiated, differentiated and hybrid pegmatites (?). The classificative scheme suffers the lack of knowledge in recognizing pegmatite textures and their overall mineralogy. These authors pretended to

discriminate the dikes on the basis of their muscovite and biotite contents. It is common observe in the pegmatites of Masino-Bregaglia the mineralogy which evolves from biotite at the border zone to muscovite in the intermediate zone and hence does not represent valid criteria to distinguish different pegmatite populations. Wenger et al., (1993) made another classification of pegmatites hosted within the Masino-Bregaglia pluton. They based their studies on the distribution of LREE and HREE on bulk composition of pegmatites hosted within and adjacent the calc-alkaline intrusion. They differentiated two groups of pegmatites. First group, named A, include pegmatites with undisturbed REE patterns, intruded into mafic rocks (amphibolites) subdivided into two categories:

(1) lower fractionated biotite type with $K_2O>Na_2O$ and minor Eu anomaly

(2) highly evolved muscovite type with $Na_2O>K_2O$ and strongly Eu anomaly

Second group, named B, include pegmatites hosted in the metamorphic Gruf unit adjacent the Masino-Bregaglia intrusion which show contaminated HREE and LREE pattern. This classification suffers of any information about mineralogical and textural characters of the pegmatites studied and once again pretends to classify pegmatites on basis of biotite/muscovite contents. A good point was the authors indicate the granitic pegmatites derive by contamination of tonalitic magma of the Masino-Bregaglia pluton. It is not too difficult to argue it: these pegmatites cross cut the Masino-Bregaglia intrusion!

Romer et al., (1996) presented U-Pb and Rb-Sr age data of different aplites, pegmatites and granodiorite dikes located along Vigezzo valley. Granodiorite porphyritic dike at Loana valley was previously studied by Bürgi and Klötzli, (1990) using Rb-Sr in biotite aged 29 m.y. Romer et al., (1996) re-analyzed the dyke and using $^{206}Pb/^{238}Pb$ in titanite fixed an age at 31.7 m.y. Aplite-pegmatite at Malesco (Vigezzo valley) with $^{207}Pb/^{235}U$ in zircons gave ages between 28 and 30 m.y. and monazite from same dike yielded a $^{207}Pb/^{235}U$ age of 29.2 m.y. The Rb-Sr analysis on muscovite gave 29.6 m.y. for such aplite-pegmatite indicating the system closed very soon after the emplacement of the dike, hence it cooled fast. The authors also analyzed a pegmatite with garnet and muscovite at Golino (Centovalli line, nearby Locarno, Switzerland) where $^{207}Pb/^{235}U$ on zircon yielded 29.1 m.y.

Gebauer (1996) obtained with SHRIMP data Pb/U zircons an age of 25.1±0.6 m.y. from a pegmatite cross-cutting the migmatites of the Southern Steep Belt at San Vittore, Mesolcina valley, Switzerland. This pegmatite was interpreted by the author to reflect the final thermal pulse connected to magmatic and fluid activity after the peak metamorphism in the SSB. Pietro Vignola (personal communication) dated at 24.1 m.y. the pegmatite of Rio Graia with U/Pb in zircon. The albitized pegmatite of the Pizzo Marcio summit was also dated using U/Pb in cheralite gave 32.7 ± 3.2 m.y. (Guastoni and Mazzoli 2007).

2.3 Masino-Bregaglia intrusion and its surrounding rocks

The Masino-Bregaglia calc-alkaline Oligocene pluton predominantly consists of tonalite at the rim and granodiorite with K-feldspar megacrysts in the core of the intrusion. In the western and southern part of the pluton a zone of magma mixing and mingling forming a contact zone to the granodiorite is often present and

usually was mapped as granodiorite (Wenk and Cornelius, 1977). The southernmost part of the tonalite is a steep tabular body oriented parallel to the Insubric line. This tabular body of tonalite extends over 50 km in an east-west direction and is always oriented parallel to the migmatites of the Southen Steep Belt and the Insubric mylonites. Its western part, along the tail of the intrusion, is named the "Iorio tonalite", whereas the eastern part (along Mera valley or Chiavenna valley) is the "Southern Bergell tonalite". The Masino-Bregaglia pluton has a nappe-like geometry (Wenk, 1973); it roots within the Southern Steep Belt north of the Insubric Line and it occupies a structural position equivalent to that of the Tambo-Suretta nappes (Rosenberg et al., 1995; Berger, 1996). At the western margin the Iorio tonalite narrows and takes on the subvertical geometry of the Southern Steep Belt adjacent to the Insubric Line. At its eastern margin, near the top of the intrusion, the Masino-Bregaglia intrusion is in contact with the South-Penninic ophiolitic units and the Austroalpine nappes of Malenco valley (Berger and Gierè, 1995). The Bergell pluton induced contact metamorphism along its eastern border (located near the top of the pluton), where the temperatures prior to contact metamorphism registred were below 450°C (Trommsdorff and Connolly, 1996)

Due to a very pronounced easterly axial plunge of up to 25° formed during and after the emplacement, increasingly deeper levels are exposed westwards within and around Bergell pluton (Berger and Gierè, 1995). NE granodioritic margin of the pluton has a laccolithic geometry and shallow level of emplacement (~5 kbar) as recorded by hornblende barometry (Reusser, 1987; Davidson et al., 1996). The SW tonalitic margin is structurally deeper (>8 kbar), also defined the "feeder zone" for the main intrusion (Davidson et al., 1996; Oberli et al., 2004) (Fig. 2.5). The isotopic measures document an extended history of crystallization and melt evolution of at least 5 Ma, defining an early interval of 33.0 to 32.0 Ma, followed by crystallization of zoned allanite from 32.0 to 28.0 Ma and formation of magmatic epidote as late as 26 Ma.

The present-day erosion surface exposes successively deeper levels of the intrusion, from the shallow roof of the intrusion in the east to the deep-seated feeder zone exposed as a tail-shaped extension in the west. The southern part of the pluton, a 50 km long tabular body of tonalite, represents the feeder of the pluton as reported by Berger et al., (1996). According to Davidson et al., (1996) the western contact of the magmatic body was emplaced and folded together with the remnants of former nappe boundaries which correspond to:

(1) Misox zone that consists of sequences of allochtonous calcareous-schists and metabasalts

(2) Chiavenna ophiolite

(3) Bellinzona-Dascio zone (BDZ) forming the Southern Steep Belt. BDZ is characterized by migmatization metamorphism with mixed gneisses and associated amphibolites, calc-schists, marbles, ultramafic rocks, relict eclogites. BDZ lies on top of the underlying Adula-Gruf nappe unit.

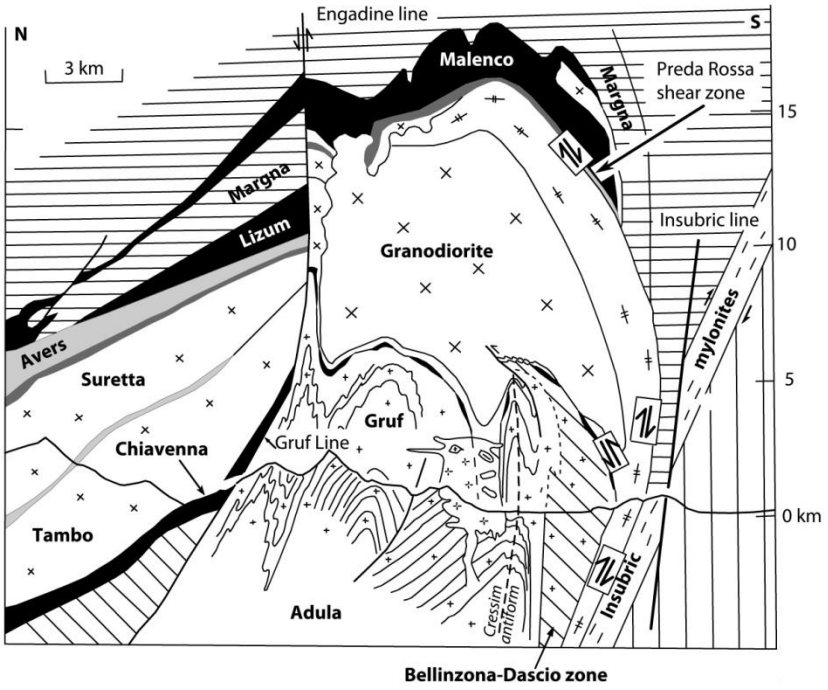

Fig 2.5 North-South section across Masino-Bregaglia intrusion and San Fedelino granitic stock along Chiavenna valley. Redrawn after Schmid et al., (1996)

2.4 Petrography of Masino-Bregaglia intrusion

The Masino-Bregaglia calc-alkaline pluton (calc-alkaline term is applied in the sense of not tholeiitic granite without positive Fe-enrichment trend with differentiation) is formed by tonalite at the rim of the intrusion and granodiorite with K-feldspar megacrysts in the core. Zoned structure of the pluton provides evidences that emplacement of granodiorite intrusion involved ballooning: the primary magma tonalite intruded country rocks and solidified from the margins inward (Rosenberg et al., 1994) (see fig. 2.5).

The tonalite is composed of plagioclase, quartz, horneblende, biotite, minor epidote and K-feldspar (Reusser, 1987). It has a well-developed foliation defined by the preferred orientation of biotite and plagioclase and a lineation defined by elongate horneblende crystals. Gabbros horneblendites, charnockites and granulites occur both in the tonalite and in the Gruf complex (Galli et al., 2011). The Gruf Complex border to the north and to the south-west the Masino-Bregaglia intrusion and predominantly consists of migmatitic quartzo–feldspathic orthogneisses, paragneisses and biotite–sillimanite–garnet–(±cordierite)-bearing metapelitic rocks (Bucher-Nurminen and Droop, 1983).

The granodiorite is composed of plagioclase, quartz, K-feldspar, biotite and less horneblende (Reusser, 1987). K-feldspar occur both as white megacrysts (up to >10 cm) and in the matrix as centimetric crystals. Near the contact with the tonalite, the granodiorite has well-developed foliation marked by the preferred orientation of biotite, whereas the alignment of K-feldspar megacrysts defines a minor lineation. In some

areas the granodiorite exhibits a distinct magmatic layering documented by accumulation of large centimetric K-feldspar oriented parallel to the layers. Both the granodiorite and tonalite contain abundant homogeneous enclaves of dioritic to monzonitic composition (Gansser and Gyr, 1964).

The Melirolo augengneiss is an intensively solid-state deformed and occasionally mylonitic epidote bearing granodiorite (Reusser, 1987) The augen are primarily 1-2 cm plagioclase but also K-feldspar and quartz are present. This deformed granodiorite occurs toward west in the southern margin of the Iorio tonalite and it also intrudes as small dikes the Tonale series. Porphyritic dikes of very similar composition were localized all along the SSB and in the Ossola valley. Schmid et al., (1996) define the Melirolo augen-gneiss contemporaneous in age with the Masino-Bregaglia intrusion because of the gradational transitions observed within the Jorio tonalite.

2.5 Novate granite

The fine-grained Novate granite (fig. 2.6) is a garnet-bearing S-type two-mica leucogranite stock derived from partial melting of crustal rocks during the Late Alpine decompression (Oschidari and Ziegler, 1992; Von Blanckenburg et al., 1992). The southeastern contact of San Fedelino leucogranite contains numerous Masino-Bregaglia tonalite blocks showing no preferred orientation within the enclosing leucogranite. The Novate granite and the associated aplite and pegmatites dike swarms crosscut the intrusion itself, the adjacent Masino-Bregaglia tonalite and Gruf complex (Wenk, 1973; Berger et al., 1996). Geochronological data indicate the Novate granite intruded at 24–25 Ma and cooled down to temperature conditions of 300–350 °C during 23–21 Ma age interval according to biotite and muscovite K–Ar and Rb–Sr ages (Hansmann, 1996; Liati et al., 2000). The Novate leucogranite was emplaced under upper crustal conditions, at the southern tip of a crustal-scale extensional shear zone, the Forcola mylonites associated with the Forcola Line, a normal fault, exposed in the northwestern end of the Novate granite and along Chiavenna valley. Extensional and vertical shearing along the Forcola shear zone provided the conditions for the magma ascent and emplacement (Ciancaleoni and Marquer, 2006).

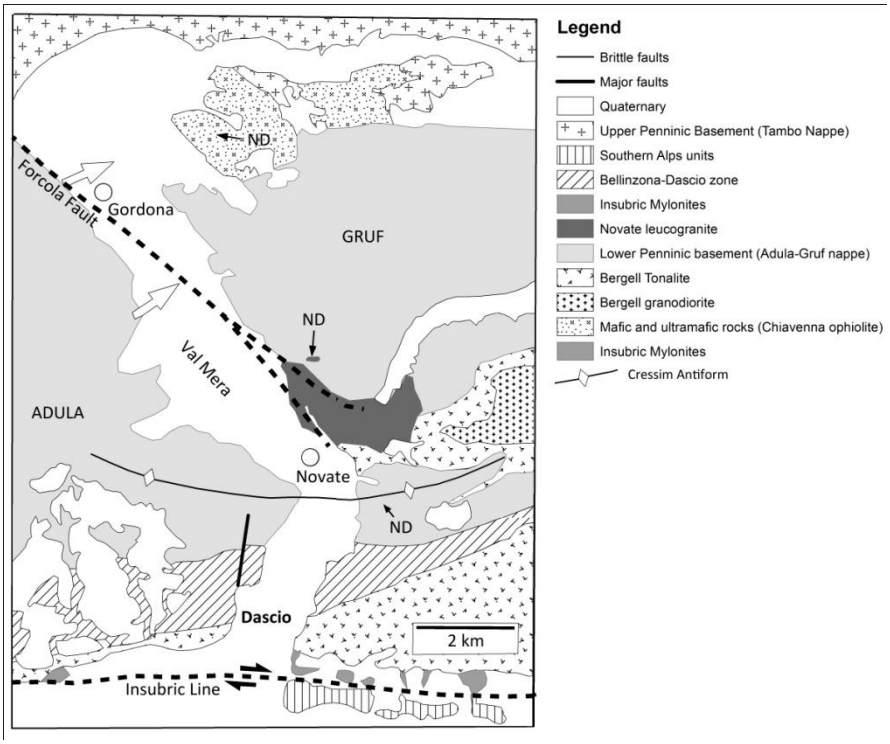

Fig. 2.6 Location of Novate S-type leucogranite at the western margin of Masino-Bregaglia tonalities. ND indicates Novate dykes which crosscut Adula Gruf nappes and Chiavenna ophiolites. Redrawn after Ciancaleoni and Marquer (2006)

2.6 Gruf Metamorphic Complex

The Gruf Complex, which is approximately 20×10 km in size, is located at the south-eastern margin of the Lepontine Dome. To the north is bordered by the Mesozoic ophiolitic Chiavenna Unit, to the east is cut by the Masino-Bregaglia intrusion, along a sharp contact, whereas to the south-west it is confined by the Novate S-type granite and the Adula nappe (fig. 2.7) A metamorphic aureola was produced by the Gruf complex within the Chiavenna ophiolite (Schmutz, 1976). No contact aureola was produced either by Masino-Bregaglia in the Gruf Complex or by the Gruf Complex in the Masino-Bregaglia pluton.

The Gruf Complex predominantly consists of migmatitic quartzo–feldspathic orthogneisses, paragneisses and biotite–sillimanite–garnet–(±cordierite)-bearing metapelitic rocks. They register mid-Tertiary metamorphic conditions in upper amphibolites facies (Bucher-Nurminen and Droop, 1983). Migmatization mostly occurred contemporaneously with (or slightly post-dating) emplacement of the Bergell Pluton (Berger et al., 1996; Davidson et al., 1996). The Gruf Complex hosts granulites and charnockites (Galli et al., 2010) and other rock types like calcisilicates, marbles and amphibolites (Motiscka, 1970). The migmatitic, isoclinaly folded Gruf migmatite gneisses can probably be correlated with the zone of Bellinzona-Dascio (Bucher-Nurminen and Droop, 1983)

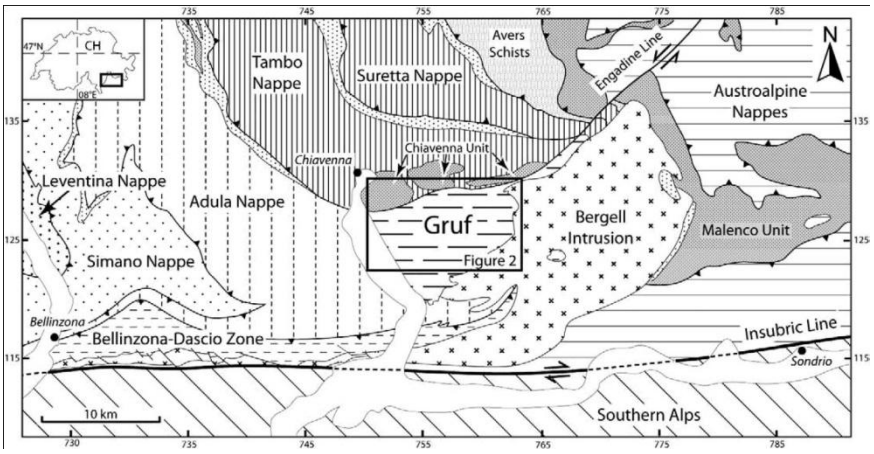

Fig. 2.7 Location of the Gruf complex at the western margin of Masino-Bregaglia intrusion. Redrawn after Bucher-Nurminen and Droop, (1983)

2.7 Thermal Lepontine Dome

The Lower and Subpennine units form a metamorphic dome, outlined by the regional metamorphic mineral zone boundaries, called Lepontine Dome (Trommsdorf, 1966; Wenk, 1970; Trommsdorf et al., 1974). Lepontine Dome is characterized by Alpine upper greenschist to amphibolite facies Barrovian type metamorphism of Oligocene to Miocene age (Frey et al., 1974) The term of Lepontine gneiss Dome region was coined by Wenk (1953) for the deepest part of the Alps and shows high grades of Tertiary metamorphism. Lepontine region extends from the Gotthard massif in the north, to the Insubric line in the south, the Simplon area in the west, to the Bergell area in the east (Fig. 2.8).

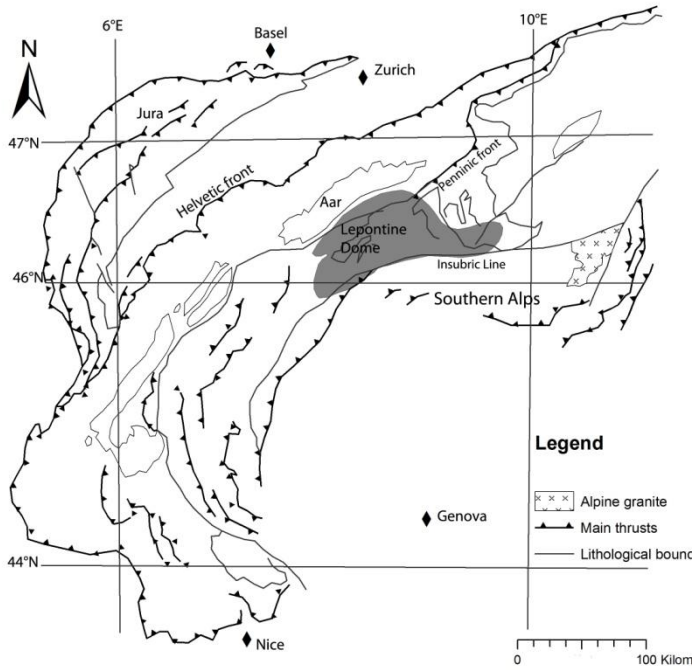

Fig. 2.8 Location of the Lepontine Dome. The amphibolites facies Isograd bounds the limit of the thermal Dome. Redrawn after Steck and Hunziker (1994).

Lepontine Dome is bordered to the north and south by elongate steep belts. The east-west striking Southern Steep Belt (SSB) is the location of back-folding and back-thrusting of the Alpine nappe stack to moderately dipping orientation into a subvertical and even overturned orientation during of late Oligocene/early Miocene (23-25 m.y.) (Heitzmann, 1987). The Northern Steep Belt (NSB) constitutes a second steep zone located some 50 km north of the SSB. It consists of Europe derived basement nappes and metasedimentary slices derived from the Valais Ocean (Frey, 1967; Probst, 1980; Steinmann, 1994) NSB is separated from SSB by a relatively flat-lying nappe stack, which we refer to as the Central Lepontine.

Todd and Engi (1997) calculated P-T thermobarometry and draw the maps of isograds in the Central Alps. The P-T maps reflect the maximum metamorphic conditions established in different times for different areas then the contour pattern of the maps represent a diachronous fields. These isograds maps are useful to trace different P-T areas but, due the orogenic belt exposes different vertical levels which reach their peak of metamorphism at different times, is not possible to define a single age for the thermal peak of metamorphism over large parts of the Alps were considered. Along the Lepontine Dome these isograds form an asymmetric dome exposed by uplift and exhumation of the deepest parts of the Alpine nappe pile. The temperature contour map shows the increase in temperature toward the south of the Dome, where the Insubric line truncates the contours map. Recorded temperatures are 525-550 °C along the northern and western limit of

amphibolite grade metamorphism and increase to 675°C to the south-central part of the field area (around Bellinzona) (Fig. 2.9) as it was already defined by Niggly et al. (1965). The pressure contour map shows pressures decreasing both to the north and the south. Maximum pressures measured are 6-7 kbar along the central axis, decreasing to 4.5 kbar to the south-east and to 5.5 kbar near the northern limit of amphibolite grade metamorphism (Fig. 2.9).

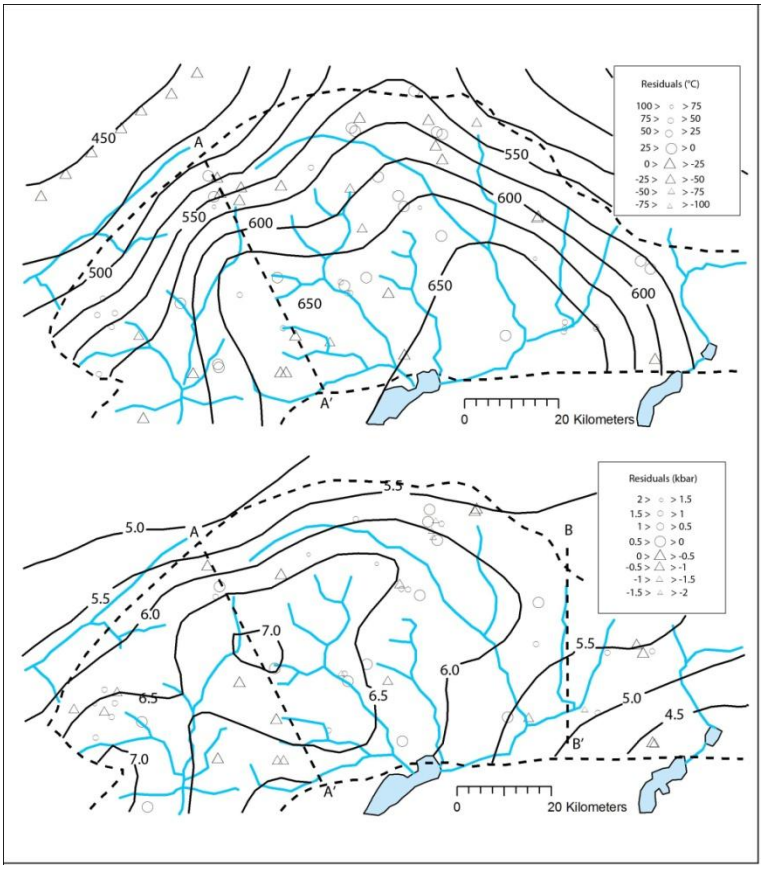

Fig. 2.9 Map of isotherms and isobars of Tertiary metamorphism Contours represent Tmax and Pmax at an elevation of 1000 mt above sea level. T and P are established on paragenetic metamorphic sequences at different times in different areas. Redrawn after Todd and Engi (1997)

Metamorphic grade increases from north to south reaching sillimanite grade near the Insubric Line. The nappe boundaries are discordantly cut by steeply inclined isograds (Fox, 1975) and the poliphasic regional metamorphism postdates nappe emplacement and nappe folding (Milnes, 1974), since isograds crosscut the respective tectonic boundaries (Trommsdorff, 1966; Niggli, 1970; Engi et al., 1995).

2.8 Migmatites of the Southern Steep Belt

The migmatite belt in the Lepontine area is hosted in the Southern Steep Belt within the pegmatite field. The Southern Steep Belt (SSB) consists of amphibolite-greenschist facies high strain zone with its boundary against the Southern Alps which truncates the southern border of Alpine high-grade metamorphic area. The SSB was strongly deformed under amphibolite facies conditions grading into the ductile mylonites (Handy et al., 2005).

Migmatites are basically simple rocks with two components. One partially melted called neosome which consists of the crystallized products from the melt. The second, called paleosome, consists of rock that did not melt. The neosome is composed of two petrologically different parts; one derived from the melt, called leucosome, and the other derived from residual solid material and dark coloured, called melanosome or residue (Sawyer 2008). All the components are most of the times deformed and strained resulting in a banded or layered appearance (Fig. 2.10).

Fig. 2.10 Layered migmatites in the Southern Steep Belt outcrop nearby Pizzo Paglia, Mesolcina valley, Bellinzona.

The main of rock types which form the SSB are two-feldspar orthogneiss and biotite-plagioclase gneiss. These gneisses are associated and interlayered with metapelites, calcareous schists, marbles, amphibolites retrogressed eclogite and metaperidotite (Wenk et al., 1974a).

In the northern portion of the Alps, the Southern Steep Belt is part of the folded units of the adjacent nappe pile, whereas in the center and the south it is characterized by a highly variable mix of rock types. In can be represented as a huge antiform, a back-folded root zone of steeply inclined north dipping Peninnic nappes (the Cressim antiform phase). From west toward east the Pennine units involved in migmatite process are Pioda di Crana, Antrona-Zermatt-Sass, Monte Rosa, Maggia, Simano, Leventina, Cima Lunga-Adula nappes (see Fig. 2.2). The Composite Lepontine serie include several mixed rock type-zones respectively named Bosco, Isorno, Moncucco, Orselina, Bellinzona-Dascio zone). It represents a melangé unit which include

large variable lithologies, like gneisses, metasediments, metabasics, ultrabasics and widespread occurrence of migmatites (Knoblauch et al., 1939; Burry et al., 2005).

Hänny et al., (1975) did geochronological studies to determine the time of migmatite formation in Bodengo valley, one of the best exposed area in the Central Alps for the study of migmatites. Migmatites and granitoid bodies from this area are Hercynian or older Variscan aged between 350-280 m.y. Romer et al., (1996) determined zircon U-Pb ages of banded migmatites gneiss at Lavertezzo (Verzasca valley, Switzerland) and aplitic leucosome veins at Corcapolo (Centovalli Line, Switzerland) which yielded Hercynian ages. These ages are in concordance with other migmatites in the Central and Eastern Alps (Köppel et al., 1980)

Burry et al., (2005) and Berger et al., (2008) evidenced that the Southern Steep Belt has high leucosome fraction but shows little evidence of hydrate-breakdown melting at the microscale. These authors studied reaction products of the metapelites forming Alpine migmatites during white mica-breakdown melting where sillimanite occurs as an incongruent melting product as follows:

$KAl_3Si_3O_{10}(OH)_2 + SiO_2 = KAlSi_3O_8 + Al_2SiO_5 + H_2O$

muscovite + quartz $_{(m)}$ = K-feldspar + aluminosilicate$_{(m)}$ + water

$(Mg,Fe)_3Al2Si_3O_{12} + KAlSi_3O_8 + H_2O = K(Mg,Fe)_3AlSi_3O_{10}(OH)_2 + Al_2SiO_5 + 2SiO_2$

garnet + orthoclase + water = biotite + aluminosilicate + quartz

They also observed the reactions of the type ms+bi+qz+feld→gt+bi+melt do occur with or without sillimanite formation. Alpine migmatites occur as grain-scale segregations or in the field as small coarse grained patches (Berzona and Lavertezzo, Centovalli Line, Switzerland), boudin-like and anastomized pools of leucosome (stromatic migmatites), elongate quartz-feldspar enriched pockets and veinlets parallel to the foliation. Leucosome segregations is diffuse and often they are rimmed by aggregates of black micas. Melting reaction products and the textural migmatite characters above mentioned have been only observed in the area of maximum Alpine metamorphic heating (around Bellinzona) and these characters disappear near Locarno to the west and toward Novate to the east. Outside this area, reaction products of muscovite dehydration melting (sillimanite + K-feldspar) are lacking or appear related to subsolidus processes rather than partial melting. Burry et al., (2005) suggest that the typically metamorphic reactions observed and the leucosome generation at the macro scale are indicative of Alpine age migmatization only around Bellinzona area (see Fig. 2.9).

Fluid sources and fluid production to generate migmatites were postulated by Berger et al., (2008) because the quantitiy of granitic melt in composition produced depends on the availability of H_2O. A potential source for fluids production was indicated by metapelite rocks. Pelitic rocks which contain a large amount of muscovite and biotite to produce melt, and the melt is granitic in composition, progressively above the temperature of the incongruent melting reactions involving these minerals at 700-800 °C. These authors assuming pressures between 0.75-0.8 Gpa and temperature below 650°C indicated that some 1.3 vol.% water could be produced from an average metapelite composition of Central Alps. They also indicated the hydrated metabasic rocks as second reliable source for acqueous fluids, which lose much of their chlorite at the

transition from greenschist to the amphibolite facies (Elmer et al., 2006). The amount of water that can be release due to the breakdown of chlorite is sensible, but the temperature estimated during Alpine aged migmatization at which metamorphic process occurred are relatively low. Indeed metagreywackes and metaandesites would begin to produce sensible percentages of melt between 750°C and 800 °C and the melting of amphibolites, to produce large volume of melt tonalitic in composition, may extensively occur at about 850°C.

Berger et al., (2008) concluded that metapelitic rocks incorporated into the SSB are not a realistic fluid source, because, at the conditions of partial melting, the released aqueous fluid is too low and it would only lead to in situ partial melting and no fluid would be released into the directly adjacent or overlying rocks to produce large batches of granitic magma. The most likely scenario, which take into consideration the most plausible thermal model for the Central Alps (see later on), is that fluids were primarily generated through dehydration of metapelites under amphibolite facies rocks which actually are deeply buried in the Southern Alps. Elsewhere such an influx of H_2O has been recognised as responsible for melting of metapelites and metamafic rocks in anatectic terranes (Ward et al., 2008). The fluid production would be caused by the effects of transpressional backthrusting of the Southern Steep Belt against colder Southern Alps. During later transpressional backthrusting this crustal segment was uplifted and exposed by localized deformation along the Insubric Line. Therefore, the migmatites of the SSB, are today at the present erosional surface, whereas the Tertiary amphibolite facies rocks of the Southern Alps remain deeply buried (Fig 2.11).

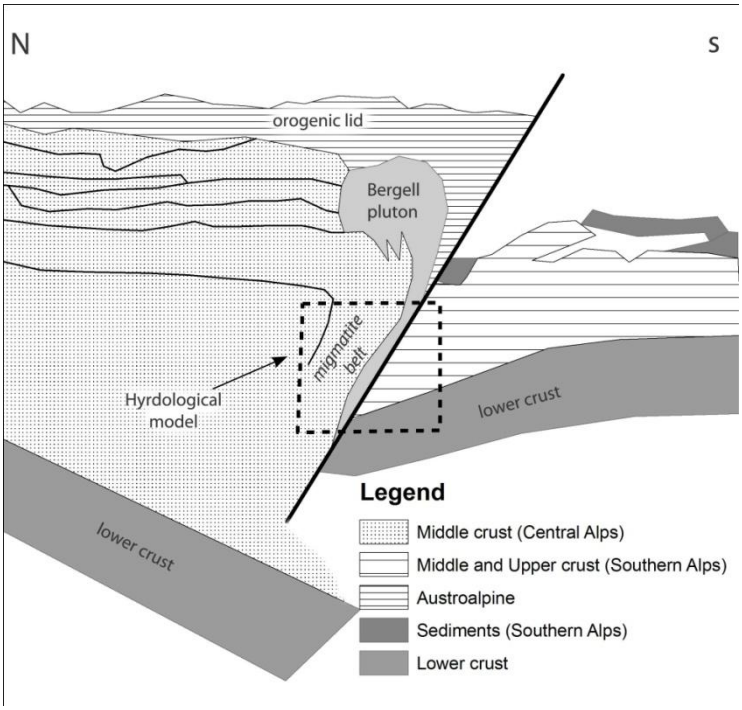

Fig. 2.11 Tectonic section of Central Alps at Oligocene. Box indicates partial melting of crust by influx of fluids from Southern Alps. Redrawn after Berger et al., (2008)

2.9 Heat advection in the Lepontine Dome

The peak metamorphic temperatures at amphibolite facies were reached in the SSB about 32 Ma (Hunziker et al., 1992; Gebauer, 1999). High temperature metamorphic conditions lasted from 35 to 25 Ma (Grujic and Mancktelow, 1996) even if Rb–Sr and Ar–Ar ages of 28 Ma in the Southern Belt already defined cooling stages (Engi et al., 1995). Fission track ages of detrital grains suggest that the core of the Lepontine became exposed at about 14 Ma (Spiegel et al., 2000) and cooling versus exhumation continued after then where, within the SSB, cooling below the ductile brittle transition is documented by numerous fission track ages (Grasemann and Mancktelow, 1993).

Todd and Engi (1997) have defined a tectonic model of the Lepontine area where the age determinations are consistent with two stages of metamorphism. The first thermal pulse created the peak thermal gradients still preserved in the northern part of the field area (Northern Steep Belt) about 35-38 m.y. during south-dipping subduction of European plate. The second thermal pulse occurred at 32 m.y. under lower pressure conditions and affected only the south-eastern part of the field area during the obduction of Adula-Cima Lunga nappes and Masino-Bregaglia pluton. During this stage was reached the amphibolite facies metamorphism in the Southern Steep Belt as the result of the pulse of heat during the obduction of Adula-Cima Lunga nappes and the magmatic bodies along the exhumation shear zone of the Insubric line.

The subduction-obduction processes along the Alpine chain produced substantial heat in the lower-upper crust transition. Thermochemical models applied to the Lepontine Dome in the Central Alps yielded by various authors (Fig. 2.12) explained the heat production with different mechanisms. The models include radioactive heating, shear heating, crustal thickness (England and Thompson, 1984; Bousquet et al., 1997). All these thermal modelling indicate that spatially condensed isotherms developed in the upper and middle crust and that overturned isotherms may have persisted in the lower crust and the mantle over prolonged periods (Roselle et al., 2002; Gerya et al., 2002; Goffé et al., 2003; Burg and Gerya, 2005). These models have in common that the significant source for heating is the "*decollement*" situated in the upper-lower crust limit. For example Berger et al., (2008) defined fluid production and melting in the continental crust along Lepontine Dome occurred during backthrusting, long after the main stage of subduction was over. A likely cause for water-assisted melting would be the development of inverted isotherms which caused partial melting in the thickened crust.

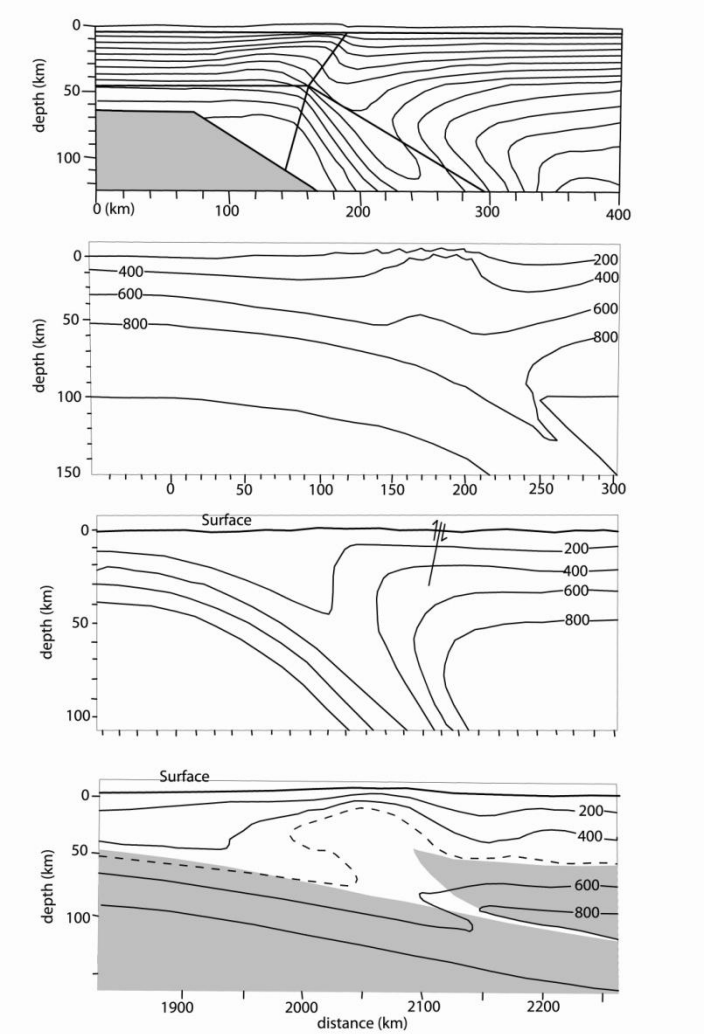

Fig. 2.12 Compilation of some published thermal models
The mantle is indicated in grey. Redrawn after several authors.

CHAPTER 3

Pegmatites of Central Alps

3.1 Preview

When I illustrated to my tutors the project of studying the pegmatite field located in the Central Alps I did not have yet realized how big the area was and how many pegmatite dikes outcrop. The area between Domodossola and the Masino-Bregaglia Oligocene intrusion hosts may be thousands aplite and pegmatite and dikes and extends for more than 90 kilometers from west toward east. First approach to the study was to begin mapping as many as possible pegmatites outcrops in the Vigezzo valley, Mesolcina valley and within the Masino-Bregaglia pluton. I tried to apply a criteria to group these pegmatites using structural field data such as strike, dip, thickness of the dikes, textural characters and mineralogical contents of the pegmatites. 95 % (or more) of the pegmatites outcropping in the Central Alps can be described as barren, mostly of these have aplitic textures, being composed of simply K-feldspar and subordinate quartz + muscovite. Only few dykes show a more complex mineralogy. As it will be discussed pegmatites from Central Alps never reach a high grade of geochemical fractionation, and mostly belong to the muscovite class as proposed by Černý and Ercit (2005). The paucity of REE enriched Alpine pegmatites may be ascribed to a combination of insufficient amounts of F, Li, B in the parental granite magmas which prevented extensive fractionation from the granitic source.

After a preliminary mapping of 80-90 dykes, It was decided to select pegmatites which showed peculiar mineralogical and textural characters. The selection was made using rare mineral accessory phases occurring in pegmatites at Vigezzo valley, Mesolcina valley and Masino-Bregaglia area. The help of local mineral collectors was also useful to localize pegmatites dykes in quite remote areas, in particular Mesolcina valley and Codera valley. Once selected the most mineralogical interesting pegmatites an additional choice was made to limit the number of dikes to study. Pegmatites bearing complex mineralogy including Sn-Nb-Ta-Y-RE-U oxides, Y-REE phosphates, Mn-Fe-phosphates, Ti-Zr-silicates, Be-Y-REE-silicates, almandine-spessartine garnets, and schorl-dravite-elbaite tourmalines were those selected for this study. The area was then divided into three zones for saving as much time as possible when the collection of data and samples in the field started. This subdivision resulted crucial for the studies because these areas, as it will see, include pegmatite with different textural, structural and geochemical characters. The first area selected extends from the village of Domodossola (Ossola valley) toward east along the Vigezzo valley where six pegmatite dikes were studied. The second area is localized in Mesolcina and Bodengo valley, include three pegmatite dikes. The third area is localized in the Codera valley, in the earth of the Masino-Bregaglia massif, where two more pegmatite dikes were studied. All the samples and pegmatites studied are respectively signed as follows (see Table 3.1 for comparison): [F] for Grignaschi quarry; [C] for Rio Graia dike; [D] for Arvogno Fluorite dike; [E] for Arvogno Albertini dike; [H] for Emerald Pizzo Marcio dike; [L] for Alpe Rosso and Summit of Pizzo

Marcio dikes; [P] for Summit of Pizzo Paglia dike; [R] for Colonnello Pizzo Paglia dike; [W] for Bodengo Road Cut dike; [A] for Garnet Codera Valley dike (A); [B] for Phosphate Codera Valley dike.

Table 3.1 Location and field characters of the pegmatite dikes studied

Sigle	Locality	Coordinates	Altitude	Strike	Dip, dip angle
F	Grignaschi quarry, Domodossola village, Ossola valley, Verbania, Italy	lat. 46° 6' 28.56"N long.8°18' 54.07"E	260 mt	N 210°-220°	N120 20°-30°
C	Rio Graia dike, Trontano village (Vigezzo valley, Verbania, Italy)	lat. 46° 7 '2.08"N long.8°20' 58.42"E	695 mt	N 210°-220°	Vertical
D	Arvogno fluorite dike, Toceno village, Crana valley, Vigezzo valley, Verbania, Piedmont, Italy	lat. 46° 9' 41.74"N long.8°27' 11.72"E	1000 mt	N330°-340°	Vertical
E	Arvogno Albertini dike, Toceno village, Crana valley, Vigezzo valley, Verbania, Piedmont, Italy	lat. 46° 9' 37.46"N long.8°27' 26.41"E	1050 mt	N250°-260°	Vertical
H	Emerald Pizzo Marcio dike, Druogno village, Vigezzo valley, Verbania, Piedmont, Italy	lat. 46° 6' 14.96"N long.8°23' 32.73"E	1790 mt	N260°-270°	N180° 75°-80°
L	Summit of Pizzo Marcio, Druogno village, Vigezzo valley, Verbania, , Piedmont, Italy	lat. 46° 6' 4.23"N long.8°23' 25.37"E	1920 mt	N250°-260°	N160° 70°-75°
P	Summit of Pizzo Paglia, Leggia village, Leggia valley, Mesolcina valley, Bellinzona, Grigioni, Switzerland	lat 46° 13' 58.55"N, long.9° 13' 1.58"E	2385 mt	N280°	Vertical
R	Colonnello dike, Pizzo Paglia, Leggia village , Leggia valley, Mesolcina valley, Bellinzona, Grigioni, Switzerland	lat 46° 14' 15.67"N long.9° 12' 57.50"E	2160 mt	N340°	N250° 80°
W	Bodengo road cut, Gordona village, Bodengo valley, Chiavenna valley, Sondrio, Lombardy, Italy	lat. 46° 16' 39.19"N long. 9° 20' 29.99"E	950 mt	N320°	Vertical
B	Garnet dike, Pedroni dal Pra, Codera valley, Novate Mezzola village, Sondrio, Lombardy, Italy	lat. 46° 17' 49.21" N long. 9° 34' 9.17" E	2740 mt	N240°-250°	Vertical
A	Phosphate dike, Pedroni dal Pra, Codera valley, Novate Mezzola village, Sondrio, Lombardy, Italy	lat. 46° 17' 45.52" N long. 9° 34' 9.13" E	2730 mt	N240°-250°	Vertical

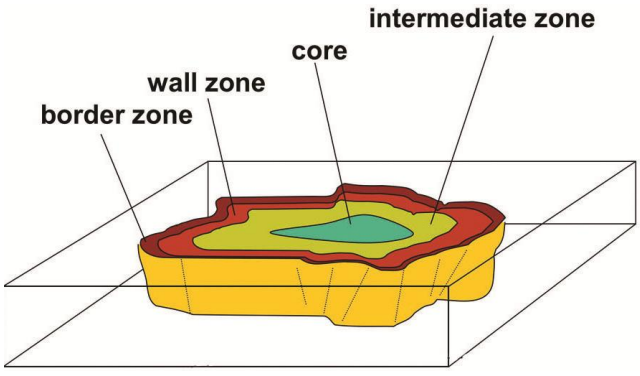

Fig. 3.1 Schematic section of a typical zoned pegmatite dike.
Redrawn after London (2008)

3.2.1 Grignaschi quarry dike (F)

This pegmatite was exposed during quarries activities for the exploitation of orthogneiss rocks. Fine grained two-mica granitic orthogneiss, which hosts the dike, belongs to the Camughera-Moncucco Lepontine series, structurally related to the Vanzone Antiform (Steck and Hunziker, 1994). Rb/Sr whole rock analysis of the orthogneiss gave an age of 271.5±5 m.y as determined by Bigioggero et al., (1981).

The Grignaschi pegmatite extends for 20 mt at the base of the wall of the quarry and reaches up to 0.5 meters in width. The pegmatite cross-cut the orthogneiss with straight parallel contacts. It has fine-grained (centimetric) border-wall zone composed of K-feldspar, albite, muscovite mica and colorless quartz. The intermediate zone (see Fig. 3.1) is medium-grained (pluricentimetric), composed of white perthite K-feldspar, albite, flakes of silvery mica and thin layers of red almandine-spessartine garnet, which form millimetric trapezohedral crystals. This portion of the pegmatite hosts accessory minerals like black schorl tourmaline prismatic crystals, up to several centimetres in length, sky-blue opaque or gemmy aquamarine prismatic hexagonal beryl crystals, up to few centimeters (Lincio, 1905; Cantadore et al., 1967). The intermediate-core of the dike is medium-grained (pluricentimetric) and composed of graphic quartz+K-feldspar intergrowth and colorless to smoky quartz masses. The dike contains a number of uncommon minerals like bavenite, columbite-tantalite-Fe, iron-sulphides, microlite, monazite-(Ce), secondary uranium phosphates, tapiolite-Fe, uraninite and zircon (De Michele, 1967).

3.2.2 Rio Graia dike (C)

The pegmatitic dike of Rio Graia was mined by mineral collectors since the early ’70 of the last century for sky blue opaque beryl crystals, they occur as well shaped euhedral hexagonal prisms up to several centimeters in length. The dike is hosted by fine-grained two mica granitic-orthogneiss with flaser K-feldspars of the Camughera-Moncucco serie (Steck and Hunziker, 1994) (Fig. 3.7). The pegmatite outcrops for 10 meters and reaches up to 8-10 meters in width; is concordant with the orthogneiss foliation and has straight contacts. The strike of the pegmatite follows the direction of the fold axis of the Vanzone Antiform (Fig. 3.2). The texture of the pegmatite is characterized by border-wall zone composed of medium-grained (pluricentimetric) white K-feldspar, silvery muscovite mica, albite and vitreous to milky quartz. The border-wall zone has muscovite enrichments and layers of millimetric up to centimetric trapezohedral crystal of red almandine-spessartine garnet. The intermedite-core zone is composed of very coarse grained (pluridecimetric up to metric) perthite K-feldspar, flakes of silvery muscovite, albite, biotite (rare), and large colorless or brownish quartz masses. In this portion of the pegmatite masses of fine-grained lamellar crystals of silvery muscovite are widespread. Tourmaline is virtually absent or very rarely was observed as black schorl in the intermediate zone of the dike. The core zone has 3-4 meters in thickness and is composed of pluridecimetric euhedral white perthitic K-feldspar crystals embedded into masses of vitreous-brownish quartz (Fig. 3.3). The pegmatite contains several uncommon minerals like bavenite, columbite-tantalite-Fe, fersmite (Vanini

and Callegari, 2002), iron-sulphides, microlite, monazite-(Ce), secondary uranium phosphates, tapiolite-Fe (Fig. 3.4), uraninite, and zircon (Mattioli, 1976; Piccoli et al., 2007).

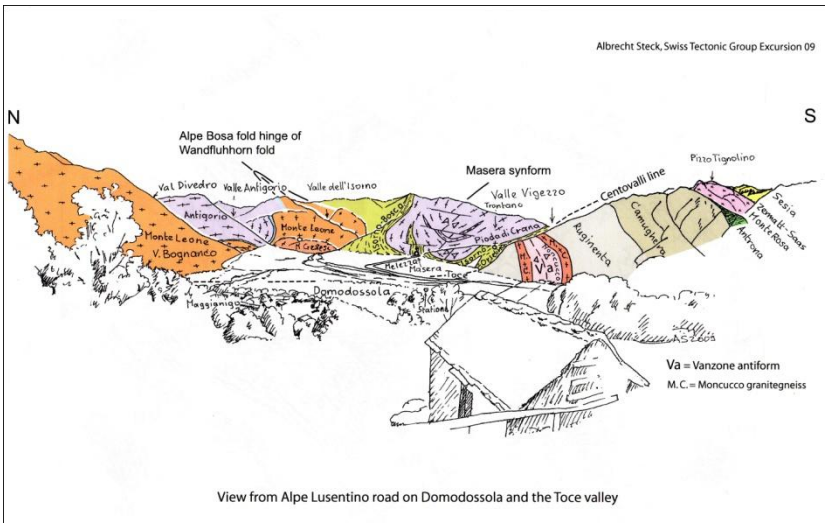

Fig 3.2 Grignaschi and Rio Graia dikes are hosted within orthogneiss of the Camughera-Moncucco series which form part of the Vanzone Antiform. (From Steck, 2009)

Fig. 3.3 Core zone of the Rio Graia pegmatite. Large crystals of K-feldspar and quartz masses are visible.

Fig. 3.4 Tapiolite-(Fe), group of polysynthetic cyclic twins up to 1.5 centimeters from Rio Graia dike.

3.2.3 Arvogno Fluorite dike (D)

Arvogno pegmatite was discovered in the early ’80 of the last century and mined by mineral collectors for a number of uncommon and rare REE-Nb-Ta oxides, phosphates, and silicates minerals. This dike is hosted and cross-cut the two mica medium-grained orthogneiss which belongs to the Pioda di Crana Lepontine nappe (Bigioggero et al., 1981). The pegmatite outcrops in the Melezzo river for about 20 meters in length,

up to 1 meter in width and has straight contacts (Fig. 3.5). It is pervaded by set of rigid fractures oblique respect the orthogneiss foliation developed from the hosting rock throughout the pegmatite. Pegmatite texture consists of border-wall fine and medium-grained zone (centimetric to pluricentimetric) composed of perthite K-feldspar, flakes of silvery green muscovite, biotite, albite, and quartz. Black millimetric to centimetric nodules with conchoidal fracture of aeschynite-polycrase-(Y) group minerals and occasionally magnetite grains are widespread in this portion of the dike. The core zone is coarse-grained (decimetric) and composed of white perthite K-feldspar, brownish-smoky vitreous quartz and lamellar albite, cleavelandite variety. This portion contains several accessory minerals like granular centimetric masses of orange yttrian-spessartine garnet and centimetric masses of green yttrian-fluorite. The core hosts aeschynite-(Y)-polycrase-(Y) group minerals, allanite-(Y), bismutinite, monazite-(Ce), titanite, uraninite, xenotime-(Y), zircon as well. Secondary cavities in the core zone, formed after the fluorite dissolution, are lined with albite, allanite-(Ce), bavenite microlite, milarite, and rarely gadolinite-(Y). The pegmatite contains rare galena nodules associated with wulfenite (Mattioli, 1986).

Fig. 3.5 Arvogno Fluorite pegmatite with zoned portions of the dike are clearly visible.

3.2.4 Arvogno Albertini dike (E)

Albertini pegmatite (in honour of the discoverer, Albertini Claudio a renowned mineral collector) was cultivated by mineral collectors since the early ’80 of the last century for the findings of REE-Nb-Ta oxides, phosphates, and silicates minerals. The dike cross-cut the two mica medium-grained orthogneiss of the Pioda di Crana Lepontine nappe. It outcrops for 4-5 meters and has 3-4 meters in thickness. The dike has coarse-grained (decimetric) border-wall zone composed of white K-feldspar, albite, brown quartz with rare accessory minerals which include allanite-(Y), bismutinite, magnetite, yttrian-spessartine and thorian-monazite-(Ce) nodules (Fig. 3.6) (Albertini and Andersen, 1989). The contact of the pegmatite with the orthogneiss shows a lobate structure. The border zone in upper portion (upper end) of the dike hosts secondary cavities formed by the dissolution of yttrian-fluorite lined with albite, aeschynite-(Y)-polycrase-(Y), gadolinite-(Y), xenotime-(Y) allanite-(Ce), titanite, yttrian-fluoroapatite and zircon. The core zone is very coarse grained (pluridecimetric) and is composed of euhedral pinkish to whitish perthite K-feldspars, brownish to colorless large masses of quartz and platy centimetric crystals of biotite.

Fig. 3.6 Centimetric brownish nodules of monazite-(Ce) from Arvogno Albertini pegmatite.

3.2.5 Emerald Pizzo Marcio (H), Alpe Rosso and Summit of Pizzo Marcio dikes (L)

The pegmatites located nearby Pizzo Marcio and Alpe Rosso area include four-five albitized dike renowned since the early ’70 of the last century for the findings of rare accessory minerals and of collection specimens with green, Cr-rich, beryl crystals (emeralds). Emerald crystals that can be faceted as gems of up to one carat were found (Fig. 3.11), in particular at the Emerald Pizzo Marcio pegmatite (Mattioli et al., 1995). Two new minerals, roggianite (Passaglia 1969) and vigezzite (Fig. 3.9) (Graeser et al. 1979), were also first described. These pegmatites are hosted in metaperidotite and serpentine schists of the Antrona-Zermatt Sass ophiolitic nappe (Fig. 3.8), are characterized by replacement processes producing total albitization and metasomatic reactions along the exocontacts with the formation of phlogopite + talc + tremolite.

The Emerald Pizzo Marcio dike (Fig. 3.7) outcrops for about 60 meters. It shows a pinch and-swell structure and reaches up to 2.5 m in width. Along the talus, below the dike, the presence of large boulders of pegmatite indicates that the pegmatite body was significantly eroded. The pegmatite forms along the exocontacts as a green-grey, decimetric, sheared micaceous unit composed by phlogopite + talc + tremolite, in some cases embedding emerald crystals of gem quality. The sheared micaceous unit also embeds large boudins of albitized pegmatite. Several sets of fractures, up to few millimeters wide, cross-cut the mass of albitized pegmatite. These fractures are locally lined by radiating green aggregates of tremolite, greenish sheets of phlogopite + talc and prismatic crystals of brownish black tourmaline (dravite80–schorl20). Most of the pegmatite body is composed of the albitized unit, characterized by massive albite (Ab90–95) with a fine- to medium-grained texture containing centimetric, pale green, milky beryl crystals up to several centimeters in length. This unit locally contains abundant millimetric secondary cavities lined with albite and minor acicular crystals of tremolite with a Mg/(Mg +Fe_{tot}) value between 0.85 and 0.90. Oxides of Nb–Ta, mainly columbite–tantalite and microlite, occur in the secondary cavities of the albitized unit or embedded in the massive albite, associated with beryllium silicates such as bavenite, bityite, meliphanite, roggianite and abundant zeolites, including chabazite-Ca, gismondine, phillipsite-Ca, stilbite-Ca and thomsonite. The core of the pegmatite was left unaffected by the albitization processes. Coarse-grained, blocky, white perthitic K-feldspar, large blades of muscovite and K-feldspar with quartz in graphic textures are here preserved, in addition to accessory phases such as prismatic crystals of pale blue beryl, occasionally covered by crystals of bavenite, prisms of schorl, corroded spessartine and tiny platy columbite-(Mn).

Alpe Rosso dike was exploited in the postwar period for sodic feldspar. During the mining activity, crystals of milky beryl, pale green in colour, were occasionally found (Roggiani 1966). The mining activity produced a trench some tens of meters in length and a few meters in width. The exocontacts of the pegmatite are preserved, and they consist of a green-grey, decimetric, sheared micaceous unit. The pegmatite dike is completely albitized. Millimetric secondary cavities, lined with albite and abundant acicular tremolite, or embedded in the massive albite, host oxides of Nb–Ta such as fersmite (Fig. 3.10), vigezzite, microlite, U-rich microlite and occasionally tapiolite-(Fe) and ferrowodginite. Beryllium silicates include bavenite, meliphanite, milarite, roggianite, and the zeolites chabazite-Ca, gismondine, phillipsite-Ca and thomsonite.

The Summit of Pizzo Marcio dike outcrops for about 40 meters and reaches up to 1.5 meters in thickness. The pegmatite is totally transformed to a medium-grained albitized unit, and it shows centimetric exocontacts composed of a greenish micaceous unit. Millimetric sporadic secondary cavities in the albitized unit are lined with albite crystals and host oxides of Nb–Ta, mainly columbite–tantalite-Mn, and Be-silicates like bertrandite. Crystals of greenish beryl are rare; accessory phases like allanite-(Ce), cheralite-(Ce), niobian titanite, spessartine, and zircon were also very rarely observed. Other oxides of Nb–Ta such as fersmite and vigezzite were not observed in this dike.

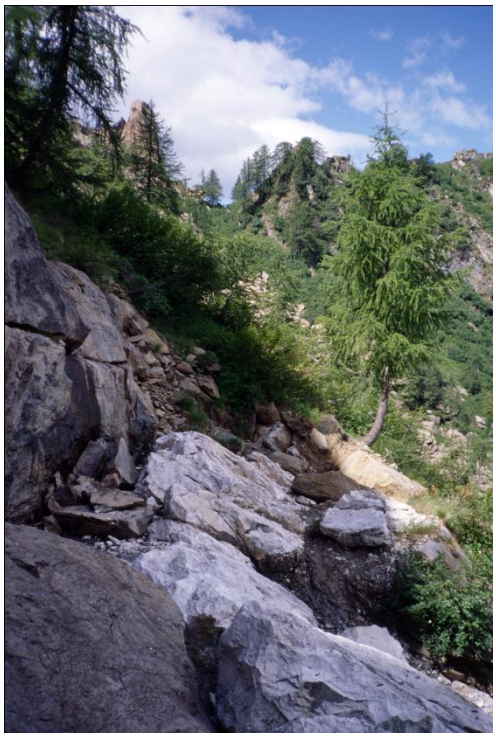

Fig. 3.7 The Emerald Pizzo Marcio albitized pegmatite dike on summer 2009.

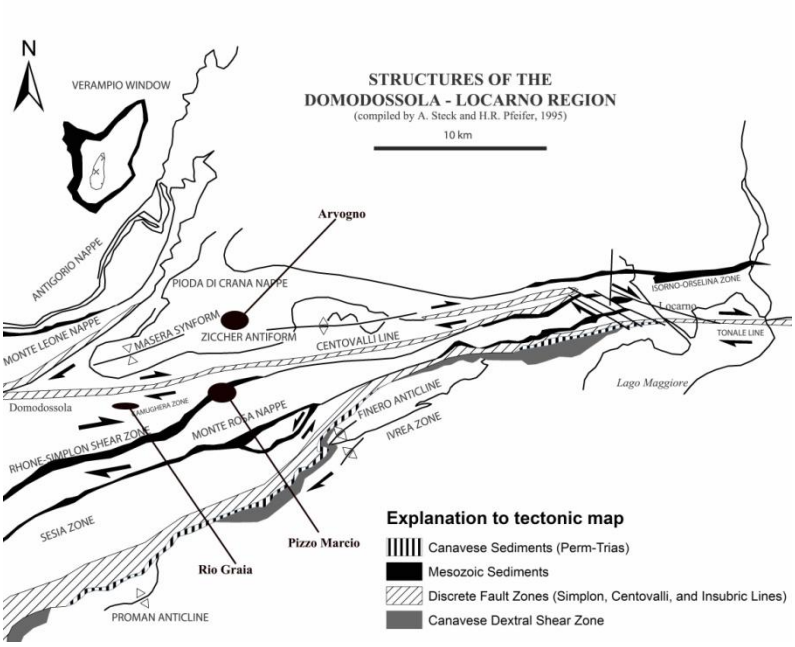

Fig. 3.8 Geological and structural sketch of Domodossola-Locarno area where Rio Graia, Arvogno and Pizzo Marcio-Alpe Rosso pegmatites are hosted. Redrawn after Steck and Pfeifer (1995)

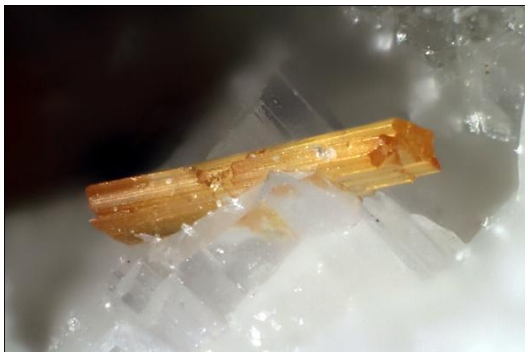

Fig. 3.9 Vigezzite, prismatic crystal of 3 millimeters from Alpe Rosso albitized dike

Fig. 3.10 Fersmite, group of crystals up to 4 millimeters from Alpe Rosso albitized dike

Fig. 3.11 Beryl var. emerald crystal and faceted gemstones up to 1.5 carats collected at the Emerald Pizzo Marcio dike.

3.2.6 Summit of Pizzo Paglia dike (P)

This pegmatite was discovered on summer 2009 during a geological field excursion. The pegmatite is both hosted in amphibolite rocks and migmatite gneiss of the Bellinzona-Dascio zone in the Southern Steep Belt area (Fig. 3.13). The dike outcrops for 20 mt and reaches up to 3-4 meters in thickness. The lower portion (lower end) of the dike is concordant with the foliation of leucocratic migmatite gneiss. Here the pegmatite reaches the maximum width (3-4 meters) due the coalescence with a lateral pegmatite dike. The border-wall zone of the pegmatite is coarse-grained (up to decimetric) composed of idiomorphic white perthite K-feldspar, albite, large aggregates of silvery muscovite mica and subordinate brownish-vitreous quartz masses. The core zone has giant texture (up to metric) composed of huge euhedral white perthite K-feldspars (Fig. 3.12) projecting into large masses of brownish to smoky vitreous quartz. In the intermediate-core zone of the pegmatite large euhedral centimetric crystal of red almandine-spessartine crystal with trapezohedral habit occur. They are associated with prisms of idiomorphic black prism schorl and, sky-blue to greenish, vitreous centimetric hexagonal prisms of beryl and greysh millimetric zircon. In the upper portion (upper end), the pegmatites is hosted by black amphibolite rock, it narrows and has one meter in width. In this section the coarse-grained (centimetric) texture is characterized by white perthite K-feldspar, albite, quartz. Centimetric primary miarolitic cavities lined with albite, K-feldspar, quartz and acicular prisms of black schorl also

occur. This portion of the pegmatite hosts black centimetric prisms of schorlite which diffuse along the exocontacts and permeate the amphibolite.

Fig. 3.12 Giant idiomorphic K-feldspars crystals in the core zone at the Summit Pizzo Paglia dike.

3.2.7 Colonnello Pizzo Paglia dike (R)

This pegmatite was also discovered on 2009. The pegmatite is discordant, hosted in the migmatite gneiss of the Southern Steep Belt (Fig. 3.13). The dike outcrops for 15 meters, reaches up 1.5 meters in width. The footwall of the dike has fine-grained layering border zone composed of K-feldspar, albite, quartz and muscovite (Webber et al., 1997). The wall zone is composed of medium-grained (centimetric) white perthite K-feldspar, albite, flakes of silvery muscovite and quartz. The intermediate zone has medium to coarse-grained texture (pluricentimetric) composed of graphic quartz+K-feldspar, albite, muscovite, red millimetric almandine-spessartine garnets, centimetric prisms of pale blue beryls and graphic black schorl (Fig. 3.15). The core zone of the pegmatite develops miarolitic pockets. This zone developed a large pocket (1meter in length x 60 centimeters in width and 50 centimeters in depth) (Fig. 3.14) where occurred brownish-smoky quartz crystals, also with scepter terminations, up to 15 centimeters in length, beryl aquamarine up to 9 x 4 x 4 centimeters, pluridecimetric idiomorphic white perthite K-feldspars, albite var. clevelandite as laminar centimetric crystals, rare black schorl prism up to 5-6 centimeters and lithiowodginite crystals up to 1.6

centimeters in length. The roofwall of the pegmatite is composed of medium-coarse grained K-feldspar, albite quartz and abundant flakes of muscovite.

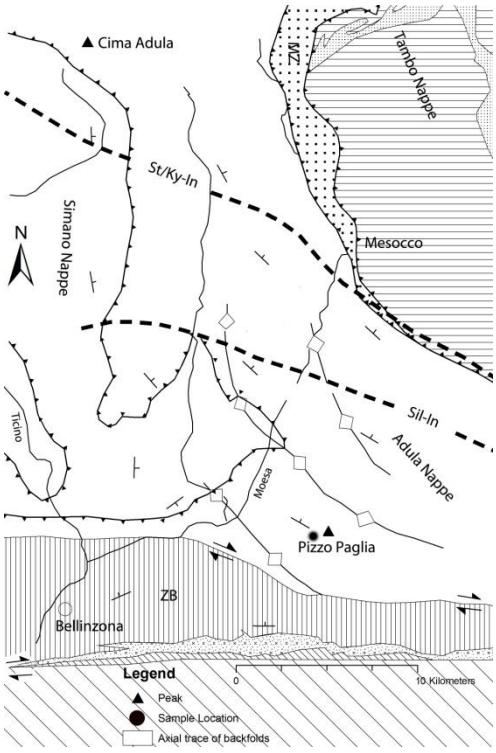

Fig. 3.13 Location of the Summit Pizzo Paglia and Colonnello pegmatite dikes. Redrawn after Nagel et al. (2002)

Fig. 3.14 Large pocket cavity in the core portion of the Colonnello pegmatite dike.

Fig. 3.15 Graphic schorl in the intermediate portion of the Colonnello pegmatite dike.

3.2.8 Bodengo Road Cut dike (W)

This small dike outcrops on the wall of the Bodengo valley road-cut. It is hosted in the contact margins between the Melirolo augengneiss and the Southern Iorio 58onalities. It is fine-grained aplite-pegmatite, discordant with the host rocks, outcrops for 10 meters and has 30-40 centimetrs in thickness. It is composed of predominat white K-feldspar, subordinate muscovite, red millimetric almandine-spessartine garnets and quartz.

3.2.9 Garnet Codera Valley dike (A)

This pegmatite belongs to swarms of pegmatite dikes outcrop along the ancient-glacial circle located in the upper Codera valley (Ghizzoni and Mazzoleni, 2005). A number of these dikes were exploited since the ’60 by mineral collectors for beautiful beryl gem quality aquamarine, weel formed idiomorphic trapezohedral red garnet crystals and black schorl prisms. The Garnet dike was heavily dig out by local collectors for garnet and aquamarine crystals. It outcrops for 30 meters and reaches up 3 meters in width in the lower portion (lower end) where coalesce with a lateral aplite-pegmatite dike. In the upper portion (upper end) it narrows and disappear within the enclosing rocks. The pegmatite is discordant, shows boudin and lobate structures along its contacts. It intrudes both the granodiorite and the tonalite of the Masino-Bregaglia pluton that here exhibit strong oriented foliation affected by synmagmatic ductile deformations (Rosenberg et al., 1994). The dike shows symmetric texture with the border zone composed of medium-grained (pluricentimetric) white K-feldspar quartz and biotite flakes which developed comb textures. Along the exocontacts pegmatite-granodiorite shear planes are also visible. The wall-intermediate zone is mainly composed of K-feldpars and graphic quartz+K-feldspar textures are locally predominant. In this portion layers of millimetric trapezohedral red almandine-spessartine garnets develop, granular black magnetite are also present. The core zone is composed of coarse-grained (pluridecimetric) smoky vitreous quartz and perthite white K-feldspar decimetric crystals (Fig. 3.16). Both these minerals are elongated along the strike of the dike due to the effect of intense ductile deformations occurred during the cooling of the dike. In the core zone accessory minerals like beryl aquamarine and red garnets crystals are not uncommon. In the border-wall zone of the dike a number of Nb-Ta and REE-U bearing minerals were described (Ghizzoni and Mazzoleni, 2005) and they include columbite-(Fe), euxenite-(Y), uraninite, monazite-(Ce), zircon (Guastoni unpublished data, 2012).

Fig. 3.16 Core zone of the Garnet Codera dike composed of elongated smoky quartz masses and white crystals of K-feldspar.

3.2.10 Phosphate Codera Valley dike (B)

The pegmatite outcrops about hundred meters east from the Garnet dike and is characterized by complex geometry and texture (Fig. 3.17). Texture and its relative complex mineralogy are index of higher geochemical fractionation respect all the other pegmatites studied so far. The Phosphate dike outcrops for 30 meters and reaches up 3 meters in width in the lower portion (lower end). Along the contacts it develops boudin and lobate structures. The pegmatite cuts discordantly the tonalite host rock which shows strong ductile pervasive foliation marked by intensively solid-state deformation. The structure of the pegmatite is complex by the abrupt change in mineralogy and grain size. It is possible to distinguish a border zone of 30 centimeters in width composed of medium grained (pluricentimetric) albite and quartz with saccarhoidal texture. This portion of the pegmatite contains Mn-rich dark green-yellow fluorelbaite with black schorl core crystals (Fig. 3.18), end-member F-rich triplite which forms black centimetric masses associated with Mn hydroxides (Vignola et al., 2012), and colorless to pale pink hexagonal prisms of beryl. The wall zone is medium-coarse grained (pluricentimetric) and consists of graphic quartz+K-feldspar, albite, subordinate quartz, black schorl and red to orange spessartine-almandine garnets with graphic textures, masses of triplite and colorless to pale pink beryl crystals. The intermediate zone is medium-coarse grained (up to decimetric) and prevail large flakes of silvery muscovite, laminar crystals of biotite, white, yellowish and pale green perthite Cr-rich K-feldspar, colourless to brownish quartz and development of graphic quartz+K-feldspar texture. The upper portion of the dike (upper end) develops elongated fine-grained bands composed of graphic quartz+K-feldspar associated with muscovite flakes bordered by coarse-grained zone (pluridecimetric) composed of K-feldspar, albite, quartz and muscovite flakes. These latter coarse grained zone is probably related to the coalescence with a lateral pegmatite dike.

Fig. 3.17 Border and wall zone of the Phosphate Codera pegmatite

Fig. 3.18 Mn-rich dark green fluorelbaite of the Phosphate Codera pegmatite

3.3 Pegmatite microstructures in thin sections

3.3.1 Grignaschi quarry dike

(F2) This section shows the contact between two-mica orthogneiss and border zone of the pegmatite. K-feldspars develop comb textures with crystals elongated and oriented perpendicular to the contact. The contact is also marked by large flakes of muscovite.

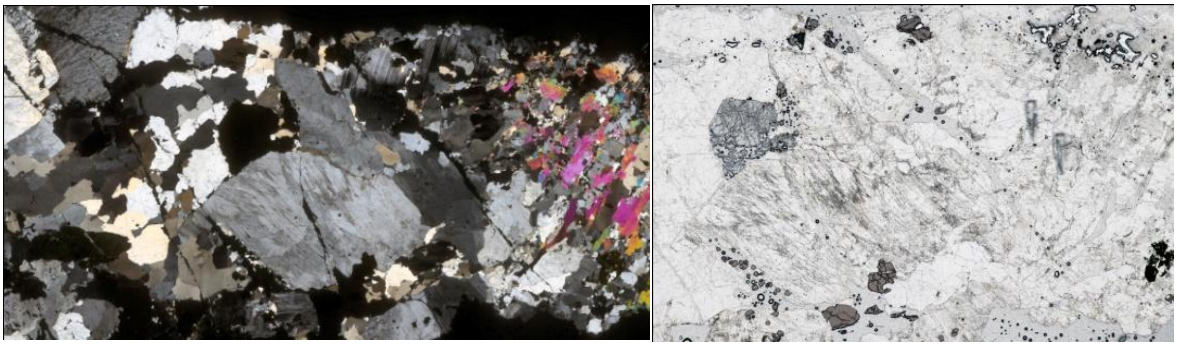

(F3) Intermediate zone of the pegmatite with large perthitic K-feldspars, polysynthetic plagioclase and polycrystalline quartz. At one nicol tourmaline crystals, green-brownish in colour, appears deeply fractured, red-brown garnets with intergranular quartz develop sets of oriented fractured around and within large K-feldspars and plagioclase.

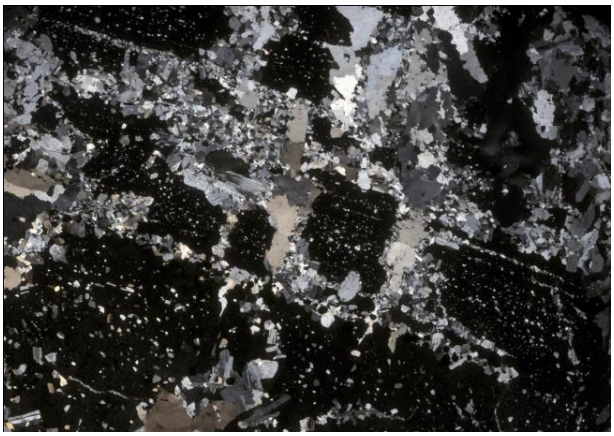

(F4) Large microcline crystal with pecilitic plagioclase lined and cut by two sets of fractures. One set is parallel to the elongated microcline composed of fine-grained plagioclase, layers of garnet and fine-granular interstitial quartz. The second set of fractures cut the microcline and is composed of large granular quartz and finer plagioclase to rim the quartz.

3.3.2 Rio Graia dike

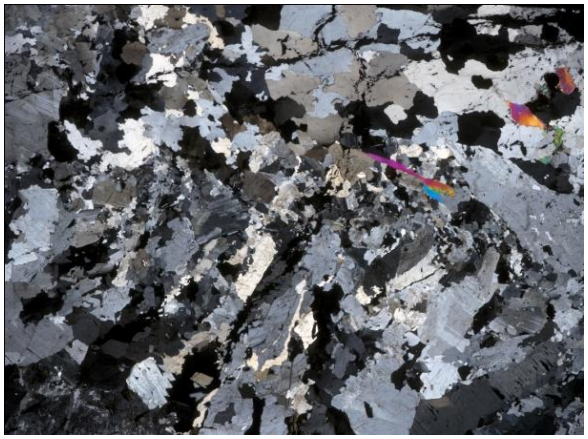

(C2) Border-wall zone of the pegmatite shows K-feldspars which develop comb texture. K-feldspars have skeletal habit which radiate from polycrystalline quartz inward the pegmatite. Rare garnets and muscovite are also observable within quartz.

(C5) Perthitic K-feldspar in the core zone of the dike. Perthitic albite shows anastomized structure

3.3.3 Arvogno fluorite dike

(D1) Contact between two mica orthogneiss and border zone of the pegmatite. An equigranular development of K-feldspar and quartz with subordinate polysynthetic plagioclase are observable.

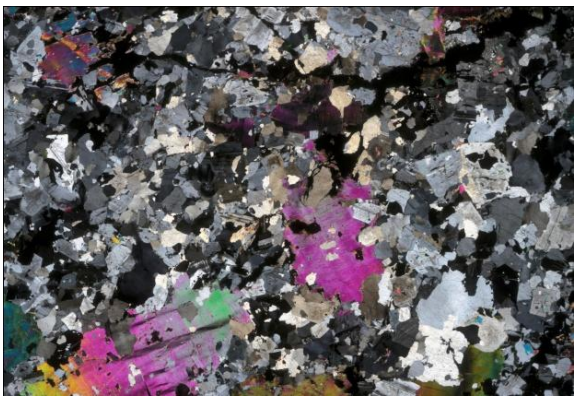

(D6) The border-wall zone of the pegmatite shows fine-grained equigranular K-feldspar, albite, quartz, large flakes of muscovite and minor plagioclase.

(D4) Perthite K-feldspar in the core zone of the dike. Albite perthite shows lobate and anastomized structures; a late stage generation of albite cleavelandite fills a set of fractures within the K-feldspar.

3.3.4 Arvogno Albertini dike

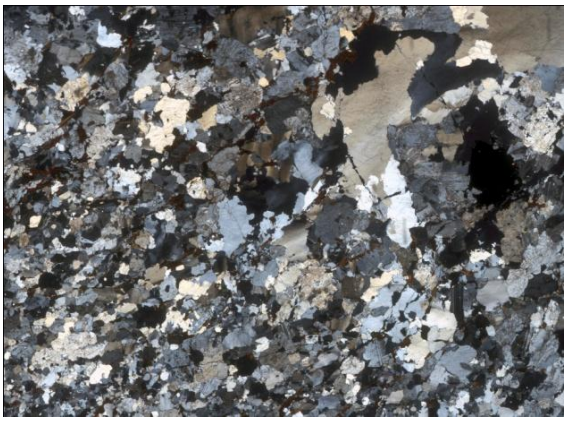

(E3) Contact between very fine grained two mica orthogneiss and the border zone of the pegmatite. Quartz grains of the pegmatite invade the host rock.

(E1) Large K-feldspar crystal of the core zone with perthitic structure. Albite perthite occurs as veinlets which crosscut the K-feldspar with different planar orientations.

3.3.5 Emerald Pizzo Marcio and Summit of Pizzo Marcio dikes

(L1) This thin section shows the albitization process of the Pizzo Marcio dikes. Thin section has been cut perpendicular respect the previous one and shows albite crystals with different grain size and characteristic interstitial trachytoid texture given by aligned albite crystals. On the left side of the section relics of beryl are visible, almost completely replaced by albite + bertrandite (beryllium silicate). The holes are secondary cavities lined with albite crystals.

3.3.6 Summit of Pizzo Paglia dike

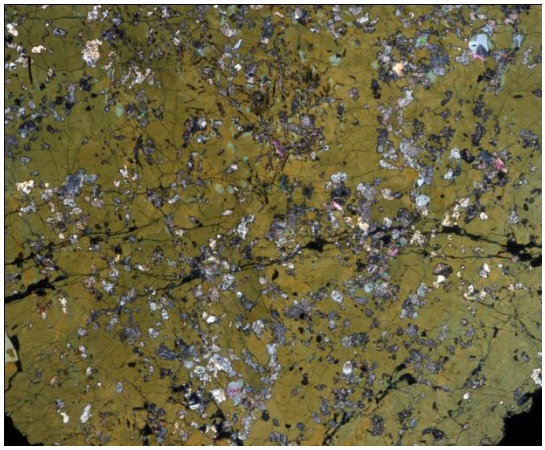

(P4) Tourmaline schorl from the enclosing amphibolite rock adjacent the dike. It formed after the pegmatite exsolved the boron-rich fluid phase during the crystallization of pegmatitic silicate liquid (Novak et al., 2004). Tourmaline shows pecilitic structure which consists of plagioclase, mica and other not identified minerals.

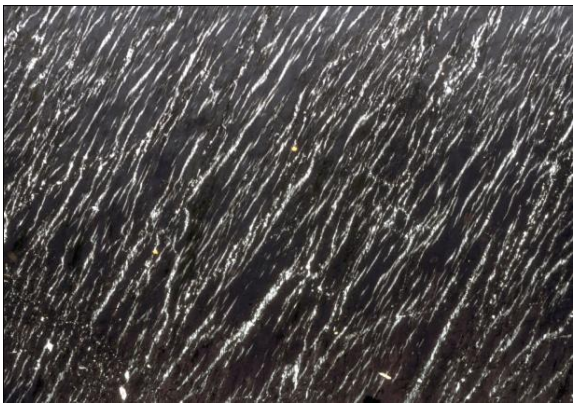

(P6) Large K-feldspar crystal of the border zone has perthitic structure with albite that runs as parallel films throughout the feldspar.

3.3.7 Colonnello Pizzo Paglia dike

(R4) The section shows the contact between leucocratic migmatite gneiss of the Southern Steep Belt and the footwall border zone of the pegmatite. The abrupt change in grain size and the straight contact are visible. K-feldspar, quartz and subordinate plagioclase have equigranular texture associated with interstitial flakes of muscovite.

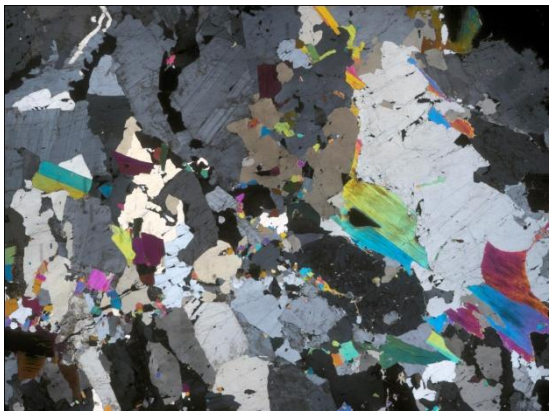

(R3) Large K-feldspars develop comb textures with crystal elongated and oriented perpendicular to the contact. Large plagioclase crystals, subordinate quartz and idiomorphic muscovite are also visible.

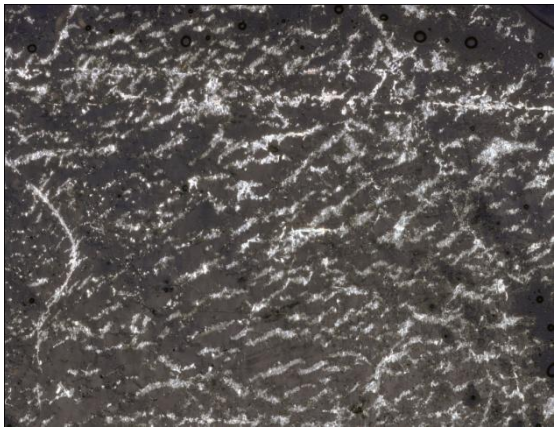

(R1) Large K-feldspar crystal of the core zone with perthitic structure. Perthitic albite forms S shaped irregular veinlets within K-feldspar.

3.3.8 Bodengo road cut dike

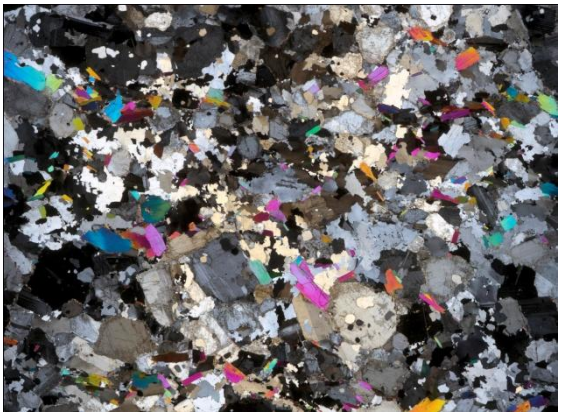

(W1) Aplite-pegmatite texture composed of equigranular K-feldspar, plagioclase, subordinate interstitial quartz and muscovite mica. Rounded garnet are also visible associated to pecilitic apatite crystals.

3.3.9 Garnet Codera dike

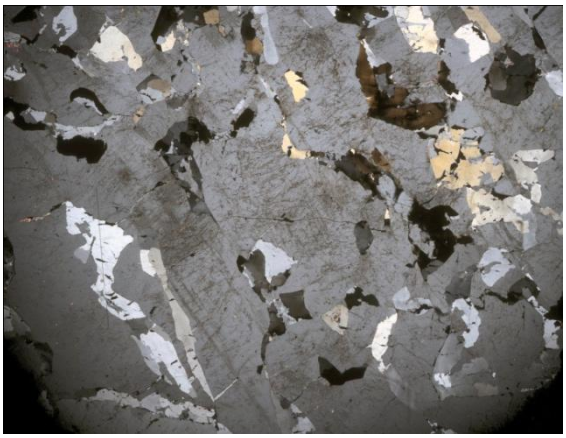

(A1) The wall-intermediate zone of the pegmatite contains graphic texture composed of large K-feldspar and intergrowth quartz. The quartz is deformed and pervasively recrystallized.

(A3) Large K-feldspar crystal of the core zone with perthitic structure. Albite perthite occurs as thin veinlets which crosscut the K-feldspar with preferred planar orientation. The veinlets are crosscut by planar perpendicular fractures that displace the perthites.

(A5) Milonitic quartz in the core zone of the pegmatite. Quartz is recrystallized and evidences preferred crystallographic orientation. Quartz subgrains show triple point junction with polygonization and grain boundary migration structures. Cataclastic, rounded K-feldspars are mantled by recrystallized quartz subgrains.

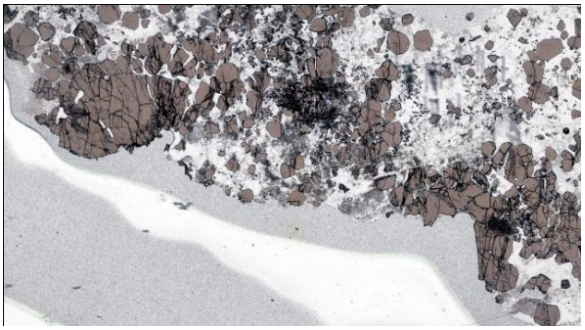

(A6) Euhedral garnet crystals embedded into quartz and K-feldspar. Smaller garnet crystals preserve their shape while larger crystals are heavily fractured. No alteration product- minerals were observed.

3.3.10 Phosphate Codera dike

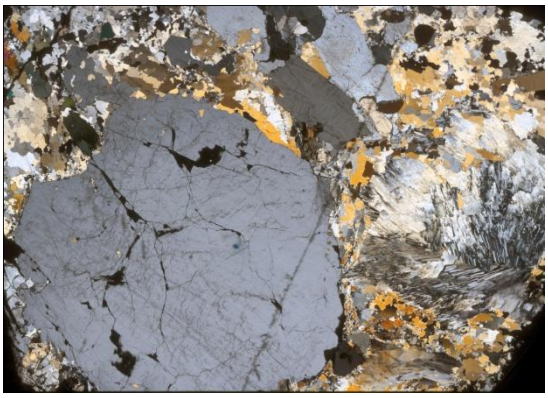

(B2) The border zone of the Phosphate pegmatite contains large euhedral beryl crystal, elongated K-feldspar crystals and trachytoid texture formed of aligned and radiated albite crystals. Subordinate green-bluish Mn-

rich elbaite is also observable. All these minerals are embedded into recrystallized, mylonitic quartz which shows preferred crystallographic orientation and variable grain-size.

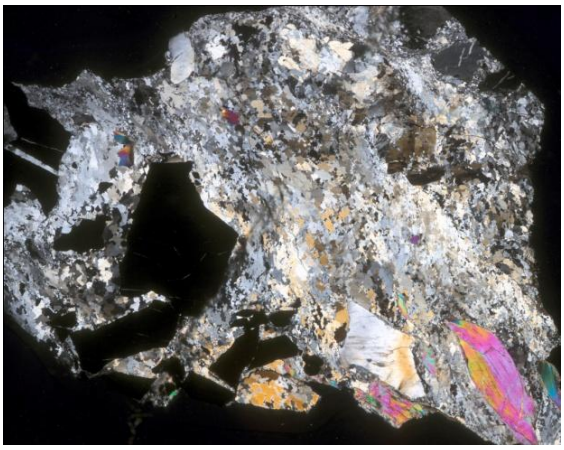

(B5) The wall zone of the pegmatite contains orange-red spessartine garnets embedded into mylonitic quartz which shows preferred crystallographic orientation and variable grain-size.

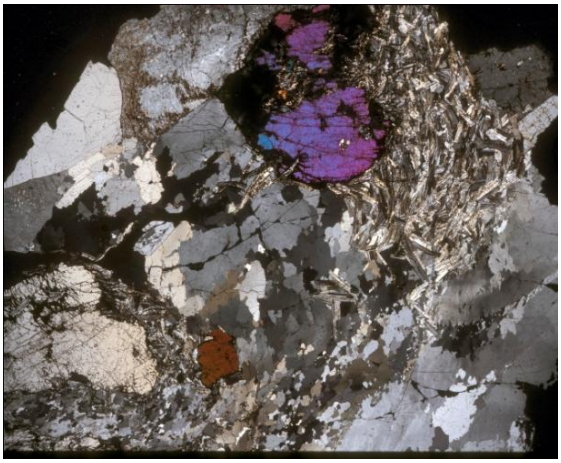

(B7) The wall zone contains masses of triplite with very high relief and anomalous interference colours up to first-order red cross-cut by set of fractures filled with manganese hydroxides. Triplite is embedded into albite var. clevelandite with trachytoid texture involved in synmagmatic deformation and recrystallized quartz grains with variable grain size. Large perthite microcline crystals are also observable in the section.

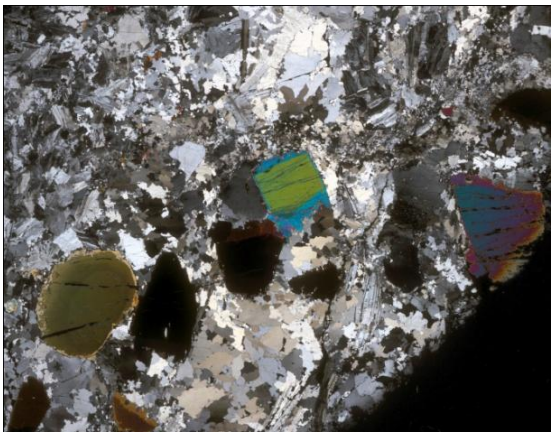

(B9) Mn-rich fluorelbaite crystals with high relief colors. Rim portions enriched in Mn-fluorelbaite component are embedded into recrystallized quartz and albite var. cleavelandite with trachytoid texture. Tourmalines show acicular terminations along the antilogue pole of the crystal.

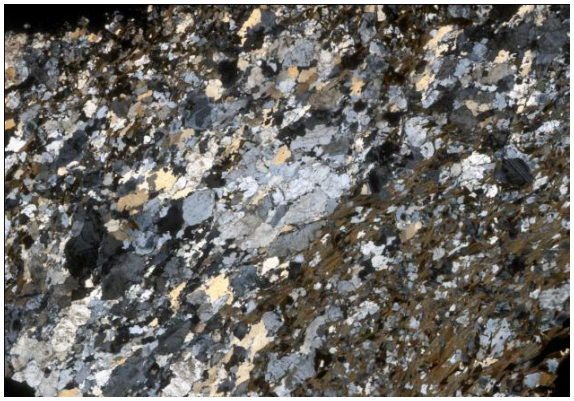

(B10) Pervasive and preferred orientation of plagioclase, biotites with shadow pressures, quartz and K-feldspar characterize the tonalite rocks along the contact zone of the pegmatite dike

CHAPTER 4

Mineralogy of pegmatites of Central Alps

4.1 Niobium- tantalum- yttrium- rare-earths-uranium oxides

4.1.1 Prewiev

REL–Li subclass granitic pegmatites of the beryl–columbite subtype, beryl–columbite–phosphate subtype commonly exhibit moderate Nb-Ta fractionation, and Nb,Ta-oxide minerals typically include columbite-(Fe) (Uher et al., 1994) ferrotapiolite and tantalite (Novák et al., 2000). However, the presence of tapiolite-(Fe), tantalite-(Fe), ishikawaite, ixiolite, wodginite and locally also abundant microlite group minerals (Wise and Černý, 1990) indicates an elevated level of Nb-Ta fractionation in some REL-Li subclass pegmatites. In addition aeschynite-group minerals and euxenite-group minerals are also typical accessory phases in REL–REE (rare-element–rare earth) subclass pegmatites of the euxenite subtype (Černý and Ercit, 2005; Škoda and Novák, 2007). For such reasons Nb-Ta, Y-REE-U bearing-minerals represent an important tool, to allow discriminate different geochemical population of pegmatites on the basis of the mineralogy of their accessory mineral phases.

Columbite serie minerals have the general formula AB_2O_6, in which, A crystallographic site is occupied by Fe^{2+}, Mn, and Mg, and B crystallographic site is occupied by Nb and Ta. Members of the columbite serie are subdivided on the basis of A and B-site chemistry. Nb as the dominant B cation are referred to as columbite, and with Ta, as tantalite serie. In the construction of species names, prefixes are used to describe A-site chemistry; thus, for example the species of columbite with Mn dominant at the A site is columbite-Mn (Burke, 2008). Columbite-group minerals show variable degrees of cation order. Most variation in the composition of columbite-serie minerals is owing to the substitution of Mn for Fe and of Ta for Nb (Ercit et al., 1995).

Minerals of the tapiolite series, $(Fe,Mn)Ta_2O_6$, occur primarily as accessory phases in REL-Li subclass granitic pegmatites, they display moderate to high levels of fractionation in Ta-mineralized granites. Commonly are associated with columbite-tantalite, microlite, wodginite, cassiterite and less frequently to fersmite (Guastoni et al., 2008). The general formula of tapiolite minerals can be expressed as AB_2O_6 where A crystallographic site is occupied by Fe^{2+} and Mn^{2+}, and B crystallographic site by Ta^{5+} and Nb^{5+} (with Ta » Nb). Ferric iron, titanium and tin may occur in minor quantities and occupy both crystallographic sites. Tapiolite-Fe refers to the Fe^{2+} end-member $FeTa_2O_6$, whereas tapiolite-Mn refers to the Mn-rich member (Wise and Černý, 1996)

Aeschynite-group minerals and euxenite-group minerals have general formula AB_2O_6, where the eight-fold coordinated A-site is occupied primarily by Y, REE, Ca, U, and Th, and the six-fold coordinated B-site is characterized by Ti, Nb, and Ta. It is indicative to allow discriminate these two groups aeschynite minerals

have orthorhombic symmetry and *Pbnm* space group, whereas euxenite-group minerals have orthorhombic symmetry and *Pcan* space group.

The minerals constituting the wodginite group are isostructural oxides, with the general formula ABC_2O_8 where A = Mn, Fe^{2+}, Li, □; B = Sn, Ti, Fe^{3+}, Ta; C = Ta, Nb. The classification is based on the chemistry of the A and B-cations taking as general definition the term wodginite itself with the general formula $MnSnTa_2O_8$. (Ercit et al., 1992)

In this study a number of Nb-Ta-Y-REE-U oxide minerals, include tantalite-columbite and tapiolite series, aeschynite, euxenite and wodginite group minerals were recognized in the pegmatites of Central Alps and their crystal-chemistry was investigated in detail. A temptative to classify pegmatites made by Wenger and Armbruster (1991) used crystal-chemistry and crystallographic data of columbites to define the degree of differentiation of pegmatitic dikes hosted in Bergell intrusion and in its aureola. What brings our attention is these minerals are very representative of the pegmatites and their presence or absence allow to discriminate the fractionation trends (geochemical evolution) in a single pegmatite body. This can be observed in the diagrams of Figure 4.1 to 4.5 where Nb-Ta-Y-REE-U oxides are represented. Table 4.1 presents a schematic distribution of Nb-Ta-Y-REE-U oxide minerals within pegmatites of the Central Alps.

Table 4.1 Classification and distribution of Nb-Ta-Y-REE-U oxides

Sigle	Locality	Name, serie, group	Formula	Simmetry	Space group
		Tantalite-Columbite serie			
F,C	Grignaschi, Rio Graia	Tantalite-(Fe)	$(Fe,Mn)(Ta,Nb,Ti)_2O_6$	Orthorhombic	*Pcan*
H,L	Summit of Pizzo Marcio Pizzo Marcio-Alpe Rosso	Tantalite-(Mn)	$(Mn,Fe)(Ta,Nb,Ti)_2O_6$	Orthorhombic	*Pcan*
		Tantalite-(Mg)	$(Mg,Fe)(Ta,Nb,Ti)_2O_6$	Orthorhombic	*Pcan*
A	Garnet Codera valley	Columbite-(Fe)	$(Fe,Mn)(Nb,Ta,Ti)_2O_6$	Orthorhombic	*Pcan*
H,L	Summit of Pizzo Marcio Pizzo Marcio-Alpe Rosso	Columbite-(Mn)	$(Mn,Fe)(Nb,Ta,Ti)_2O_6$	Orthorhombic	*Pcan*
		Columbite-(Mg)	$(Mg,Fe)(Nb,Ta,Ti)_2O_6$	Orthorhombic	*Pcan*
		Tapiolite serie			
F,C, H	Grignaschi, Rio Graia Pizzo Marcio-Alpe Rosso	Tapiolite-(Fe)	$(Fe,Mn)(Ta,Nb,Ti)_2O_6$	Tetragonal	$P4_2/mnm$
		Tapiolite-(Mn)	$(Mn,Fe)(Ta,Nb,Ti)_2O_6$	Tetragonal	$P4_2/mnm$
		Aeschynite group			*Pbnm*
E	Arvogno Albertini	Aeschynite-(Y)	$(Y,Ca,REE)(Ti,Nb,Ta)_2(O,OH)_6$	Orthorhombic	*Pbnm*
		Aeschynite-(Ce)	$(Ce,Ca,REE)(Ti,Nb,Ta)_2(O,OH)_6$	Orthorhombic	*Pbnm*
		Nioboaeschynite-(Y)	$(Y,Ca,REE)(Nb,Ti,Ta)_2(O,OH)_6$	Orthorhombic	*Pbnm*
		Nioboaeschynite-(Ce)	$(Ce,Ca,REE)(Nb,Ti,Ta)_2(O,OH)_6$	Orthorhombic	*Pbnm*
		Tantalaeschynite-(Y)	$(Y,Ca,REE)(Ta,Ti,Nb)_2O_6$	Orthorhombic	*Pbnm*
		Rynersonite	$Ca(Ta,Nb,Ti)_2O_6$	Orthorhombic	*Pbnm*
H	Pizzo Marcio-Alpe Rosso	Vigezzite	$(Ca,Ce)(Nb,Ta,Ti)_2O_6$	Orthorhombic	*Pbnm*

		Euxenite group			
A	Garnet Codera valley	Euxenite-(Y)	$(Y,U,Ca,REE)(Nb,Ti,Ta)_2(O,OH)_6$	Orthorhombic	*Pcan*
E	Arvogno Albertini	Polycrase-(Y)	$(Y,U,Ca,REE)(Ti,Nb,Ta)_2(O,OH)_6$	Orthorhombic	*Pcan*
		Uranopolycrase-(Y)	$(U,Y,Ca,REE)(Ti,Nb,Ta)_2(O,OH)_6$	Orthorhombic	*Pcan*
		Tanteuxenite-(Y)	$(Y,U,Ca,REE)(Ta,Nb,Ti)_2(O,OH)_6$	Orthorhombic	*Pcan*
H	Pizzo Marcio-Alpe Rosso	Fersmite	$(Ca,Ce,REE)(Nb,Ta,Ti)_2(O,OH)_6$	Orthorhombic	*Pcan*
		Wodginite group			
		Wodginite	$MnSnTa_2O_8$	Monoclinic	*C*2/*c*
R	Colonnello Pizzo Paglia	Lithiowodginite	$LiSnTa_2O_8$	Monoclinic	*C*2/*c*
H	Pizzo Marcio-Alpe Rosso	Ferrowodginite	$FeSnTa_2O_8$	Monoclinic	*C*2/*c*
		Ferrotitanowodginite	$Fe(Ti,Sn)Ta_2O_8$	Monoclinic	*C*2/*c*
		Titanowodginite	$Mn(Ti,Sn)Ta_2O_8$	Monoclinic	*C*2/*c*

4.1.2 Grignaschi and Rio Graia dike: mineral-chemistry of tantalite-columbite and tapiolite-(Fe)

Both these pegmatite dike are charaterized by the presence of tantalite-columbites and tapiolite-(Fe) distributed in the intermediate-core zone of the pegmatites. At Grignaschi tantalite-columbite forms platy striated black, metallic crystals up to 1 centimeters in length embedded in K-feldspar or quartz, whereas at Rio Graia it forms platy tabular crystals up to 2-3 centimetrs in length embedded into K-feldspar. Tapiolite-(Fe) at Grignaschi and Rio Graia form black, metallic rounded polysynthetic cyclic twin crystals embedded in K-feldspar or quartz.

In both localities (Table 4.2) chemical analysis give Ta/(Ta+Nb) ratio in tantalite-columbite serie in the range of 51 to 57 *p.f.u.*. At Rio Graia the core portion of the crystal is composed of columbite-(Fe) and the Ta/(Ta+Nb) ratio decreases to 0.42. Mn/(Mn+Fe) ratio is quite homogeneous within the range of 0.21-0.24 *p.f.u.*.. Columbite-tantalites do not incorporate other elements except for SnO_2 up to 0.23 wt% and UO_2 up to 0.10 wt % in tantalites from Rio Graia. Tapiolite-(Fe) is invariably conspicuously enriched in Ta and Fe in comparison to tantalite. Both localities have almost identical Ta/(Ta+Nb) and Mn/(Mn+Fe) ratios.

Table 4.2 Grignaschi and Rio Graia dike, representative compositionsof tantalite-columbite and tapiolite-Fe

	Rio Graia	Rio Graia	Rio Graia	Rio Graia	Grignaschi	Grignaschi
	G7 border	G7 intermediate	G7 core	G6	F1	F2
Elements Wt%	Tantalite-(Fe)	Tantalite-(Fe)	Columbite-(Fe)	Tapiolite-(Fe)	Tapiolite-(Fe)	Tantalite-(Fe)
MgO	0.08	0.09	0.00	0.05	0.00	0.00
CaO	0.00	0.00	0.00	0.00	0.00	0.00
TiO_2	1.04	1.6	1.49	3.61	3.28	1.73
Sc_2O_3	0.00	0.00	0.00	0.00	0.00	0.00
MnO	3.42	3.62	4.09	0.43	0.58	3.73
FeO	12.62	12.92	13.14	14.38	15.29	13.24
Y_2O_3	0.00	0.00	0.00	0.00	0.00	0.00
Nb_2O_5	25.37	29.66	36.91	10.65	9.54	27.40
SnO_2	0.18	0.22	0.23	0.25	0.20	0.18
Ta_2O_5	56.61	52.09	44.06	69.98	70.28	51.84
WO_3	0.00	0.00	0.00	0.00	0.00	0.00
Gd_2O_3	0.00	0.00	0.00	0.00	0.00	0.00

Tb_2O_3	0.00	0.00	0.00	0.00	0.00	0.00
Dy_2O_3	0.00	0.00	0.00	0.00	0.00	0.00
Er_2O_3	0.00	0.00	0.00	0.00	0.00	0.00
Yb_2O_3	0.00	0.00	0.00	0.00	0.00	0.00
ThO_2	0.00	0.00	0.00	0.00	0.00	0.00
UO_2	0.00	0.10	0.07	0.21	0.00	0.00
TOT	99.32	100.3	99.99	99.56	99.17	98.12
			Formula proportions normalized to 6 oxygen atoms			
p.f.u.						
Mg	0.01	0.01	0.00	0.01	0.00	0.00
Ca	0.00	0.00	0.00	0.00	0.00	0.00
Ti	0.06	0.08	0.08	0.21	0.19	0.09
Sc	0.00	0.00	0.00	0.00	0.00	0.00
Mn	0.21	0.21	0.23	0.03	0.04	0.23
Fe	0.77	0.76	0.74	0.93	1.00	0.80
Y	0.00	0.00	0.00	0.00	0.00	0.00
Nb	0.83	0.94	1.13	0.37	0.34	0.89
Sn	0.01	0.01	0.01	0.01	0.01	0.01
Ta	1.12	0.99	0.81	1.47	1.49	1.02
W	0.00	0.00	0.00	0.00	0.00	0.00
Gd	0.00	0.00	0.00	0.00	0.00	0.00
Tb	0.00	0.00	0.00	0.00	0.00	0.00
Dy	0.00	0.00	0.00	0.00	0.00	0.00
Er	0.00	0.00	0.00	0.00	0.00	0.00
Yb	0.00	0.00	0.00	0.00	0.00	0.00
Th	0.00	0.00	0.00	0.00	0.00	0.00
U	0.00	0.00	0.00	0.00	0.00	0.00
Cation Sum	3.01	3.00	3.00	3.03	3.07	3.04
Y+REE	0.00	0.00	0.00	0.00	0.00	0.00
Ca+U+Th	0.00	0.00	0.00	0.00	0.00	0.00
U	0.00	0.00	0.00	0.00	0.00	0.00
Nb+Ta+Ti+W	2.01	2.01	2.02	2.05	2.02	2.00
Mn/(Mn+Fe)	0.21	0.22	0.24	0.03	0.04	0.22
Ta/(Ta+Nb)	0.57	0.51	0.42	0.80	0.81	0.53

4.1.3 Arvogno Albertini dike: mineral-chemistry of aeschynite-(Y)/polycrase-(Y)

Aeschynite-(Y)/polycrase-(Y) form black, reddish brown crystals metallic, with granular to conchoidal fracture. The habitus is platy, tabular, barrel or prismatic, sometimes elongated, and the crystals can reach up to two centimetres in length. They are hosted in K-feldspar or smoky quartz due the effect of irradiation. The data presented in the table 4 are from Albertini and Andersen (1989) and refers to the Arvogno pegmatite dike. Analysis (Table 4.3) were selected on the basis of the most characteristic habitus of the crystals: all the chemical analysis were recalculated. As it can be observed all the Nb-Ta-Y-REE-U oxides fall in the aeschynite-(Y) versus polycrase-(Y) compositions. Albertini and Andersen (1989) classified these Nb-Ta oxides as euxenite-(Y) or polycrase-(Y). Only by measuring the unit cell parameters of these minerals is possible discriminate these two group of minerals. Indeed aeschynites have *Pbmn* space group whereas euxenites have *Pcan* space group.

Nb-Ta-Y-REE-U oxides of the Albertini pegmatite have strong HREE enrichment with Y+REE in the range of 0.70 to 0.84 *p.f.u.* Dysprosium has the highest content in the range of 2.64 to 3.35 wt %. U+Th is quite variable and varies from 0.07 to 0.22 *p.f.u.* These minerals suffer the effects of metamictization due to the

presence of significative amounts of uranium and thorium like occur in minerals with similar crystal-chemical characters (Warner and Ewing, 1993; Hanson et al., 1999).

Table 4.3 Arvogno Albertini dike,representative compositions of aeschynite-(Y)-polycrase-(Y)

	Albertini Type 2	Albertini Type 3	Albertini Type 5
Elements Wt%	Aeschynite-(Y) versus Policrase-(Y)	Aeschynite-(Y) versus Policrase-(Y)	Aeschynite-(Y) versus Policrase-(Y)
MgO	0.00	0.00	0.00
CaO	0.54	0.92	0.24
TiO_2	22.13	20.29	24.68
Sc_2O_3	0.00	0.00	0.00
MnO	0.31	0.23	0.25
FeO	2.28	1.47	1.52
Y_2O_3	14.74	16.57	20.74
Nb_2O_5	24.4	17.39	24.38
SnO_2	0.00	0.00	0.00
Ta_2O_5	10.02	26.3	13.57
WO_3	0.00	0.00	0.00
Gd_2O_3	1.80	1.63	1.94
Tb_2O_3	0.9	0.73	0.88
Dy_2O_3	3.33	2.64	3.35
Er_2O_3	1.51	1.09	1.55
Yb_2O_3	1.84	1.24	1.05
ThO_2	3.22	3.42	1.67
UO_2	11.73	5.36	3.95
TOT	98.75	99.28	99.77
	Formula proportions normalized to 6 oxygen atoms		
p.f.u.			
Mg	0.00	0.00	0.00
Ca	0.04	0.06	0.02
Ti	1.07	1.00	1.13
Sc	0.00	0.00	0.00
Mn	0.02	0.01	0.01
Fe	0.12	0.08	0.08
Y	0.50	0.58	0.67
Nb	0.71	0.52	0.67
Sn	0.00	0.00	0.00
Ta	0.18	0.47	0.22
W	0.00	0.00	0.00
Gd	0.04	0.04	0.04
Tb	0.02	0.02	0.02
Dy	0.07	0.06	0.07
Er	0.03	0.02	0.03
Yb	0.04	0.02	0.02
Th	0.05	0.05	0.02
U	0.17	0.08	0.05
Cation Sum	3.06	3.01	3.05
Y+REE	0.70	0.74	0.85
Ca+U+Th	0.26	0.19	0.09
U	0.17	0.08	0.05
Nb+Ta+Ti+W	1.96	1.99	2.02
Mn/(Mn+Fe)	0.14	0.11	0.11
Ta/(Ta+Nb)	0.20	0.47	0.25

4.1.4 Pizzo Marcio–Alpe Rosso dikes: mineral-chemistry of fersmite and vigezzite

Fersmite forms yellowish or greenish prismatic,millimetric, striated crystals, in some cases with a dark reddish to brownish core composed of columbite–tantalite + microlite. Idiomorphic crystals of fersmite were observed in the secondary cavities associated with albite and tremolite or embedded in massive albite with other oxides of Nb–Ta. Vigezzite forms brown to reddish, millimetric, platy, prismatic crystals, in some cases with a dark core composed of thorian vigezzite embedded in massive albite and associated with albite and tremolite.

The analytical data indicate that fersmite (Table 4.4) in samples PZ1, PZ15, and PZ16, are rather homogeneous with Ta/(Ta+Nb) in the range of 0.15 to 0.19 *p.f.u.* Tantalum-rich fersmite (PZ12) is significantly different, as the Nb_2O_5 content dramatically decreases down to 41.79 wt%, and consequently the Ta_2O_5 increases up to 43.04 wt% with Ta/(Ta+Nb) up to 0.38 *p.f.u.* This latter value probably represents the highest Ta_2O_5 content of fersmite measured in the literature. Fersmite from Pizzo Marcio-Alpe Rosso do not incorporate other elements except for Ce_2O_3 up to 0.32 wt%. The composition of vigezzite (Table 4.4) sample PZ18 reveals chemical differences with respect to the chemical data from the holotype vigezzite reported by Graeser et al. (1979). In addition to high values of Ce_2O_3, significant contents of Nd_2O_3, Sm_2O_3 and Gd_2O_3 were also measured. High TiO_2 and Ce_2O_3 values indicate that vigezzite forms a partial solid-solution with nioboaeschynite-(Ce), an isostructural AB_2O_6 member of the aeschynite group (Rosenblum and Mosier 1975), The increase in Ta content also indicate a shift toward partial solid-solution with rynersonite, another isostructural AB_2O_6 member of the aeschynite group (Foord and Mrose, 1978). Moreover, the composition of vigezzite from Pizzo Marcio-Alpe Rosso dikes shifts at the core toward thorian vigezzite, even if such content is not enough to form a Th-dominant end-member of this group (0.13 *p.f.u.* Th), as reported by Bayliss et al. (2005). Unit-cell parameters of vigezzite (PZ18) correspond to an orthorhombic cell with: *a* 11.048(1), *b* 7.536(1), *c* 5.368(1) Å, and the cell data agree with those for vigezzite of Alpe Rosso reported by Giuseppetti and Tadini (1990).

Table 4.4 Emerald Pizzo Marcio-Alpe Rosso dikes, representative compositions of fersmite and vigezzite

	Pizzo Marcio Alpe Rosso	Pizzo Marcio Alpe Rosso	Pizzo Marcio Alpe Rosso	Pizzo Marcio Alpe Rosso	Pizzo Marcio Alpe Rosso	Pizzo Marcio Alpe Rosso	Pizzo Marcio Alpe Rosso	Pizzo Marcio Alpe Rosso
	PZ1	PZ15	PZ16	PZ12	PZ18 core1	PZ18core2	PZ18intermediate	PZ18rim
Elements Wt%	Fersmite	Fersmite	Fersmite	Fersmite	Vigezzite	Vigezzite	Vigezzite	Vigezzite
MgO	0.00	0.00	0.00	0.00	0.00	0.00	0.00	0.00
CaO	15.59	16.86	16.74	14.52	8.69	8.86	10.81	13.61
TiO_2	1.40	1.39	0.75	0.18	10.48	10.46	7.69	6.16
Sc_2O_3	0.00	0.00	0.00	0.00	0.00	0.00	0.00	0.00
MnO	0.16	0.19	0.20	0.62	0.00	0.00	0.00	0.00
FeO	0.00	0.00	0.00	0.24	0.62	0.63	0.34	0.30
Y_2O_3	0.00	0.00	0.00	0.00	0.00	0.00	0.00	0.00
Nb_2O_5	59.36	61.99	58.40	41.79	31.77	27.51	35.01	36.25
SnO_2	0.00	0.00	0.00	0.00	0.00	0.00	0.00	0.00
Ta_2O_5	23.58	18.33	23.29	43.04	32.60	36.98	38.52	41.29
WO_3	0.00	0.00	0.00	0.00	0.00	0.00	0.00	0.00
Ce_2O_3	0.11	0.32	0.00	0.00	4.51	3.98	4.28	2.01
Nd_2O_3	0.00	0.00	0.00	0.00	1.39	1.38	1.11	0.31

Sm_2O_3	0.00	0.00	0.00	0.00	0.44	0.88	0.44	0.17
Gd_2O_3	0.00	0.00	0.00	0.00	0.10	0.42	0.10	0.13
Dy_2O_3	0.00	0.00	0.00	0.00	0.00	0.00	0.00	0.00
Yb_2O_3	0.00	0.00	0.00	0.00	0.00	0.00	0.00	0.00
ThO_2	0.00	0.00	0.00	0.00	8.65	8.26	2.20	0.00
UO_2	0.00	0.00	0.00	0.00	0.00	0.00	0.00	0.00
TOT	100.20	99.08	99.38	100.39	100.02	99.36	100.50	100.23
				Formula proportions normalized to 6 oxygen atoms				
p.f.u.								
Mg	0.00	0.00	0.00	0.00	0.00	0.00	0.00	0.00
Ca	0.98	1.05	1.06	1.00	0.61	0.64	0.74	0.93
Ti	0.06	0.06	0.03	0.01	0.52	0.53	0.37	0.29
Sc	0.00	0.00	0.00	0.00	0.00	0.00	0.00	0.00
Mn	0.01	0.01	0.01	0.03	0.00	0.00	0.00	0.00
Fe	0.00	0.00	0.00	0.01	0.03	0.04	0.02	0.02
Y	0.00	0.00	0.00	0.00	0.00	0.00	0.00	0.00
Nb	1.58	1.63	1.57	1.22	0.94	0.84	1.02	1.04
Sn	0.00	0.00	0.00	0.00	0.00	0.00	0.00	0.00
Ta	0.38	0.29	0.38	0.75	0.58	0.68	0.67	0.71
W	0.00	0.00	0.00	0.00	0.00	0.00	0.00	0.00
Ce	0.01	0.01	0.00	0.00	0.11	0.10	0.10	0.05
Nd	0.00	0.00	0.00	0.00	0.03	0.03	0.03	0.01
Sm	0.00	0.00	0.00	0.00	0.02	0.02	0.01	0.01
Gd	0.00	0.00	0.00	0.00	0.01	0.01	0.01	0.01
Dy	0.00	0.00	0.00	0.00	0.00	0.00	0.00	0.00
Yb	0.00	0.00	0.00	0.00	0.00	0.00	0.00	0.00
Th	0.00	0.00	0.00	0.00	0.13	0.13	0.03	0.00
U	0.00	0.00	0.00	0.00	0.00	0.00	0.00	0.00
Cation Sum	3.02	3.05	3.05	3.02	2.98	3.02	3.00	3.07
Y+REE	0.01	0.01	0.00	0.00	0.17	0.16	0.15	0.08
Ca+U+Th	0.98	1.05	1.06	1.00	0.74	0.77	0.77	0.93
U	0.00	0.00	0.00	0.00	0.00	0.00	0.00	0.00
Nb+Ta+Ti+W	2.02	1.98	1.98	1.98	2.04	2.05	2.06	2.04
Mn/(Mn+Fe)	1.00	1.00	1.00	0.75	0.00	0.00	0.00	0.00
Ta/(Ta+Nb)	0.19	0.15	0.19	0.38	0.38	0.45	0.40	0.41

4.1.5 Pizzo Marcio–Alpe Rosso dikes: mineral-chemistry of tantalite-columbite

Columbite–tantalite serie minerals form brown-grey granular rounded crystals or millimetric, brown to reddish, platy, prismatic crystals (PZ4), hosted by massive albite or within secondary albite cavities.

Sample PZ4 consists of columbite-(Mn) with up to 49.7 wt% Nb_2O_5. Analysis (Table 4.5) reveal significant Mg up to 0.19 wt% TiO_2, and up to 0.13 wt% CaO. Sample PZ7 is Mg-rich columbite showing up to 2.08 wt% MgO, up to 58.34 wt% Nb_2O_5 in addition to detectable Sn values, up to 0.22 wt% SnO2. Sample PZ10 consists of tantalite-(Mn) that shows very variable Nb/Ta values, with the highest Ta enrichments toward the rim of the crystal (up to 81.48 wt%) with Ta/(Ta+Nb) ratio which equals to 0.90 *p.f.u.*. Sample PZ12 consists of columbite-(Mn) with an average of 41.13 wt% Nb_2O_5, with detectable MgO (0.58 wt%) and SnO_2 (0.30 wt%). Sample PZ14 consists of columbite-(Mn) with an average of 59.16 wt% Nb_2O_5, detectable MgO (0.82 wt%) and SnO_2 (0.22 wt%).

Table 4.5 Summit-Emerald Pizzo Marcio-Alpe Rosso dikes, representative compositions of tantalite-columbite serie

	Summit of Pizzo Marcio PZ4	Pizzo Marcio Alpe Rosso PZ7	Pizzo Marcio Alpe Rosso PZ10 core	Pizzo Marcio Alpe Rosso PZ10 rim	Pizzo Marcio Alpe Rosso PZ12	Pizzo Marcio Alpe Rosso PZ14
Elements	Columbite-(Mn)	Columbite-(Mn)	Tantalite-(Mn)	Tantalite-(Mn)	Columbite-(Mn)	Columbite-(Mn)
Wt%						
MgO	0.40	2.08	0.43	0.19	0.58	0.82
CaO	0.13	0.07	0.00	0.00	0.00	0.00
TiO_2	0.19	0.17	0.19	0.17	0.17	0.14
Sc_2O_3	0.00	0.00	0.00	0.00	0.00	0.00
MnO	12.35	7.99	11.18	9.72	12.04	12.42
FeO	4.64	7.34	3.37	3.25	4.00	5.35
Y_2O_3	0.00	0.00	0.00	0.00	0.00	0.00
Nb_2O_5	49.77	58.34	21.31	5.22	41.13	59.16
SnO_2	0.20	0.22	0.20	0.20	0.30	0.10
Ta_2O_5	33.07	24.65	64.05	81.48	42.45	23.08
WO_3	0.00	0.00	0.00	0.00	0.00	0.00
Gd_2O_3	0.00	0.00	0.00	0.00	0.00	0.00
Tb_2O_3	0.00	0.00	0.00	0.00	0.00	0.00
Dy_2O_3	0.00	0.00	0.00	0.00	0.00	0.00
Er_2O_3	0.00	0.00	0.00	0.00	0.00	0.00
Yb_2O_3	0.00	0.00	0.00	0.00	0.00	0.00
ThO_2	0.00	0.00	0.00	0.00	0.00	0.00
UO_2	0.00	0.00	0.00	0.00	0.00	0.00
TOT	100.75	100.86	100.73	100.17	100.67	101.07
			Formula proportions normalized to 6 oxygen atoms			
p.f.u.						
Mg	0.04	0.19	0.05	0.02	0.06	0.07
Ca	0.04	0.01	0.00	0.00	0.00	0.00
Ti	0.01	0.01	0.01	0.01	0.01	0.01
Sc	0.00	0.00	0.00	0.00	0.00	0.00
Mn	0.67	0.41	0.70	0.68	0.68	0.64
Fe	0.25	0.37	0.21	0.22	0.22	0.27
Y	0.00	0.00	0.00	0.00	0.00	0.00
Nb	1.43	1.60	0.71	0.19	1.24	1.62
Sn	0.01	0.01	0.01	0.01	0.01	0.01
Ta	0.57	0.41	1.29	1.82	0.77	0.38
W	0.00	0.00	0.00	0.00	0.00	0.00
Gd	0.00	0.00	0.00	0.00	0.00	0.00
Tb	0.00	0.00	0.00	0.00	0.00	0.00
Dy	0.00	0.00	0.00	0.00	0.00	0.00
Er	0.00	0.00	0.00	0.00	0.00	0.00
Yb	0.00	0.00	0.00	0.00	0.00	0.00
Th	0.00	0.00	0.00	0.00	0.00	0.00
U	0.00	0.00	0.00	0.00	0.00	0.00
Cation Sum	3.02	3.01	2.98	2.95	2.99	3.00
Y+REE	0.00	0.00	0.00	0.00	0.00	0.00
Ca+U+Th	0.04	0.01	0.00	0.00	0.00	0.00
U	0.00	0.00	0.00	0.00	0.00	0.00
Nb+Ta+Ti+W	2.01	2.02	2.01	2.02	2.02	2.01
Mn/(Mn+Fe)	0.73	0.53	0.77	0.76	0.76	0.70
Ta/(Ta+Nb)	0.29	0.20	0.64	0.90	0.38	0.19

4.1.6 Emerald–Alpe Rosso dikes: mineral-chemistry of tapiolite-(Fe) and ferrowodginite

Tapiolite-(Fe)+ferrowodginite form grey-brown pseudo-octahedral crystals associated with microlite and embedded in massive albite. Chemical analysis (Table 4.6) of tapiolite-(Fe) (PZ19) shows Ta_2O_5 contents of up to 86.53 wt% and FeO up to 8.91 wt%. Ferrowodginite (PZ19a) contains up to 76.58 wt% Ta_2O_5 and variable Fe/Mn values, with Fe slightly predominant over Mn Considering that tapiolite-(Fe) (Ta/(Ta+Nb) equals to 0.99 *p.f.u.*) is compositionally very similar to tantalite-(Fe) and ferrowodginite (Ta/(Ta+Nb) equals to 0.92 *p.f.u.*), and is chemically analogous to ixiolite, single-crystal X-ray-diffraction analyses were performed to establish the nature of these minerals. The cell data obtained from the single-crystal data collected for ferrowodginite correspond to a monoclinic cell with: *a* 9.430(7), *b*11.423(9), *c* 5.071(5) Å, b 90.97(7)°, and agree with the cell of ferrowodginite reported by Ercit *et al*. (1992). The unit-cell parameters of tapiolite-(Fe) obtained from the single-crystal data collected correspond to a tetragonal cell with *a* 4.754(1), *c* 9.218(2) Å, and agree well with the cell of tapiolite-(Fe) reported by Wise & Černý (1996)

Table 4.6 Emerald Pizzo Marcio-Alpe Rosso dikes representative compositions of ferrowodginite and tapiolite-(Fe)

	Pizzo Marcio Alpe Rosso PZ19	Pizzo Marcio Alpe Rosso PZ19a
Elements Wt%	Tapiolite-(Fe)	Ferrowodginite
MgO	0.11	0.99
CaO	0.00	0.00
TiO_2	0.12	1.31
Sc_2O_3	0.00	0.00
MnO	3.95	5.24
FeO	8.91	5.60
Y_2O_3	0.00	0.00
Nb_2O_5	0.53	3.89
SnO_2	0.24	5.66
Ta_2O_5	86.53	76.58
WO_3	0.00	0.00
Gd_2O_3	0.00	0.00
Tb_2O_3	0.00	0.00
Dy_2O_3	0.00	0.00
Er_2O_3	0.00	0.00
Yb_2O_3	0.00	0.00
ThO_2	0.00	0.00
UO_2	0.00	0.00
TOT	100.39	99.27
Formula normalized to 6 and 8 oxygen atoms		
p.f.u.		
Mg	0.01	0.16
Ca	0.00	0.00
Ti	0.01	0.11
Sc	0.00	0.00
Mn	0.28	0.48
Fe	0.63	0.51
Y	0.00	0.00
Nb	0.02	0.19
Sn	0.01	0.25
Ta	2.00	2.27
W	0.00	0.00

Gd	0.00	0.00
Tb	0.00	0.00
Dy	0.00	0.00
Er	0.00	0.00
Yb	0.00	0.00
Th	0.00	0.00
U	0.00	0.00
Cation Sum	2.96	3.97
Y+REE	0.00	0.00
Ca+U+Th	0.00	0.00
U	0.00	0.00
Nb+Ta+Ti+W	2.03	2.57
Mn/(Mn+Fe)	0.31	0.48
Ta/(Ta+Nb)	0.99	0.92

4.1.7 Colonnello Pizzo Paglia dike: mineral-chemistry of lithiowodginite

Lithiowodginite is a lithium, tantalum, tin oxide and represent an indicator of elevated level of Nb-Ta fractionation in REL-Li subclass pegmatites. This mineral was observed in miarolitic pockets of the granitic pegmatite of the Colonnello dike where forms black, metallic, barrel-prismatic crystals up to 1.6 centimeters in length. Electron microprobe analysis (Table 4.7) have deficient closure (98 wt%), the lithium calculated by stoichiometry in the range of 1.75 to 2.4 Li_2O wt % is the only compatible element which can fill the vacancy at the A site of the wodginite structure, characterized by general formula ABC_2O_8 (Ercit et al., 1992) Lithiowodginite of Colonnello dike has Ta/(Ta+Nb) ratio in the range of 0.92-0.94 *p.f.u.* and Mn/(Mn+Fe) between 0.69-0.70 *p.f.u.* It does not incorporate other elements except for UO_2 up to 0.11 wt%.

Table 4.7 Colonnello dike, representative compositions of lithiowodginite

	Colonnello Pizzo Paglia G8 core	Colonnello Pizzo Paglia G8 rim
Elements Wt%	Lithiowodginite	Lithiowodginite
Li_2O	2.4	1.75
MgO	0.00	0.00
CaO	0.00	0.00
TiO_2	0.58	0.48
Sc_2O_3	0.00	0.00
MnO	8.33	8.31
FeO	3.91	3.58
Y_2O_3	0.00	0.00
Nb_2O_5	3.33	2.69
SnO_2	13.92	14.84
Ta_2O_5	67.37	68.27
WO_3	0.00	0.00
Gd_2O_3	0.00	0.00
Tb_2O_3	0.00	0.00
Dy_2O_3	0.00	0.00
Er_2O_3	0.00	0.00
Yb_2O_3	0.00	0.00
ThO_2	0.00	0.00
UO_2	0.11	0.10
TOT	99.95	100.02

Formula normalized to 8 oxygen atoms		
p.f.u.		
Li	1.01	0.74
Mg	0.00	0.00
Ca	0.00	0.00
Ti	0.05	0.04
Sc	0.00	0.00
Mn	0.74	0.74
Fe	0.34	0.32
Y	0.00	0.00
Nb	0.16	0.13
Sn	0.58	0.63
Ta	1.91	1.96
W	0.00	0.00
Gd	0.00	0.00
Tb	0.00	0.00
Dy	0.00	0.00
Er	0.00	0.00
Yb	0.00	0.00
Th	0.00	0.00
U	0.00	0.00
Cation Sum	4.79	4.56
Y+REE	0.00	0.00
Ca+U+Th	0.00	0.00
U	0.00	0.00
Nb+Ta+Ti+W	2.12	2.13
Mn/(Mn+Fe)	0.69	0.70
Ta/(Ta+Nb)	0.92	0.94

4.1.8 Garnet Codera dike: mineral-chemistry of columbite-(Fe)

Columbite-(Fe) at Codera dike occurs as black, metallic, tabular or platy crystals with granular fracture up to two centimeters in length embedded in K-feldspar. Sample G2 consists of columbite-(Fe) and is rather homogeneous in composition. The core of the crystal has up to 69.83 wt% Nb_2O_5 and the rim decreases to 66.52 wt %. Columbite-(Fe) incorporate other elements like WO_3 up to 1.20 wt %, SnO_2 up to 0.28 wt%, UO_2 up to 0.81 wt % . Low REE values were also measured and include Y_2O_3 (0.05-0.10 wt%), Nd_2O_3 (0.05-0.08 wt %), Gd_2O_3 (0.05-0.10 wt%). Sample G3 consists of columbite-(Fe); the core of the crystal has up to 67.99 wt% Nb_2O_5 and the rim decreases to 66.08 wt %. Columbite-(Fe) incorporate other elements like WO_3 up to 1.20 wt %, SnO_2 up to 0.34 wt%, UO_2 up to 0.30 wt % .

Table 4.8 Garnet Codera dike, representative compositions of columbite-(Fe)

Elements Wt%	Garnet Codera G2 rim Columbite-(Fe)	Garnet Codera G2 int Columbite-(Fe)	Garnet Codera G2 core Columbite-(Fe)	Garnet Codera G2 core Columbite-(Fe)	Garnet Codera G3 rim Columbite-(Fe)	Garnet Codera G3 rim Columbite-(Fe)	Garnet Codera G3 int-dark Columbite-(Fe)	Garnet Codera G3 core Columbite-(Fe)
MgO	0.24	0.24	0.21	0.14	0.33	0.30	0.32	0.23
CaO	0.00	0.00	0.00	0.00	0.00	0.00	0.00	0.00
TiO_2	5.44	5.32	4.55	3.74	5.54	3.27	6.51	4.10
Sc_2O_3	1.11	1.08	0.93	0.83	0.81	0.84	0.80	0.45
MnO	7.74	7.56	7.88	8.94	4.55	6.27	4.61	6.56
FeO	11.54	11.57	11.31	10.03	14.46	13.68	13.14	12.53
Y_2O_3	0.09	0.10	0.06	0.05	0.00	0.00	0.00	0.00

Nb_2O_5	66.52	67.45	68.29	69.83	61.02	66.08	65.26	67.99
SnO_2	0.28	0.26	0.19	0.13	0.29	0.19	0.34	0.17
Ta_2O_5	4.86	4.90	5.06	5.24	11.58	9.44	5.20	7.25
WO_3	1.11	0.80	1.20	0.70	1.11	0.21	1.20	0.40
Nd_2O_3	0.00	0.08	0.06	0.05	0.00	0.00	0.00	0.00
Sm_2O_3	0.00	0.00	0.00	0.00	0.00	0.00	0.00	0.00
Gd_2O_3	0.05	0.10	0.09	0.05	0.00	0.00	0.00	0.00
Dy_2O_3	0.00	0.00	0.00	0.00	0.00	0.00	0.00	0.00
Yb_2O_3	0.00	0.00	0.00	0.00	0.00	0.00	0.00	0.00
ThO_2	0.00	0.00	0.00	0.00	0.00	0.00	0.00	0.00
UO_2	0.81	0.80	0.22	0.20	0.29	0.09	0.30	0.25
TOT	99.79	100.26	100.05	99.93	99.98	100.37	97.68	99.93
			Formula proportions normalized to 6 oxygen atoms					
p.f.u.								
Mg	0.02	0.02	0.02	0.01	0.03	0.03	0.03	0.02
Ca	0.02	0.00	0.00	0.00	0.00	0.00	0.00	0.00
Ti	0.23	0.22	0.19	0.16	0.24	0.14	0.28	0.18
Sc	0.05	0.05	0.05	0.04	0.04	0.04	0.04	0.02
Mn	0.37	0.36	0.38	0.43	0.22	0.30	0.22	0.32
Fe	0.55	0.54	0.53	0.47	0.70	0.66	0.63	0.60
Y	0.00	0.00	0.00	0.00	0.00	0.00	0.00	0.00
Nb	1.7	1.71	1.74	1.78	1.59	1.71	1.69	1.75
Sn	0.01	0.01	0.00	0.00	0.01	0.00	0.01	0.00
Ta	0.07	0.07	0.08	0.08	0.18	0.15	0.08	0.11
W	0.02	0.01	0.02	0.01	0.02	0.00	0.02	0.01
Nd	0.00	0.00	0.00	0.00	0.00	0.00	0.00	0.00
Sm	0.00	0.00	0.00	0.00	0.00	0.00	0.00	0.00
Gd	0.00	0.00	0.00	0.00	0.00	0.00	0.00	0.00
Dy	0.00	0.00	0.00	0.00	0.00	0.00	0.00	0.00
Yb	0.00	0.00	0.00	0.00	0.00	0.00	0.00	0.00
Th	0.00	0.00	0.00	0.00	0.00	0.00	0.00	0.00
U	0.01	0.01	0.00	0.00	0.01	0.00	0.00	0.00
Cation Sum	3.05	3.00	3.01	2.98	3.04	3.03	3.00	3.01
Y+REE	0.00	0.00	0.00	0.00	0.00	0.00	0.00	0.00
Ca+U+Th	0.03	0.01	0.00	0.00	0.01	0.00	0.00	0.00
U	0.01	0.01	0.00	0.00	0.01	0.00	0.00	0.00
Nb+Ta+Ti+W	2.02	2.01	2.03	2.03	2.03	2.00	2.07	2.05
Mn/(Mn+Fe)	0.40	0.40	0.42	0.37	0.24	0.31	0.26	0.35
Ta/(Ta+Nb)	0.04	0.04	0.04	0.04	0.10	0.08	0.04	0.06

4.1.9 Garnet Codera dike: mineral-chemistry of U-rich euxenite-(Y) and euxenite-(Y)

U-rich euxenite-(Y) and euxenite-(Y) at Codera dike occurs as black, reddish-brown, platy or prismatic crystals with conchoidal vitreous fracture up to 1 centimeter in length embedded in K-feldspar. Sample G1 consists of U-rich euxenite-(Y) and is rather heterogeneous in composition. The core has Nb_2O_5 up to 37.3 wt %, UO_2 up to 20.82 wt%, Y_2O_3 up to 6.74 wt %. The border zone of the crystal displays Nb_2O_5 up to 34.97 wt %, UO_2 up to 15.87 wt%, Y_2O_3 up to 8.58 wt %. Sample G1 is enriched with LREE and HREE and displays sensible contents in SnO_2 (up to 1.34 wt%) and WO_3 (up to 1.80 wt %). Sample G4 consists of euxenite-(Y) and is rather homogenous in composition. The core of the crystal has Nb_2O_5 up to 37.45 wt %, UO_2 up to 11.65 wt%, Y_2O_3 up to 9.97 wt %. The border of the crystal has Nb_2O_5 up to 34.94 wt %, UO_2 up to 10.82 wt%, Y_2O_3 up to 10.12 wt %. G4 sample is also enriched with LREE and HREE and displays sensible contents in SnO_2 (up to 1.99 wt%) and WO_3 (up to 1.85 wt %).

Table 4.9 Garnet Codera dike representative compositions of U-rich euxenite-(Y) and euxenite-(Y)

Elements Wt%	Garnet Codera G1 patches U-rich euxenite-(Y)	Garnet Codera G1 U-rich euxenite-(Y)	Garnet Codera G4 core Euxenite-(Y)	Garnet Codera G4 int Euxenite-(Y)	Garnet Codera G4 rim Euxenite-(Y)
MgO	0.11	0.09	0.12	0.16	0.08
CaO	0.21	0.26	0.32	0.26	0.36
TiO_2	3.77	3.98	3.78	4.16	4.11
Sc_2O_3	0.36	0.66	0.79	0.89	1.37
MnO	1.31	1.11	1.16	1.19	1.48
FeO	8.9	9.03	8.25	8.27	7.64
Y_2O_3	6.74	8.58	9.89	9.97	10.12
Nb_2O_5	37.3	34.97	37.45	36.16	34.94
SnO_2	1.34	1.06	1.30	1.24	1.99
Ta_2O_5	10.5	14.01	14.02	14.03	16.79
WO_3	0.70	1.80	1.88	1.85	1.75
Nd_2O_3	1.18	1.12	1.32	1.15	1.31
Sm_2O_3	0.84	0.67	0.51	0.55	0.59
Gd_2O_3	1.34	1.13	1.10	1.14	1.12
Dy_2O_3	1.28	0.89	0.45	0.57	0.62
Yb_2O_3	0.56	1.01	0.82	0.92	0.58
ThO_2	1.75	1.59	1.60	1.65	1.55
UO_2	20.82	15.87	11.65	11.74	10.82
TOT	99.01	97.83	96.41	95.87	97.22
	Formula proportions normalized to 6 oxygen atoms				
p.f.u.					
Mg	0.00	0.00	0.00	0.00	0.00
Ca	0.02	0.02	0.02	0.02	0.03
Ti	0.20	0.21	0.20	0.22	0.22
Sc	0.02	0.04	0.05	0.05	0.08
Mn	0.08	0.07	0.07	0.07	0.09
Fe	0.53	0.54	0.49	0.49	0.45
Y	0.26	0.33	0.37	0.38	0.38
Nb	1.21	1.13	1.19	1.16	1.11
Sn	0.04	0.03	0.04	0.04	0.06
Ta	0.20	0.27	0.27	0.27	0.32
W	0.01	0.03	0.03	0.03	0.03
Nd	0.03	0.03	0.03	0.03	0.03
Sm	0.02	0.02	0.01	0.01	0.01
Gd	0.03	0.03	0.02	0.03	0.03
Dy	0.03	0.02	0.01	0.01	0.01
Yb	0.01	0.02	0.02	0.02	0.01
Th	0.03	0.03	0.03	0.03	0.02
U	0.33	0.25	0.18	0.19	0.17
Cation Sum	3.05	3.07	3.03	3.05	3.05
Y+REE	0.38	0.45	0.46	0.48	0.47
Ca+U+Th	0.38	0.30	0.23	0.24	0.22
U	0.33	0.25	0.18	0.19	0.17
Nb+Ta+Ti+W	1.62	1.64	1.69	1.68	1.68
Mn/(Mn+Fe)	0.13	0.11	0.12	0.12	0.17
Ta/(Ta+Nb)	0.14	0.19	0.18	0.19	0.22

4.1.10 Backscatter images of niobium- tantalum- yttrium- rare-earths-uranium oxides

Backscatter images (BES) were collected at the Museum of Natural History of Milan on thin sections, carbon coated, using SEM JEOL-5600 LV operating at low vacuum conditions at 20 KeV, 15ηPa under 50-200X magnify.

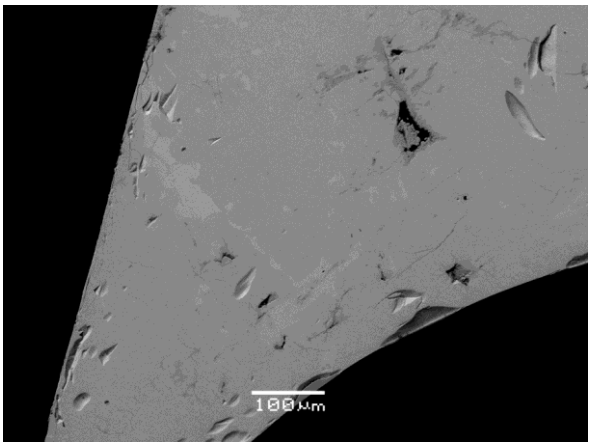

Sample G1. Backscatter image of euxenite-(Y) from Garnet Codera pegmatite dike. The picture shows brighter light gray portions within the crystal in form of patches which are composed of U-rich euxenite-(Y). The darker grey portion is composed of euxenite-(Y) with lower Nb, REE and U contents.

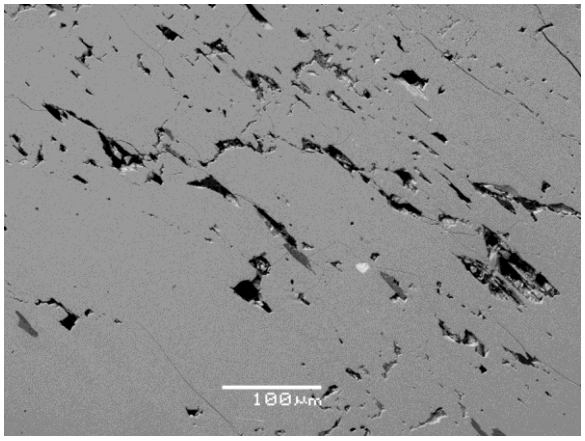

Sample G2. Backscatter image of columbite-(Fe) from Garnet Codera pegmatite dike. The brighter light gray patches, few microns in length, are composed of euxenite-(Y) which appear to be exsolution within the dark grey mass composed of Sc-bearing columbite-(Fe).

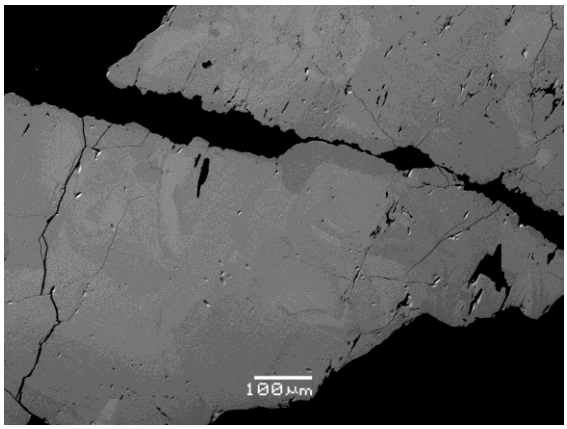

Sample G3. Backscatter image of columbite-(Fe) from Garnet Codera pegmatite dike. The crystal shows lighter and darker gray patches and zoned areas. The darker portions are richer in Nb and Fe whereas the light grey areas are richer in Ta and Mn.

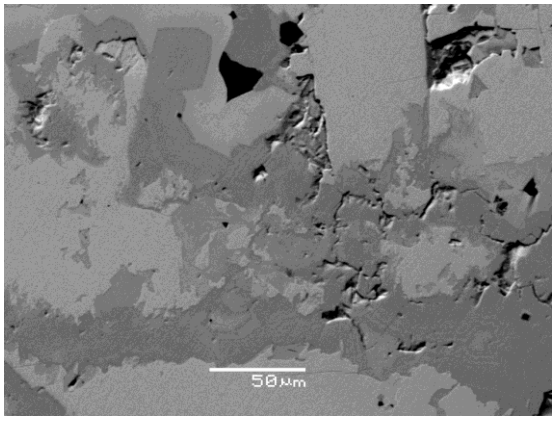

Sample G6. Backscatter image of tapiolite-(Fe) and microlite from Rio Graia pegmatite dike. The portion of the crystal is composed of light gray areas of tapiolite-(Fe) and darker gray zoned patches of microlite exsolutions which replace tapiolite-(Fe).

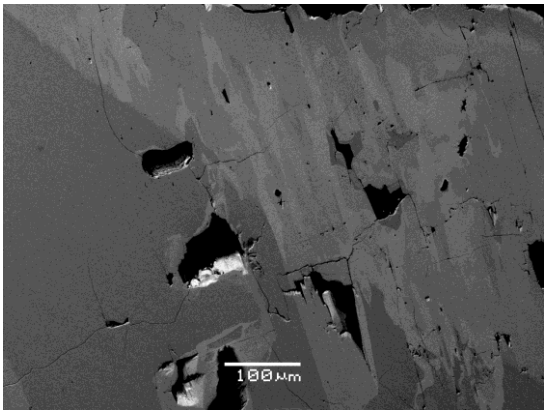

Sample G6. Backscatter image of tantalite-(Fe) and columbite-(Fe) from Rio Graia pegmatite dike. The image shows different gray tonalities where the lighter gray portion is tantalite-(Fe) the medium gray is

tantalite-(Fe) with higher niobium content whereas the darker gray is composed of columbite-(Fe) with high Ta content.

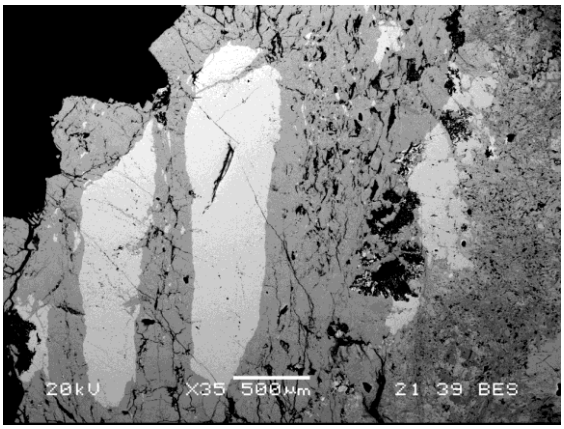

Sample PZ19. Backscatter image of tapiolite-(Fe) and ferrowodginite from Alpe Rosso-Pizzo Marcio albitized pegmatite dikes. The brighter gray area is tapiolite-(Fe), partially replaced by dark gray microlite. Patchy and fine-grained ferrowodginite (darker areas on the right of the image) are invaded by microlite Replacement process of microlite after tapiolite-(Fe) could follow a reaction scheme similar to the diagrams reported by Lumpkin & Ewing (1992) where:

$0.5H_2O + Ca^{2+} + FeTa_2O_6 \rightarrow H^+ + Fe^{2+} + CaTa_2O_{6.5}$

tapiolite-(Fe) microlite

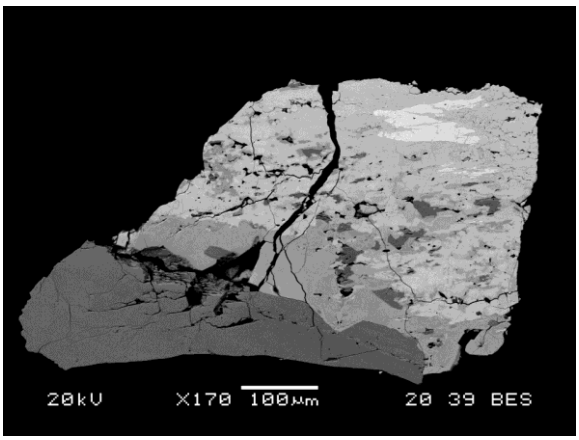

Sample PZ12 and PZ17. Backscatter image of fersmite tantalite-(Mn)and microlite from Alpe Rosso-Pizzo Marcio albititzed pegmatite dikes The brighter area in the upper portion of the back-scattered image contains relics of tantalite-(Mn) replaced by microlite with different grey tones characterized by variable Nb/Ta values whereas darker gray areas is composed of fersmite overgrown on microlite. Replacement process follow a reaction scheme similar to the diagrams reported by Lumpkin & Ewing (1992) where:

$0.5H_2O + Ca^{2+} + Mn(Ta,Nb)_2O_6 \rightarrow H^+ + Mn^{2+} + Ca(Ta,Nb)_2O_{6.5} \rightarrow 0.5H_2O + Mn^{2+} + Ca(Ta,Nb)_2O_6$

tantalite-(Mn) microlite fersmite

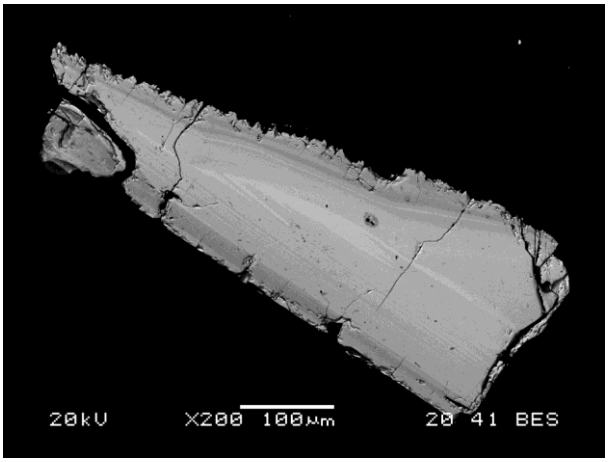

Sample PZ18. Backscatter image of vigezzite Alpe Rosso-Pizzo Marcio albitized pegmatite dikes. Vigezzite has fine oscillatory zoning, characterized by Th–REE enrichment in the core of the crystal.

4.2 Tourmalines in the pegmatites of the Central Alps

4.2.1 Prewiev

Tourmaline group minerals are common accessory minerals in pegmatites. These minerals can origin comb-structured fringes; they develop perpendicular to the dike direction and develop toward the wall-intermediate zone of the pegmatites. Massive replacement of host rock by tourmalinization may also occur around highly fractionated pegmatites (Novák, 2000a; Černý, 2005). Tourmaline cemented breccia represent another type of occurrence for this borosilicate. There are several examples of pneumatolitic stages where tourmaline form fine-grained cement composed of massive granular tourmaline, sometimes is associated with polymetallic ore deposits (Fletcher, 1977). Tourmaline breccias in pegmatites were also described by London (2008) for White Picacho district pegmatites. Perhaps in this case the structures London describes more resemble graphic tourmaline intergrowths than cemented breccia tourmalines. Many Li-bearing pegmatites have black tourmaline fringes at the core margins which evolve toward coloured Li-dominant tourmaline in the core zone or in the miarolitic pockets in gem bearing pegmatites. In this latter case tourmalines tend to develop in miarolitic pockets color zoning textures perpendicular to the c-axis of the crystal. The crystal-chemistry and classification of tourmaline have been revised and redefined by Novák et al., (2009) Tourmaline is an acentric rhombohedral (*R*3*m* space group) borosilicate with the general chemical formula $XY_3Z_6(T_6O_{18})(BO_3)_3V_3W$ (Hawthorne and Henry 1999). This simplified general formula makes no assumptions about site occupancy. Relative crystallographic site occupancies of anions and cations are subdivided into the following without taking into consideration relative abundances of individual ions:

X-site: Na, K, Ca

Y-site: Li, Al, Mg, Ti, V, Cr, Mn, Fe^{2+}, Fe^{3+}, Co, Ni, Cu, Zn

Z-site: Al, Mg, V, Cr, Fe^{3+}

T-site. B, Al, Si

B-site: B

V-site : OH, O

W-site : OH, O, F

The number of currently recognized and plausible tourmaline species is potentially large. To simplify the classification and the number of species in the potential list are included only those tourmalines which occur more commonly or were described more frequently in literature (Table 4.10). In the table 4.11 the occurrence of tourmaline in pegmatites from Central Alps is also reported and figures 4.6 to 4.8 give crystal-chemical classification of selected tourmaline compositions.

Table 4.10 Tourmaline classification

Name	**Chemical Formula**
Buergerite	$Na\ Fe^{3+}_3\ Al_6\ Si_6O_{18}\ (BO_3)_3\ (O)_3\ (OH)$
Dravite	$Na\ Mg_3\ Al_6\ Si_6O_{18}\ (BO_3)_3\ (OH)_3\ (OH)$
Elbaite	$Na\ Li^{1+}_{1.5}Al^{3+}_{1.5}\ Al_6\ Si_6O_{18}\ (BO_3)_3\ (OH)_3\ (OH)$
Fluor-elbaite	$Na\ Li^{1+}_{1.5}Al^{3+}_{1.5}\ Al_6\ Si_6O_{18}\ (BO_3)_3\ (OH)_3\ (F)$
Fluor-rossmanite	$\square\ Li^{1+}Al^{3+}_2\ Al_6\ Si_6O_{18}\ (BO_3)_3\ (OH)_3\ (F)$
Fluor-schorl	$Na\ Fe^{2+}_3Al_6\ Si_6O_{18}\ (BO_3)_3\ (OH)_3\ (F)$
Foitite	$\square\ Fe^{2+}_2Al^{3+}\ Al_6\ Si_6O_{18}\ (BO_3)_3\ (OH)_3\ (OH)$
Liddicoatite	$Na\ Li^{1+}_2Al^{3+}\ Al_6\ Si_6O_{18}\ (BO_3)_3\ (OH)_3\ (OH)$
Olenite	$Na\ Al_3\ Al_6\ Si_6O_{18}\ (BO_3)_3\ (O)_3\ (OH)$
Povondraite	$Na\ Mg_2\ Fe^{3+}\ Fe_6^{3+}\ Si_6O_{18}\ (BO_3)_3\ (OH)_3\ (O)$
Rossmanite	$\square\ Li^{1+}Al^{3+}_2\ Al_6\ Si_6O_{18}\ (BO_3)_3\ (OH)_3\ (OH)$
Schorl	$Na\ Fe^{2+}_3\ Al_6\ Si_6O_{18}\ (BO_3)_3\ (OH)_3\ (OH)$
Uvite	$Ca\ Mg_3\ MgAl_5\ Si_6O_{18}\ (BO_3)_3\ (OH)_3\ (OH)$

Table 4.11 Distribution of tourmalines in the pegmatites of Central Alps

Sigle	Locality	Name
F	Grignaschi	Schorl
C	Rio Graia	Schorl (rare)
H	Pizzo Marcio-Alpe Rosso	Dravite, dravite-schorl, schorl
D	Arvogno fluorite dike	
E	Arvogno Albertini dike	
P	Summit Paglia dike	Schorl
R	Colonnello Paglia dike	Schorl
W	Bodengo road cut dike	
A	Garnet Codera dike	Schorl (rare)
B	Phospahte Codera dike	Mn-rich elbaite, Mn-rich Fluor-elbaite, Mn-rich elbaite-schorl

4.2.2 Pizzo Marcio-Alpe Rosso dikes: mineral-chemistry of dravite and schorl

Tourmaline crystals from Emerald pegmatite of Pizzo Marcio are brownish black centimetric crystals, embedded in massive albite (PZT1), bluish to dark green millimetric prisms, lining sets of fractures cross-cutting the albitized pegmatite associated with tremolite (PZT2), and bluish green idiomorphic crystals, lining the secondary cavities of the wall-intermedate albitized pegmatite zone (PZT3). The tourmaline in samples PZT1, PZT2 and PZT3 compositionally vary from schorl–dravite (PZT1) to Fe-rich dravite (PZT2) and dravite (PZT3) (Table 4.12). The basis for the formula calculation was taken from Hawthorne et al. (1993); cation site-occupancies of an aluminum–magnesium-disordered dravite was assigned. This means that a distinct amount of Mg was assigned to the Y-site, and no Fe^{3+} value was calculated on the basis of stoichiometry to fill the Y-site. Fe_2O_3, FeO, B_2O_3, Li_2O, and H_2O contents were calculated by stoichiometry. Calculation of site occupancies were made with B=3 *p.f.u.*; Li=3 *p.f.u.* - ΣY-site; OH+F=4 *p.f.u.* Sample PZT1 has Fe/Mg value decreasing slightly toward the rim of the crystal (PZT1b). Sample PZT2 shows a higher Mg content (up to 11.07 wt%) and a significant Cr content (up to 0.37 wt% Cr2O3). Sample PZT3 has the highest Mg content (up to 12.06 wt% MgO), and a significant Ca content (up to 1.66 wt% CaO). Unit-cell parameters of the Fe-rich dravite obtained by collecting single-crystal data correspond to a trigonal cell with *a* 15.959(2), *c* 7.2210(10) Å.

Table 4.12 Representative compositon of dravite-schorl from Emerald Pizzo Marcio dike

	Emerald-Pizzo Marcio	**Emerald-Pizzo Marcio**	**Emerald-Pizzo Marcio**	**Emerald-Pizzo Marcio**
	PZT1a	**PZT1b**	**PZT2**	**PZT3**
Elements Wt%	Dravite-schorl	Dravite	Dravite	Dravite
Si_2O wt%	36.14	36.66	36.87	35.55
TiO_2	0.08	0.10	0.05	0.17
B_2O_3*	10.39	10.57	10.75	10.59
Al_2O_3	29.55	30.35	28.90	27.72
Fe_2O_3*	1.47	0.95	4.46	6.58
MgO	5.75	6.32	11.07	12.06
CaO	0.32	0.37	1.29	1.66
MnO	0.21	0.16	0.06	0.00
FeO*	10.01	9.50	1.01	0.00
Cr_2O_3	0.00	0.00	0.37	0.21
Li_2O*	0.20	0.16	0.19	0.00
Na_2O	2.63	2.55	2.25	1.74
H_2O*	3.59	3.65	3.71	3.66
F	0.00	0.00	0.00.	0.00
Sum	100.34	101.34	100.98	99.94
	Formula proportions normalized to 31 oxygen atoms			
X-site				
□	0.09	0.12	0.08	0.16
Ca	0.06	0.07	0.22	0.29
Na	0.85	0.81	0.70	0.55
Sum	1.00	1.00	1.00	1.00
Y-site				
Al	0.00	0.00	0.00	0.00
Ti	0.01	0.01	0.01	0.02
Mg	1.43	1.55	2.67	2.95
Mn	0.03	0.02	0.01	0.00
Fe^{2+}	1.40	1.31	0.14	0.00
Cr	0.00	0.00	0.05	0.03
Li	0.13	0.11	0.12	0.00
Sum	3.00	3.00	3.00	3.00
Z-site				
Al	5.82	5.88	5.46	5.19
Fe^{3+}	0.18	0.12	0.54	0.81
Sum	6.00	6.00	6.00	6.00
T-site				
Si	6.04	6.03	5.96	5.83
Al	0.00	0.00	0.04	0.17
Sum	6.04	6.03	6.00	6.00
B-site				
B	3.00	3.00	3.00	3.00
Sum	3.00	3.00	3.00	3.00
V_3+W-site				
OH	4.00	4.00	4.00	4.00
F	0.00	0.00	0.00	0.00
Sum	4.00	4.00	4.00	4.00

4.2.3 Colonnello Pizzo Paglia dike: mineral-chemistry of schorl

Schorl crystals from Colonnello pegmatite for the study were collected in the core zone of the dike lining the bottom of a miarolitic pocket associated with albite var.cleavelandite quartz, microcline, beryl aquamarine and lithiowodginite. Schorl crystals reach up to 4 centimeters in length and growth free-standing into the pocket. The tourmaline in sample R5 compositionally is schorl vacant at the X-site (up to 0.36 *p.f.u.*) has negligible MgO content up to 0.44 wt %. B_2O_3, Li_2O, and H_2O contents were calculated by stoichiometry whereas F contents was not measured (Table 4.13).

Table 4.13 Schorl from Colonnello dike

	Colonnello Pizzo-Paglia
	R5
Elements Wt%	
Si_2O wt%	35.62
TiO_2	0.11
B_2O_3*	10.25
Al_2O_3	34.34
Fe_2O_3	0.00
MgO	0.44
CaO	0.11
MnO	0.15
FeO	14.30
Cr_2O_3	0.00
Li_2O*	0.00
Na_2O	1.83
H_2O*	2.90
F	n.a.
Sum	100.12
Normalized to 31 oxygen atoms	
X-site	
□	0.36
Ca	0.02
Na	0.60
Sum	1.00
Y-site	
Al	0.86
Ti	0.01
Mg	0.11
Mn	0.02
Fe^{2+}	2.03
Cr	0.00
Li	0.00
Sum	3.03
Z-site	
Al	6.00
Fe^{3+}	0.00
Sum	6.00
T-site	
Si	6.03
Al	0.00
Sum	6.03
B-site	
B	3.00
Sum	3.00
V_3+W-site	
OH	3.28
F	n.a.
Sum	3.28

4.2.4 Phosphate Codera dike: mineral-chemistry of Mn-rich elbaite, Mn-rich Fluor-elbaite, Mn-rich schorl-elbaite

The border zone of Phopshate Codera dike is composed of albite with subordinate quartz with saccarohidal grained texture. This portion of the pegmatite contains Mn-rich dark green-yellow elbaite crystals with black schorl core up to several centimeters in length aassociated with a pure end-member F-rich triplite and colorless to pale pink hexagonal prisms of beryl. All tourmalines analyzed have high Mn content up to 5.80 wt % corresponding to 0.83 p.f.u. occupancy at the Y-site (Tables 4.14 and 4.15). Tourmaline composition include Mn-rich elbaite, Mn-rich Fluor-elbaite, Mn-rich schorl-elbaite. The basis for the formula calculation

was taken from Ertl et al. (2003). B_2O_3, Li_2O and H_2O were calculated by stoichiometry whereas fluorine *Kα* line interferes with Fe and Mn*Lα* lines, requiring a correction for the measured F values as follows: F = F meas – (–0.000055 FeO2 + 0.0889 FeO – 0.0044) + 0.015 MnO (Kalt et al. 2001).

Table 4.14 Mn-rich elbaite, Mn-rich Fluor-elbaite, Mn-rich schorl-elbaite from Phosphate Codera dike

	Phosphate Codera	**Phosphate Codera**	**Phosphate Codera**	**Phosphate Codera**	**Phosphate Codera**	**Phosphate Codera**	**Phosphate Codera**	**Phosphate Codera**
	3grandec	**3grandef**	**3grandeg**	**1basaleb**	**1basalec**	**1basalee**	**1basalef**	**1basale**
Elements Wt%								
Si_2O wt%	32.98	34.87	34.14	33.86	32.38	33.27	32.84	32.24
TiO_2	0.25	0.13	0.24	0.25	0.24	0.23	0.18	0.08
B_2O_3*	10.44	10.78	10.42	10.71	10.28	10.48	10.35	10.24
Al_2O_3	39.64	40.28	38.45	41.14	38.31	39.25	38.70	38.19
Fe_2O_3	0.00	0.00	0.00	0.00	0.00	0.00	0.00	0.00
MgO	0.10	0.08	0.23	0.09	0.22	0.18	0.22	0.18
CaO	0.04	0.04	0.03	0.17	0.10	0.07	0.07	0.15
MnO	5.03	4.90	4.62	4.45	3.32	3.79	3.31	3.53
FeO	2.09	1.61	1.72	2.37	6.21	6.12	6.43	6.90
ZnO	0.00	0.00	0.00	0.00	0.00	0.00	0.00.	0.00
Li_2O*	1.03	1.27	1.16	1.03	0.61	0.57	0.58	0.47
Na_2O	2.42	2.95	2.37	2.34	2.20	1.96	2.00	2.03
K_2O	0.00	0.00	0.00	0.00	0.00	0.00	0.00	0.00
H_2O*	3.03	3.30	2.91	3.22	3.22	3.29	3.29	3.18
F	1.40	0.91	1.45	1.02	0.68	0.71	0.61	0.74
O=F	-0.59	-0.38	-0.61	-0.43	-0.29	-0.30	-0.26	-0.31
Sum	97.86	100.74	97.13	100.22	97.48	99.62	98.32	97.62
			Formula proportions normalized to 31 oxygen atoms					
X-site								
□	0.21	0.25	0.32	0.24	0.24	0.29	0.31	0.25
Ca	0.02	0.01	0.01	0.01	0.01	0.01	0.01	0.01
Na	0.77	0.74	0.67	0.76	0.75	0.70	0.68	0.75
Sum	1.00	1.00	1.00	1.00	1.00	1.00	1.00	1.00
Y-site								
Al	1.31	1.12	1.31	1.24	1.32	1.04	1.24	1.28
Ti	0.04	0.02	0.03	0.03	0.03	0.02	0.03	0.02
Mg	0.05	0.07	0.05	0.02	0.04	0.09	0.02	0.04
Mn	0.64	0.50	0.68	0.63	0.64	0.51	0.83	0.69
Fe^{2+}	0.28	1.01	0.46	0.43	0.51	1.02	0.43	0.40
Li	0.68	0.19	0.47	0.65	0.46	0.32	0.45	0.57
Sum	3.00	3.00	3.00	3.00	3.00	3.00	3.00	3.00
Z-site								
Al	6.00	6.00	6.00	6.00	6.00	6.00	6.00	6.00
Fe^{3+}	0.00	0.00	0.00	0.00	0.00	0.00	0.00	0.00
Sum	6.00	6.00	6.00	6.00	6.00	6.00	6.00	6.00
T-site								
Si	5.50	5.47	5.45	5.61	5.35	5.58	5.46	5.52
Al	0.50	0.53	0.55	0.39	0.65	0.42	0.54	0.48
Sum	6.00	6.00	6.00	6.00	6.00	6.00	6.00	6.00
B-site								
B	3.00	3.00	3.00	3.00	3.00	3.00	3.00	3.00
Sum	3.00	3.00	3.00	3.00	3.00	3.00	3.00	3.00
V_3+W-site								
OH	3.29	3.63	3.44	3.39	3.61	3.69	3.28	3.41
F	0.71	0.37	0.56	0.61	0.39	0.31	0.72	0.59
Sum	4.00	4.00	4.00	4.00	4.00	4.00	4.00	4.00

Table 4.15 Representative compositions of Mn-rich elbaite, Mn-rich Fluor-elbaite, Mn-rich schorl-elbaite

	Phosphate Codera 1basalea	Phosphate Codera 1basalei	Phosphate Codera 1basalep	Phosphate Codera 1basaleq	Phosphate Codera 1basaler	Phosphate Codera 1basalez	Phosphate Codera 2allunga	Phosphate Codera 3grandea
Elements Wt%								
Si_2O wt%	33.78	32.32	33.20	33.99	32.89	33.19	32.15	33.75
TiO_2	0.32	0.15	0.21	0.23	0.22	0.12	0.20	0.16
B_2O_3*	10.67	10.28	10.57	10.52	10.68	10.33	10.24	10.61
Al_2O_3	40.72	38.36	40.64	39.21	41.62	37.69	38.90	40.26
Fe_2O_3	0.00	0.00	0.00	0.00	0.00	0.00	0.00	0.00
MgO	0.22	0.27	0.21	0.09	0.18	0.35	0.07	0.16
CaO	0.09	0.03	0.04	0.02	0.04	0.05	0.04	0.01
MnO	4.63	3.47	4.86	4.52	4.62	3.58	5.80	4.97
FeO	2.07	7.12	3.36	3.09	3.75	7.24	3.05	2.89
ZnO	0.00	0.00	0.00	0.00	0.00	0.00	0.00	0.00
Li_2O*	1.04	0.27	0.71	0.98	0.70	0.47	0.66	0.86
Na_2O	2.44	2.27	2.09	2.37	2.39	2.15	2.08	2.37
K_2O	0.00	0.00	0.00	0.00	0.00	0.00	0.00	0.00.
H_2O*	3.03	3.22	3.14	3.08	3.33	3.29	2.90	3.13
F	1.38	0.70	1.07	1.17	0.76	0.59	1.34	1.14
O=F	-0.58	-0.29	-0.45	-0.49	-0.32	-0.25	- 0.56	- 0.48
Sum	99.81	98.14	99.65	98.78	100.86	98.80	96.87	99.83
			Formula proportions normalized to 31 oxygen atoms					
X-site								
□	0.21	0.25	0.32	0.24	0.24	0.29	0.31	0.24
Ca	0.02	0.01	0.01	0.00	0.01	0.01	0.01	0.01
Na	0.77	0.74	0.67	0.76	0.75	0.70	0.68	0.75
Sum	1.00	1.00	1.00	1.00	1.00	1.00	1.00	1.00
Y-site								
Al	1.31	1.12	1.31	1.24	1.32	1.04	1.24	1.28
Ti	0.04	0.02	0.03	0.03	0.03	0.02	0.03	0.02
Mg	0.05	0.07	0.05	0.02	0.04	0.09	0.02	0.04
Mn	0.64	0.50	0.68	0.63	0.64	0.51	0.83	0.69
Fe^{2+}	0.28	1.01	0.46	0.43	0.51	1.02	0.43	0.40
Li	0.68	0.19	0.47	0.65	0.46	0.32	0.45	0.57
Sum	3.00	3.00	3.00	3.00	3.00	3.00	3.00	3.00
Z-site								
Al	6.00	6.00	6.00	6.00	6.00	6.00	6.00	6.00
Fe^{3+}	0.00	0.00	0.00	0.00	0.00	0.00	0.00	0.00
Sum	6.00	6.00	6.00	6.00	6.00	6.00	6.00	6.00
T-site								
Si	5.50	5.47	5.45	5.61	5.35	5.58	5.46	5.52
Al	0.50	0.53	0.55	0.39	0.65	0.42	0.54	0.48
Sum	6.00	6.00	6.00	6.00	6.00	6.00	6.00	6.00
B-site								
B	3.00	3.00	3.00	3.00	3.00	3.00	3.00	3.00
Sum	3.00	3.00	3.00	3.00	3.00	3.00	3.00	3.00
V_3+W-site								
OH	3.29	3.63	3.44	3.39	3.61	3.69	3.28	3.41
F	0.71	0.37	0.56	0.61	0.39	0.31	0.72	0.59
Sum	4.00	4.00	4.00	4.00	4.00	4.00	4.00	4.00

4.3 Phosphates

4.3.1 Triplite of the Phosphate Codera dike

A number of phosphate including Mn-rich graftonite, $(Ca,Mn)(Fe,Mn)_2(PO_4)^2$, ferrisicklerite, $Li_{1-x}(Fe^{3+},Mn^{2+})PO_4$, manganoan apatite, Ca,Mn2+,Fe2+Mg)(PO4)3Cl, staněkite, Fe3+Mn2+O(PO4) and Mn-rich vivianite, $(Fe^{2+})_3(PO_4)_2 \cdot 8H_2O$, were described in a granitic pegmatite at Soe` Valley, nearby Gordona

(Central Alps, Italy) by Guastoni et al. (2007). The pegmatite contains several accesory minerals which include Be-silicates and Nb-Ta oxides Guastoni and Grammatica, 2001; Guastoni and Demartin, 2003).

A second occurrence of phosphates in granitic pegmatites in Central Alps is located at the Phosphate Codera dike where an end-member F-rich triplite (Table 4.16), a manganese fluo-phosphate of chemical formula $Mn_2(PO_4)F$, forms black centimetric masses associated with fluorapatite and Mn hydroxides were investigated (Vignola et al., 2012). Triplite occurs in rounded centimetric masses fractured and filled by Mn oxides in the border zone of the pegmatite emebedded in albite with subordinate quartz both with saccarohidal texture. This portion of the pegmatite contains Mn-rich dark green-yellow elbaite with black schorl core crystals and colorless to pale pink hexagonal prisms of beryl. The unit-cell parameters of triplite obtained from the single-crystal data collected correspond to a monoclinic cell with *a* 12.109(2), *b* 6.516(1), *c* 10.117(1) Å, β 106.16 (2)°, they agree well with the cell of triplite reported by Waldrop (1969). Triplite from Codera valley plots close to end-member composition $Mn_2(PO_4)F$, along with triplite found in a tungsten ore at Reagan Mining District (Aurum, White Pine Co., Nevada), described by Hess and Hunt (1913).

Table 4.16

Triplite Phosphate Codera	
	wt%
P_2O_5	32.33
Al_2O_3	0.01
FeO	3.25
MnO	56.68
CaO	2.48
MgO	0.15
Na_2O	0.00
K_2O	0.00
F	8.68
Σ	**103.59**
-O=F	-3.65
total	**99.94**
formula	on 1 P
p.f.u.	
P	1.000
Al	0.000
Fe2+	0.10
Mn	1.75
Ca	0.10
Mg	0.01
Na	0.00
K	0.00
F	1.00
O	3.96

4.4.1 WDS

Electron-microprobe analyses of fersmite, vigezzite, ferrowodginite and tapiolite-(Fe) from Pizzo Marcio-Alpe Rosso were performed on polished samples using an Applied Research Laboratories (ARL) electron microprobe fitted with six wavelength-dispersion spectrometers (WDS) at the National Research Council – IDPA microprobe laboratory, Department of Earth Sciences, Milan. The WDS analyses were performed using an accelerating voltage of 20 kV, a sample current on brass of 15 nA, and a counting time of 10 or 20 s on peak and 5 or 10 s on backgrounds. Pure metals for Nb, Ta, W and Sn, kaersutite for Mg, Ca, Si, Fe, Al, Na, K, Ti, pollucite for Cs, rhodonite for Mn, chromite for Cr, apatite-(CaF)mfor F, and synthetic standards (synthetic uranium oxide for U and synthetic lithium metaborate glasses prepared as specified in Mannucci *et al.* (1986), for REE and Th) were employed. In all the oxides of Nb–Ta examined, the concentrations of Sc, Sr, Y, Zr, Ba, Pb were found to be below the limits of detection (0.01 wt%). The results were processed for matrix effects using a modified version of the magic IV program, and the interference among the REE were corrected as specified by Mannucci *et al.* (1986).

The chemical composition of columbite-tantalite, euxenite-(Y), ferrotapiolite-(Fe) and lithiowodginite from Central Alps pegmatites were determined using a Cameca-Camebax SX50 electron microprobe at the University of Padova operating in wavelength-dispersive mode with a focused beam (~1 μm in diameter), an acceleration voltage of 20 kV, and a beam current of 20 nA, with 10 and 5 s counting times for peak and background, respectively. X-ray counts were converted to oxide wt% using the PAP correction program supplied by Cameca (Pouchou and Pichoir 1985). The following natural and synthetic standards, spectral lines and detector types were used in the analysis: wollastonite (Si*K*α, Ca*K*α, TAP), corundum (Al*K*α, TAP), apatite (P*K*α, TAP), Fe_2O_3 (Fe*K*α, LiF), Zr-Y-REE-silicates (Zr*L*α, Y*L*α, REE*L*α, and Nd*L*β, LiF), synthetic UO_2 and ThO_2 (U*M*α and Th*M*α, PET), metallic Nb (Nb*L*α, PET), and Ta, Sn and W (Ta*L*α Sn*L*α, and W*L*α, LiF).

Triplite chemical composition was determined with quantitative electron microprobe analysis on polished thin section using a JEOL JXA-8200 microprobe in wavelength-dispersive mode at the Earth Sciences Department, University of Milano. The system operated at an accelerating voltage of 15 kV, beam current of 15 nA and counting time of 30 s on the peaks and 10 s on the backgrounds. Minerals (graftonite for P, Fe, Mn and Ca, grossular for Si and Al, K-feldspar for K, forsterite for Mg, omphacite for Na, and apatite for F) were used as standards. The raw data were corrected for matrix effects using the protocol implemented in the JEOL suite of programs.

4.4.2 Single crystal X-ray diffraction

The unit-cell data of vigezzite were collected using an Enraf Nonius CAD-4 single-crystal diffractometer with Mo*K*a X-ray source. The cell data of tapiolite-(Fe) and ferrowodginite were collected with an Area-Detector Bruker SMART CCD single-crystal diffractometer with Mo*K*a X-ray source: both X-ray data were

collected at the Department of Structural Chemistry and Inorganic Stereochemistry of the University of Milan. The unit cell data for Fe-rich dravite were collected using a Nonius Kappa CCD single-crystal diffractometer with Mo*K*α X-ray source at the Institut für Mineralogie und Kristallographie, Geozentrum, Universität Wien, Vienna. Crystallographic data were obtained at room temperature from homogeneous fragments having dimensions of about 0.1 3 0.1 3 0.2 mm.

The unit cell data for triplite were collected using Single-crystal X-ray diffraction data were obtained with an Xcalibur - Oxford Instruments diffractometer equipped with a CCD, using graphite-monocromatized Mo*K*α X-radiation, and operated at 50 kV and 40 mA.

4.5 Diagrams of Nb-Ta-Y-REE-U oxides

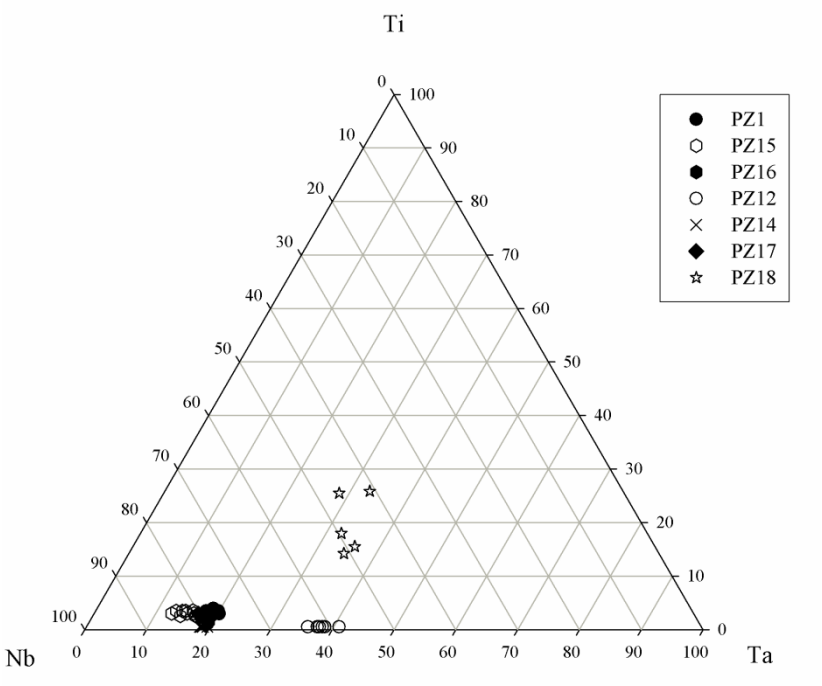

Fig.4.1 Triangular plot of fersmite and vigezzite of Alpe Rosso-Pizzo Marcio albitized pegmatites

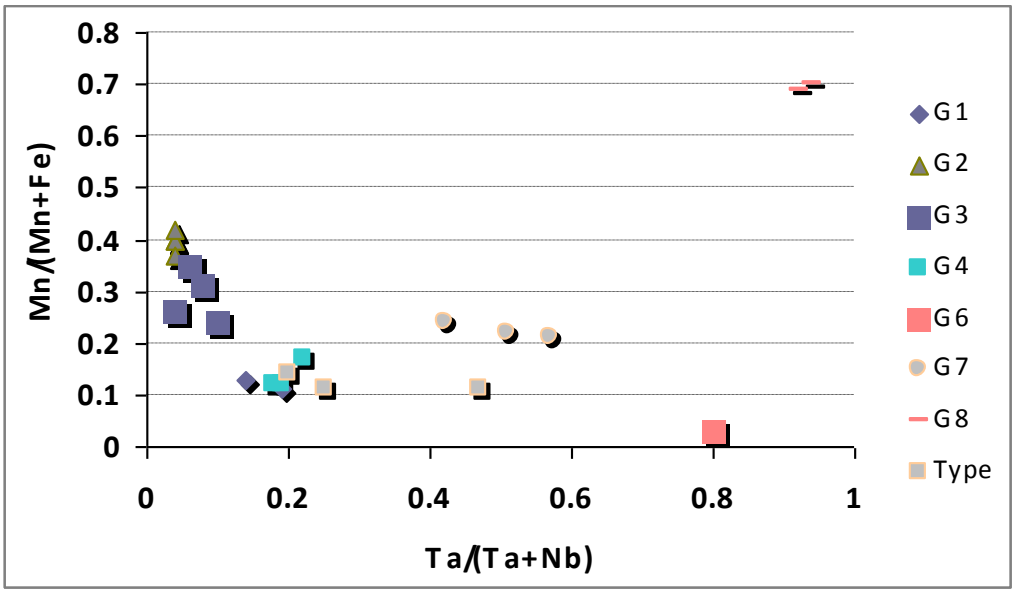

Fig. 4.2 The diagram shows well defined fields for niobo-tantalates of Central Alps pegmatites. They include the first given by columbite-(Fe) (G2 and G3); the second given by aeschynite-(Y) and euxenite-(Y) (G1, G4 and type); the third given by tantalite-(Mn) (G7); the fourth by tapiolite-(Fe) (G6); the fifth by lithiowodginite (G8).

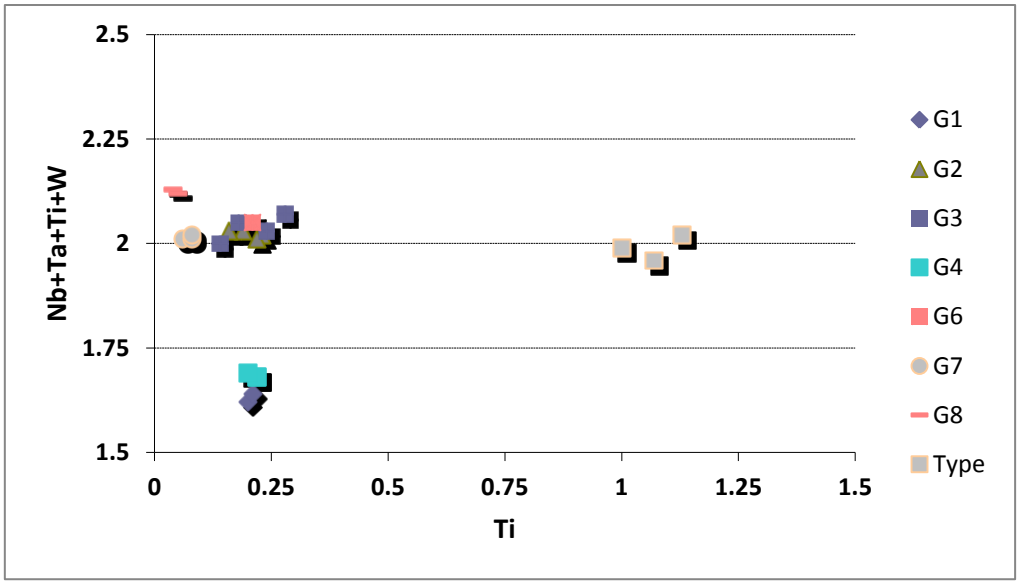

Fig. 4.3 This diagram allows to separate three major fields. The first field, low in titanium and high in niobium and tantalum include columbite-(Fe), tantalite-(Fe), tapiolite-(Fe), and lithiowodginite (G2, G3, G6, G7, G8) The second field, low in titanium include euxenite-(Y) (G1 and G4). The third field, high in titanium, niobium and tantalum, include aeschynite-(Y) (Type).

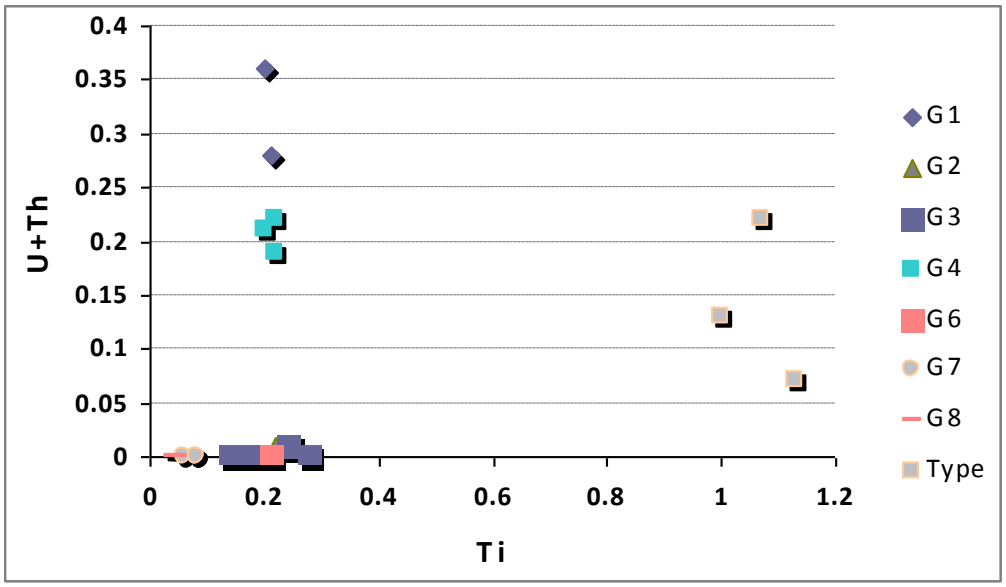

Fig. 4.4 This diagram discriminates euxenite-(Y) with high U and low titanium contents of Codera Garnet pegmatite (G1 and G4) by aeschynite-(Y) of Arvogno pegmatites (Type) characterized by high U and Ti contents. Columbite-(Fe), tantalite-(Fe) lithiowodginite and tapiolite-(Fe) have low Ti and U is absent in the structure of these niobium-tantalates minerals.

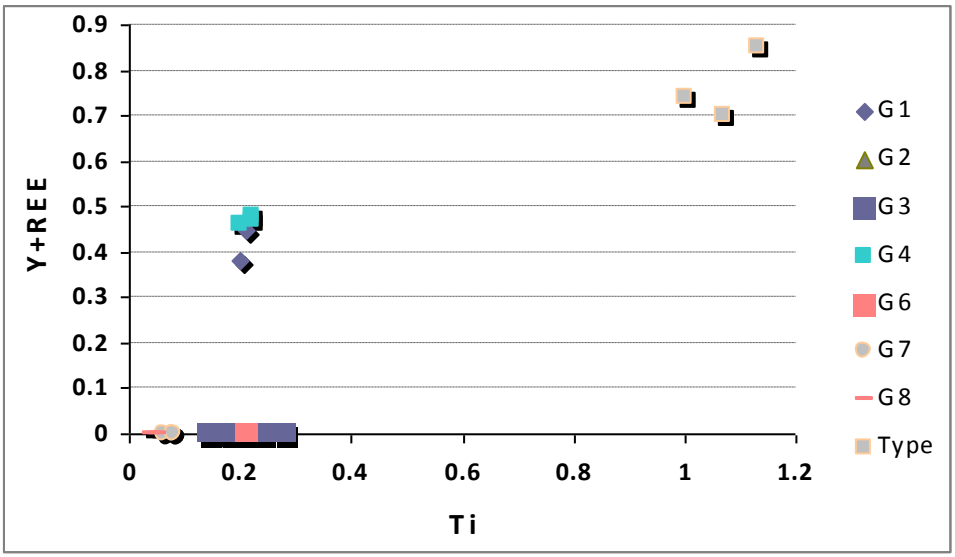

Fig. 4.5 Y+REE versus Ti diagram shows three distinct fields. One characterized by Y and REE absence e and low titanium content which include columbite-(Fe), tantalite-(Fe) lithiowodginite and tapiolite-(Fe). The second has high Y+REE and low Ti content with euxenite-(Y) of Garnet Codera pegmatite. The third is given by higher Y+REE and high Ti content with aeschynite-(Y) of Arvogno pegmatite

4.6 Diagrams of tourmalines

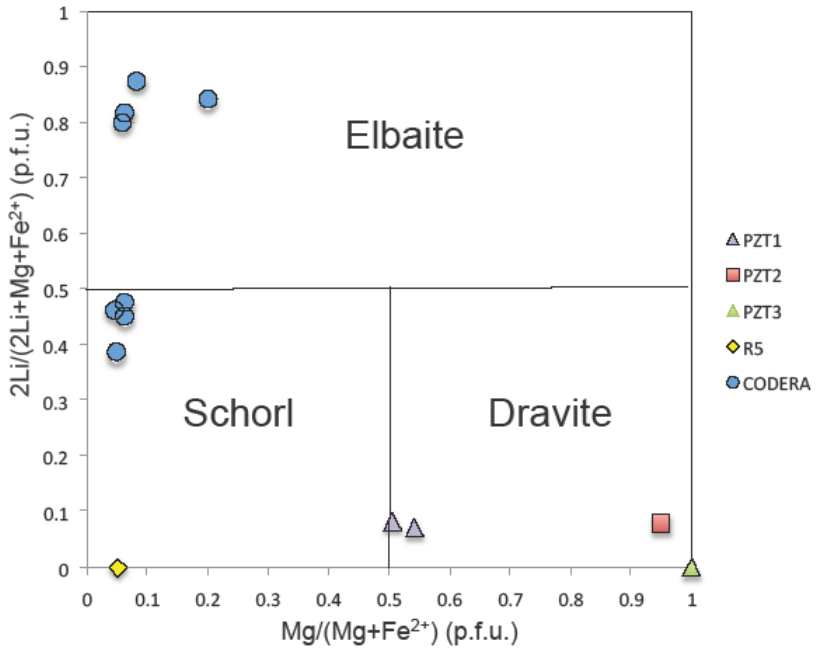

Fig. 4.6 Representative classification of tourmaline from pegmatites of Central Alps

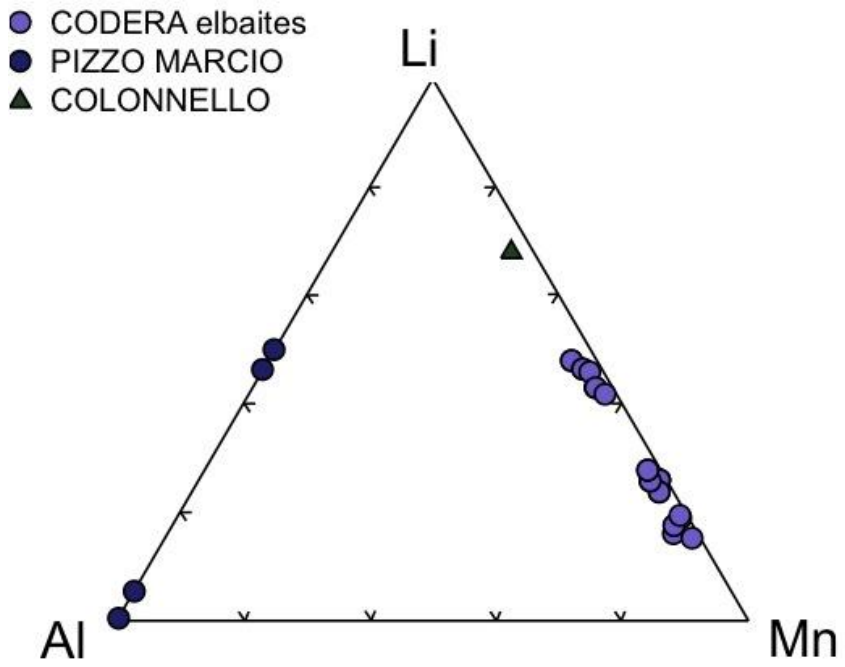

Fig. 4.7 Ternary diagram of Y-site occupancy of selected tourmaline composition from pegmatites of Central Alps

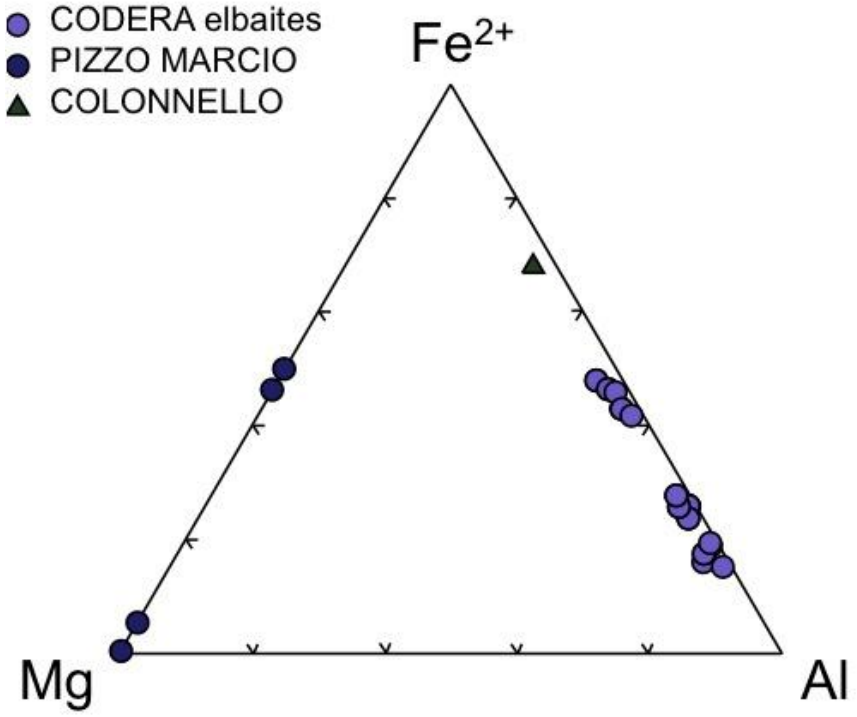

Fig. 4.8 Ternary diagram of Y-site occupancy of selected tourmaline composition from pegmatites of Central Alps

CHAPTER 5

Geochemistry of Masino-Bregaglia intrusion and its surrounding rocks

5.1 Introduction

The Bergell calc-alkaline Oligocene pluton consists of tonalite (also known as serizzo) at the rim and granodiorite (also known as ghiandone) with K-feldspar megacrysts in the core of the intrusion. The southernmost part of the tonalite intrusion has its western part (west of Val Mera or Valle Chiavenna) composed of "Iorio tonalite", whereas the far eastern part as "Southern Bergell tonalite". The Melirolo augengneiss is an intensively solid-state deformed and occasionally mylonitc epidote bearing granodiorite occurs in the southern margin of the Iorio tonalite (Reusser, 1987). Within and around the intrusion several types of small stocks and dikes of gabbro and horneblendite were also distinguished; coarse-grained orthopyroxene-bearing olivine-clinopyroxene horneblendite; fine-medium grained clinopyroxene-horneblende gabbro; pegmatitic-horneblende gabbro. These mafic precursors are considered to represent the early phases of the Masino-Bregalia intrusion (Diethelm, 1985). In the southern-western area of the intrusion (Chiavenna valley) fine-grained 24–25 M.y. Novate granite, a garnet-bearing S-type two-mica leucogranite and the associated aplite, microgranite dike swarms occur and they cross-cut the back-folding nappes and Masino-Bregaglia (Wenk, 1973; Berger et al., 1996).

The western aureola of the intrusion hosts the Gruf Complex. This metamorphic unit predominantly consists of migmatitic quartzo–feldspathic orthogneisses, paragneisses and biotite–sillimanite–garnet–(±cordierite)-bearing metapelitic rocks. Metapelites suffered mid-Tertiary metamorphic conditions of upper amphibolites facies (Bucher-Nurminen and Droop, 1983). According to Berger et al., (1996) and Davison et al., (1996) the paragenetic sequences above mentioned which define the migmatization mostly occurred contemporaneously with, or slightly post-dating, emplacement of the Bergell Pluton (Berger et al., 1996; Davidson et al., 1996).

The Gruf Complex hosts dark Mg–Al-rich sapphirine-bearing granulites granulite rocks, first defined and studied by Cornelius (1916) and Wenk et al. (1974a). Galli et al., (2011) made detailed studies of these rocks and defined the presence of charnockites associated with granulites distributed over the entire Gruf Complex. Granulites are dark, massive, composed of massive sapphirine–orthopyroxene–cordierite–garnet-granulite±spinel or sapphirine-rthopyroxene–sillimanite–cordierite–garnet- granulite±spinel. Charnockites are leucocratic, medium- to coarse-grained and weakly foliated. These rocks are composed of quartz (40%), plagioclase (30%), perthitic alkali feldspar (15%), rounded garnet (5%), brownish orthopyroxene (5%), rare biotite (3%) and ilmenite (1%).

Table 5.1 Representative compositions of pegmatites hosting rocks

	Migmatite Paglia colonnello R4	**Gneiss Grigna F1**	**Gneiss Arvogno fluorite D3**	**Gneiss Arvogno Albertini E4**	**Tonalite Codera granati A4**	**Gneiss Rio Graia C1**
SiO_2	48.82	71.84	75.64	76.22	66.33	71.44
Al_2O_3	21.65	14.29	12.95	12.83	16.46	14.90
Fe_2O_3	9.53	2.99	1.22	0.97	3.94	1.80
MgO	5.38	0.70	0.25	0.18	1.92	0.38
CaO	2.90	1.69	1.04	0.59	3.73	1.18
Na_2O	3.72	4.00	3.81	3.96	4.19	3.67
K_2O	5.01	2.82	4.09	4.27	1.84	5.40
TiO_2	1.06	0.42	0.13	0.09	0.46	0.25
P_2O_5	0.25	0.19	0.03	0.03	0.21	0.15
MnO	0.15	0.05	0.06	0.05	0.08	0.03
LOI	1.2	0.70	0.5	0.5	0.5	0.6
TOTAL	99.67	99.69	99.72	99.69	99.66	99.80
ppm						
Sc	15	8	5	4	11	5
Ba	689	272	137	114	273	620
Be	10	6	7	4	5	4
Cs	40	66	29	8	31	29
Ga	32	20	16	14	20	15
Hf	5	5	4	4	4	3
Nb	10	15	19	20	12	11
Rb	391	258	236	257	199	246
Sn	19	15	7	4	8	9
Sr	258	103	60	52	250	108
Ta	1	2	3	3	1	2
Th	13	14	42	35	14	11
U	6	4	12	6	3	2
V	180	26	8	7	83	16
Zr	23	175	109	84	135	107
Y	37	28	29	32	11	19
La	6	29	29	18	46	22
Ce	13	63	60	41	81	45
Pr	2	8	7	5	8	5
Nd	6	29	24	19	26	21
Sm	2	6	5	4	3	4
Eu	0.31	0.81	0.37	0.30	0.73	0.85
Gd	3	6	5	4	3	4
Tb	1	1	1	1	0	1
Dy	4	5	5	5	2	4
Ho	1	1	1	1	0	1
Er	2	3	2	3	1	2
Tm	1	0	0	1	0	0
Yb	3	3	3	4	1	2
Lu	1	0	0	1	0	0
Mo	0	0	0	0	0	0
Cu	4	3	1	2	14	1
Pb	4	1	2	3	2	3
Zn	115	40	34	21	68	36

Ni	53	3	1	1	8	3
As	0	3	0	0	0	0
Cd	0	0	0	0	0	0
Sb	0	0	0	0	0	0
Bi	0	0	0	0	0	1

5.2 Geochemical diagrams

In this paragraph are presented a serie of diagrams which relates the geochemical characters of Masino-Bregaglia intrusion and its surroundings rocks within the studied area. Geochemical data of the various rock types of the Masino-Bregaglia intrusion and its surrounding rocks were plot together with the bulk compositions of the pegmatite dikes. The source data for Masino-Bregaglia intrusive rocks were taken from the bibliography of Richardson et al., (1976), Wenk et al., (1997) and von Blanckenburg et al., (1992). The geochemical data on granulite and charnockites were taken from Galli et al., (2010) whereas bulk compositions of pegmatites are taken from samples collected by the author on the field. Source data from bibliography suffer limitation due the fact heterogenous data of Masino-Bregaglia rocks were published. In particular trace elements and rare earths elements of granitoid rocks only exist those from the work published by von Blanckenburg et al., (1992).

5.2.1 AFM

In the AFM ternary diagram the plots of tonalite (except for few dispersed samples), granodiorite and granite define a well constrained calc-alkaline trend for the Oligocenic Masino-Bregaglia intrusion. Microgranites dikes, aplites and San Fedelino two-mica granite fall toward the alkali left end fractionated rocks where pegmatites, which represent the most fractionated rocks, define their trend in the lower left apex of the ternary diagram. Migmatites and charnockites of the Gruf Complex also define an alkaline trend and fall within the granodiorite-granites field. Alkaline shoshonitic lamprophyres (Wenk et al., 1977), gabbros and granulites are dispersed toward the FeO and MgO edges of the diagram (Fig. 5.1).

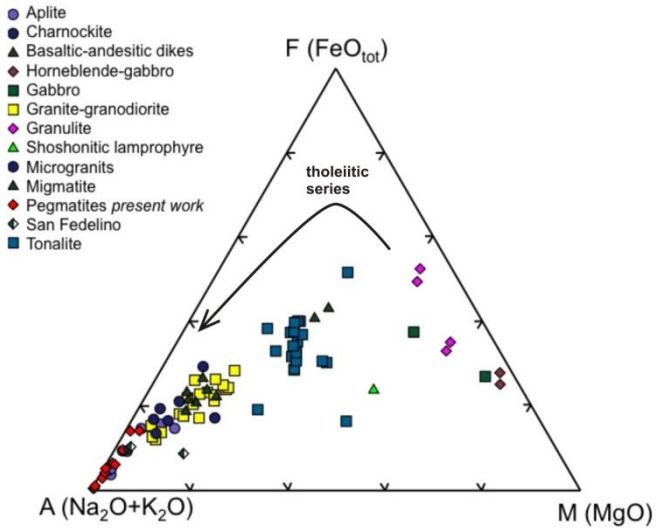

Fig. 5.1 AFM diagram

5.2.2 FeO/(FeO + MgO) versus SiO_2

FeO/(FeO + MgO) binary diagram is characterized by peraluminous leucogranite field which fall in the range 0.72-0.80 FeO/(FeO + MgO), as proposed in the classification scheme of granitic rocks of Frost et al., (2001). Within the peraluminous granitoids fall some granites of the Masino-Bregaglia intrusion, microgranitic dikes, San Fedelino granite, some aplites (related to the mica contents) and the pegmatites from Central Alps. Grignaschi, Rio Graia and Bodengo road cut pegmatite,dikes have the highest FeO/(FeO + MgO) ratios (Fig. 5.2)

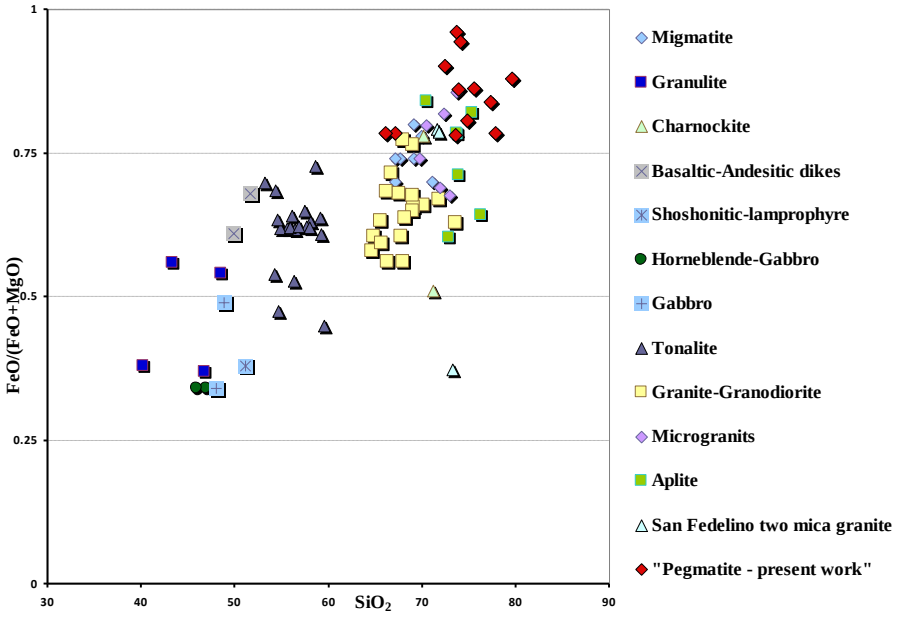

Fig. 5.2 FeO/(FeO + MgO) versus SiO_2 diagram

5.2.3 (MALI) index: (Na_2O+K_2O-CaO) versus SiO_2

The Modified Alkali-Lime Index (MALI) diagram characterized by (Na2O+K2O-CaO) contents as proposed by Frost et al., (2001) utilized to plot the Masino-Bregaglia, surrounding rocks and pegmatites show that two distinct fields can be discriminated; the first field, where tonalities fall, have calc-alkalic trend, where the term calc-alkalic describes suites of rocks that show moderate enrichment in calcium over the alkalis (Peacock 1931). The second field includes granites, granodiorites, aplites, microgranitic dikes, San Fedelino two mica granite, charnockites of the Gruf Complex and bulk pegmatites reveals an alkali-calcic trend which is characterized by the highest MALI rock index (Fig. 5.3).

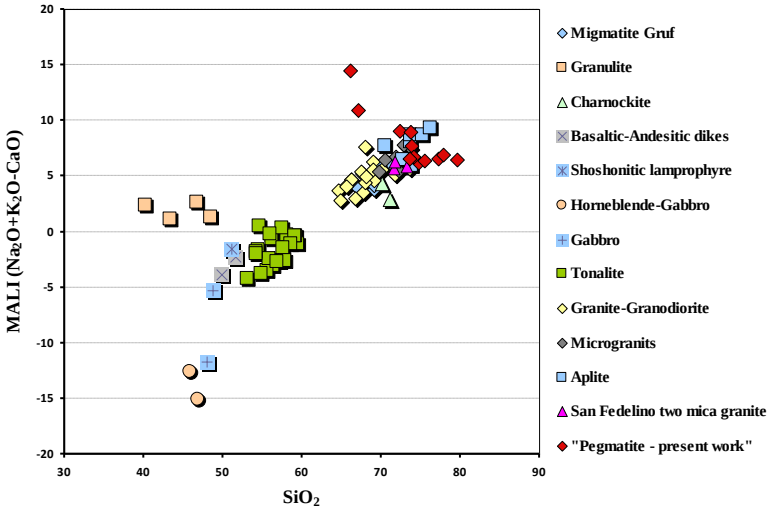

Fig. 5.3 (Na_2O+K_2O-CaO) versus SiO_2 diagram

5.2.4 (MALI) index: (Na_2O+K_2O-CaO) versus K_2O

MALI rock index versus K_2O allows to discriminate two distinct regions of the diagram. The first region within MALI ranges between -5 to 1 encloses tonalites, basaltic-andesite dikes and few gabbros. The second region within MALI ranges between 3 to 10 encloses granites, granodiorites, aplites, microgranitic dikes, San Fedelino two mica granite, charnockites of the Gruf Complex and whole rock composition of the pegmatites. The highest MALI content, which equals to 10.91 belongs to the albitized pegmatites of Pizzo Marcio (Fig. 5.4).

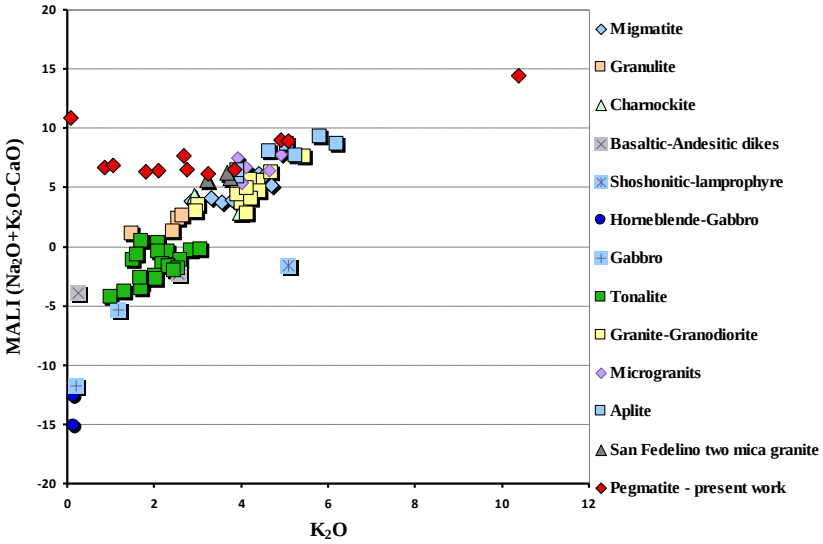

Fig 5.4 (Na_2O+K_2O-CaO) versus K_2O diagram

5.2.5 (ASI) index: Al/(Ca-1.67P+Na+K) versus P_2O_5

The ASI index defines the field of tonalites, granodiorites and granites which fall between 0.85 and 1.34. P_2O_5 content falls for the granitoid rocks and bulk pegmatites in the range between 0 to 0.35 wt% P_2O_5 for most of the bulk compositions plotted in the diagram. Some dispersed tonalite, gabbro and basaltic-andesitic dikes taken from the bibliography have higher P_2O_5 values. Aplites and pegmatites also have low P_2O_5 contents except for Codera phosphate dike (0.27 P_2O_5 wt%), Codera Garnet dike (0.10 P_2O_5 wt%) and Bodengo road cut dike (0.20 P_2O_5 wt%). These sensible higher phosphorous contents would be retained in almandine-spessartine garnet and triplite as revealed by these contained in these pegmatites.

A general rule for granitoid rocks indicates that when the crystallization of plagioclase occurs it drops Ca content in the liquid melt. The remaining Ca content allows to use P and crystallize apatite (London, 1997). S-type granite magmas derived from the incipient partial melting of metapelites, if equilibrium is attained during melting, should be strongly peraluminous (ASI = 1.3–1.4) regardless of the activity of H_2O in melt (Holtz et al., 1992; Wolf and London, 1995; Patiño Douce, 1996). San Fedelino two-mica granite has 1.22-1.27 ASI range, tonalities have 0.99 to 1.13 ASI range, with some exceptions up to 1.34 ASI, whereas granites and granodiorites have 0.95-1.27 ASI range (Fig. 5.5)

High ASI contents are typical of peraluminous and Ca-poor liquids derived from metapelites. It is plausible that all apatite that is exposed to the melt will dissolve at the source, and hence that the P_2O_5 of initial melt will be limited by the abundance of apatite. Metapelite derived magmas is that they will be undersaturated with respect to apatite at the source and begin to fractionate plagioclase but not apatite with crystallization upon ascent.

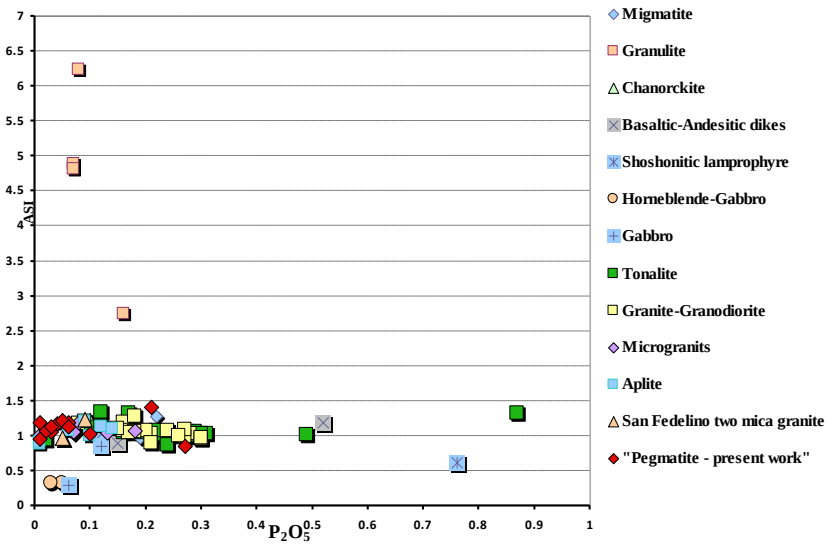

Fig 5.5 Al/(Ca-1.67P+Na+K) versus P_2O_5 diagram

5.2.6 (ASI) index: Al/(Ca-1.67P+Na+K) versus SiO_2

The Aluminum Saturation Index (ASI) defined by molecular ratio Al/(Ca-1.67P+Na+K) as defined by Frost et al., (2001) does not allow to discriminate well defined fields within metaluminous (ASI < 1) or peraluminous (ASI > 1) in which the data plotted would fall. It is evident that tonalites, granodiorites, granites of the Masino-Bregaglia intrusion occupy both metaluminous or peraluminous fields. Only microgranitic dikes, San Fedelino two-mica granite and charnockites show peraluminous characters and fall above ASI > 1 (Fig. 5.6).

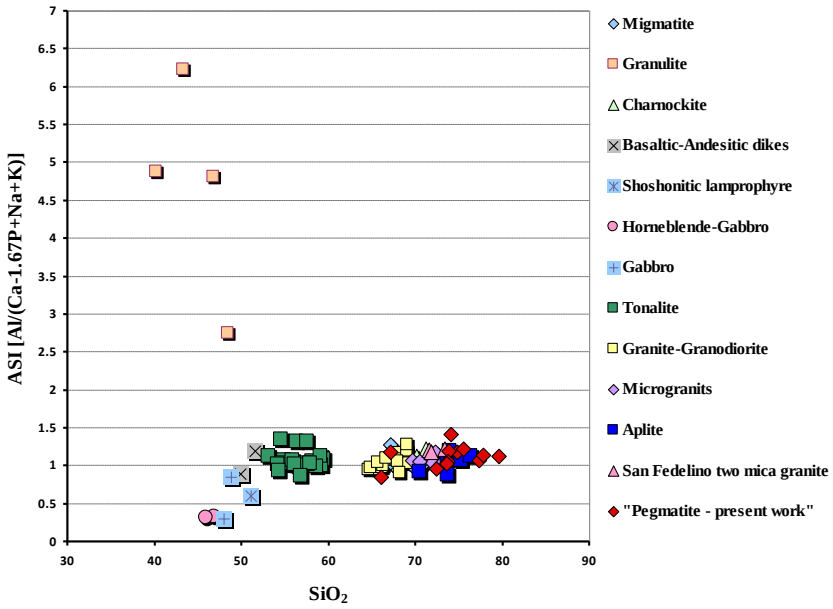

Fig. 5.6 Al/(Ca-1.67P+Na+K) versus SiO_2 diagram

CHAPTER6

Geochemistry of pegmatites

6.1 Introduction

Granitic pegmatites of the rare-element and miarolitic classes display extreme fractionation and accumulation of LILE (large-ion litophile elements) like K, Rb, Sr, Cs, Ba; HFSE (high field strength elements) like Zr, Hf, Nb, Ta, REE, U, Th; light elements, volatiles and semi-volatiles like Li Be, B, F, P .All these lements are beyond the limits observed in other granitic rocks. The geochemical signatures of rare-element pegmatites are all the more interesting because they represent the extremes of fractionation trends encountered in the final stages of granitic differentiation, in leucocratic metaluminous to peraluminous granites (Černý, 1985). Pegmatites with an established signature (LCT or NYF) acquire their geochemical character when magmatic fractionation redistributes elements between the newly formed granitic melt and the restitic crystalline phases which reside in the parental granitic melt. Indeed fractional crystallization from the parental granitic melt appears to be principal means by which pegmatite liquid melts acquire their trace-element signature once move away. The mechanisms of fractionation which drives the evolution from granite to pegmatite are still on debate (London, 2008). Anyway a schematic different scenarios to explain how pegmatite differentiate may be taken into consideration :

(1) an evolving magma chamber where different generations of pegmatite dikes which cross cut each other on the surface and evolve with different geochemical signatures

(2) fractionation and geochemical evolution over the distance in pegmatite fields starting from its source, granitic in origin (Trueman and Černý, 1982)

(3) escape of pegmatite liquids through a filter pressing mechanisms from a rare-metal granitic magma chamber of zoned pluton.

All the models above presented do not consider geodynamic situation where a pegmatite field is intruded into a polymetamorphic orogenic chain which developed a P-T metamorphic path. For example the pegmatite field of Central Alps intersects different nappes emplaced at different crustal levels and characterized by different lithologies. This case will represent the argument of discussion in the chapter devoted to explain the origin of the pegmatite field of the Central Alps

6.2 Silicate melts, hypercritical fluids, and geochemical fractionation of rare elements

6.2.1 Behaviour of F, B, P in silicate melts-vapour system

H_2O, volatiles and semi-volatiles elements (boron, fluorine and phosphorous) play their fundamental role favouring the miscibility between liquidus and pegmatite silicate melts as described by London (1987; 1988; 1989, 1992). The role of H_2O, as a component of granitic melts depresses solidus and liquidus temperatures

(Tuttle and Bowen ,1958; Luth et al., 1964) lowers melt viscosities (Burnham, 1975; Shaw, 1965, 1972) and promotes coarse grain size (Fenn, 1977).

Fluorine, like H_2O, lowers solidus and liquidus temperatures, enhances cation diffusivities, and decreases melt viscosities (Wyllie and Tuttle, 1961; Manning, 1981). An important difference between F and H_2O is that $D(F)^{vapour/melt}$ is <1 in metaluminous and peraluminous granitic bulk compositions (Kogarko et al., 1968; Manning, 1981; Webster et al., 1987) Fluorine decreases the solubility of H_2O in melt so that at equal H_2O contents of volatile-undersaturated magma at the same P and T the activity of H_2O is higher in F-bearing melts than in F-absent melts. In silicate melts, F appears to bond with alkalis and aluminum (Manning et al., 1980; Mysen and Virgo, 1985). In the haplogranite system, fluorine lowers the activity of albite with expansion of the liquidus field of quartz toward the $NaAlSi_3O_8$ apex. (London, 1987, 1988).

Boron lowers the solidus of H_2O-saturated haplogranite by 60°C or more at 5 wt% B_2O_3 (Wyllie and Tuttle, 1964; Chorlton and Martin, 1978; Pichavant, 1981). Boron increases the solubility of H_2O in silicate melts, at 200 MPa_{H2O} the system eucryptite-Ab-Qz-$Li_2B_4O_7 \cdot H_2O$ contains a large field of complete silicate-liquid-H_2O miscibility (London, 1986). Boron also decreases the viscosity of silicate melts (London, 1986) presumably through depolymerization caused by combined effects of B and H_2O. Like for F-bearing systems, the addition of B to silicate melts leads to expansion of the liquidus field of quartz toward the $NaAlSi_3O_8$ apex in the haplogranite ternary Ab-Qz-Kfeld diagram (Pichavant, 1981, London, 1986)

In silicate melts, phosphorous forms distorted PO_4 tetrahedra that have limited solubility in silicate-liquid granitic melts (Ryerson and Hess, 1980; Mysen et al., 1981). Indeed the addition of P to granitic liquid melts promotes phosphate-silicate liquid immiscibility (Visser et al., 1978). Phosphorous is generally partitioned into silica-poor, basic melts along with other high field-strength cations such as rare-earths, scandium, titanium (Ryerson and Hess, 1980; Watson and Capobianco, 1981; Watson and Green, 1981).

Experimental studies performed by Huffman et al., (1986) envisaged that phosphorous may increase the solubility of H_2O in silicate melt. These observations were confirmed by the experimental studies of London (1987) with macusanite rhyolite glass and addition of B, P, F obtained sensible increase in silicate-melt-aqueous vapour miscibility. London by adding boron and phosphorous, but not F, increased H_2O solubility in melt to approximately 9-10 wt% H_2O at superliquidus T and 200-300 MPa. At high concentrations of B, P, F near or complete silicate-liquid-H_2O miscibility is attainable. B, P and F reduce the activity of albite, and correspondingly increase the activity of muscovite+quartz in hydrous granitic melt or aqueous vapour. The macusanite experiments (London, 1986) provide evidence that muscovite can coexist with peralkaline Na-B-F-rich vapour.

6.2.2 The role of compatible and incompatible elements in pegmatites

The partitioning behaviour of elements defined in terms of compatibility and incompatibility is the mechanism which allows the fractionation of pegmatites from their source plutons. Compatibility elements are those that partition in the pegmatite forming mineral phases like the silicates; incompatible elements are those that partition into the fluid phases over the crystallized ones. The partitioning behaviour of rare-

elements in the crystal structures of pegmatite-forming minerals depends by crystal-chemical and by physical factors. The most popular factors invoked are the pressure, the temperature of fluids, and the concentration of the element in fluids. Other factors to play attention are the velocity of diffusion in the crystal, the SiO_2 activity, and the role of complexing and transporting agents of scandium, yttrium, rare-earths and HFSE elements in liquid melts by fluorine, phosphorous or H_2O (Wood, 1990; Liu and Byrne, 1997; Gramaccioli et al., 2000; Guastoni et al., 2012).

Examples from literature may help to understand the behaviour of incompatible elements in pegmatites. Solodov (1971) claimed that 5.000 ppm Li is the minimal concentration required to precipitate Li rich minerals in granitic pegmatites. In the metaluminous systems Ab-Qz-H_2O and Ab-Or-Qz-H_2O the addition of 1-4 wt% Li_2O depresses liquidus by approximately 80°90°C at 100-200 MPa, and shifts minimum melt compositions away from SiO_2 in Ab-Qz-Or haplogranite ternary diagrams (Wyllie and Tuttle, 1964; Stewart, 1978; Martin, 1983). High Rb contents are diffuse in highly fractionated rare-element pegmatites; K/Rb ratios are largely dependent of the biotite or K-feldspar crystallization. These minerals play an important role in K/Rb decreasing ratio with advancing crystallization of pegmatites, owing to rapid depletion of K by incorporation in K-feldspar and relative accumulation of Rb in the residual melt. K/Rb ratio may also vary because Rb is generally incorporated in the crystal-structure of K-feldspar (Murray and Rogers, 1973; Teerstra et al., 1998). Černý et al, (1984) found Rb in K-feldspar to range from 180 to 880 ppm (and K/Rb from 390 to 95 ppm), over a distance of 1.5 m from the border zone to the core-margin in the Věžná pegmatite of the beryl-columbite type. Cs concentration, among LILE, remains at very low levels of concentration in pegmatite and granitic rocks. In order of increasing concentration, due to incorporation in the crystal structures, the main candidates for incorporating Cs are K-feldspar, micas, beryl and pollucite in the pegmatites. The Ba/Rb ratio rates is one of the most sensitive indicators of fractionation (Taylor, 1963). Within the field of rare-element pegmatites the steep gradients in Ba content are the rule in the less fractionated ones. For example, Shmakin (1979) showed Ba in K-feldspar to decrease from 8800 ppm in the outer zone to 20 ppm. in core margin of the pegmatite at the New York mine, Black Hills, South Dakota, U.S.A. Pegmatites with high fractionation levels of Mn always contain Mn-enriched mineral accessory phases. Typically these pegmatites contain columbite-(Mn), tantalite-(Mn), spessartine, and Fe-Mn phosphates enriched in fluorine. This trend characterizes most of the geochemical evolved pegmatites worldwide and this geochemical trend is also peculiar of the Codera phosphate pegmatite dike where Mn-enriched accessory minerals are diffuse. Gallium is an incompatible element which can be notable enriched in rare-element pegmatites. (Gordiyenko, 1970; Miller et al. 1984) The Ga content may reach as high as 50 to 80 ppm, (Černý 1982b) Albite, muscovite tourmaline commonly are the primary constituents and the main concentrators of this element in granitic pegmatites. The behaviour of HFSE, in particular Zr and Hf, tends to increase in differentiated peralkaline, agpaitic suites, with considerable accumulation of both elements in related pegmatites. In contrast the concentration of Zr + Hf in metaluminous to peraluminous igneous series of calc-alkaline chemistry is very simple a gives low concentration, restricted to an early crystallizing zircon. Zr/Hf have higher values in complex pegmatites, but not comparable with the peralkaline ones, despite their

high overall degree of fractionation. (Černý and Silvola, 1980). Fractionation of Nb and Ta pegmatites were documented in relatively primitive types of pegmatite with NYF geochemical signature (Černý et al., 1985) typically those containing Nb-Y-dominant minerals such as aeschynite-(Y), euxenite-(Y), polycrase-(Y). Ta-dominant species are restricted to the highly fractionated complex type of rare-element pegmatites and they include minerals like wodginite, tantalite-Mn rynersonite and microlite in addition to Sn-Bi-Sb-Cs-based tantalum dominant oxides like microlite group and simpsonite. Pegmatites of Central Alps evidences well constrained trends of Nb/Ta fractionation. Aeschynite-(Y), columbite-(Fe) euxenite-(Y), mark NYF geochemical characters of pegmatites at the Fluorite Arvogno, Albertini Arvogno and Codera Garnet dikes. Microlite, ferrowodginite, tantalite-(Mn), tapiolite-(Fe), fersmite and vigezzite are associated with LCT pegmatites at the Grigaschi, Rio Graia and Pizzo Marcio dike. Geochemical evolved miarolitic pegmatite, the Colonnello dike, contains lithiowodginite as the only tantalum constituent, whereas tantalum-niobium oxides minerals look completely absent in the highest fractionated pegmatite of Central Alps, the Codera phosphate dike.

Mineral-melt partition coefficients of REE are quite variable and they behave both as compatible and incompatible during fractionation in pegmatites. Garnet, biotite, clynopiroxene and less extent muscovite are HREE (Gd, Tb, Dy, Ho, Er, Tm, Yb, Lu) and LREE (La, Ce, Pr, Nd, Pm, Sm) selective (Adam et al., 1993), Y and Sc have ionic charge and chemical characters similar with HREE and tend to partition with these group of elements during the crystallization processes (Gramaccioli et al., 2000). HREE and LREE are constituent of common accessory minerals in pegmatites such as zircon, xenotime-(Y), apatite and REE-carbonates. The (Y,REE,U,Th)–(Nb,Ta,Ti) oxide minerals are nearly ubiquitous constituents of REE-enriched granitic pegmatite. They consist of many mineral groups and individual species; the prominent ones are minerals of the euxenite, aeschynite, pyrochlore, samarskite and fergusonite groups. Typical mineralogical assemblages in pegmatites identify selective enrichments in terms of REE if the mineral components crystallize in border-wall zone or in the core zones or miarolitic pockets. HREE bearing-minerals are more widespread in the border-intermediate zones whereas LREE bearing- minerals crystallize more frequently in miarolitic pockets. Indeed several limitations occur due changing in composition and chemical zoning in REE-bearing minerals especially when they are analyzed in the core portions with respect border zones of the same crystal REE tend to decrease abruptly (Pezzotta et al., 1999; Pezzotta et al., 2005; Guastoni et al., 2008; Guastoni and Nestola, 2010; Guastoni et al., 2012). HREE are important constituent of NYF pegmatites related to I and A-type granites whereas the LREE tend to predominate in peralkaline agpaitic pegmatite suites (Wooley, 1987; Martin and De Vito 2005; Guastoni et al., 2009). As general rule the deep crustal sources with sensible contents of garnets and clinopyroxene will generate LREE-rich melts (agpaitic-carbonatitic suites) whereas crustal sources which contain amphibole, biotite and phlogopite will generate HREE-rich melts (NYF and A-type granite-pegmatites) (Martin and De Vito, 2005; London, 2008).

6.2.3 Grignaschi and Rio Graia pegmatites: geochemistry of trace elements

Pegmatites of Rio Graia and Grignaschi quarry may be grouped because of their structural, textural and mineralogical affinities as already discussed above. Trace elements analysis of Rio Graia pegmatite dike were determined with samples from border zone pegmatite, aplite apophysis, K-feldspar core, fine-grained muscovite masses at the intermediate-core zone and beryl of the core zone, whereas trace elements data of Grignaschi quarry correspond to the border-intermediate zone of the pegmatite dike. Ga average content is 20÷41 ppm, Ba 16÷29 ppm, Cs 36÷339 ppm (at Rio Graia the Cs measured in beryl consists of 1374 ppm), Rb 394÷706 ppm (at Rio Graia the Rb measured in K-feldspar of the core zone corresponds to 1339 ppm and Rb in muscovite at 1862 ppm), Sr 9÷18 ppm, Y 3÷10 ppm, LREE 3÷13 ppm, HREE 3÷5 ppm, U 1÷5 ppm, Eu 0.04÷0.16 ppm, Sc 0÷2 ppm, Hf 0÷2 ppm and Zr/Hf ratio 9÷17 ppm. In addition, but not reported in the Tables 6.1 and 6.2, K-feldspar at Rio Graia has Pb equals to 7 ppm whereas beryl has Zn equals to 10 ppm.

6.2.4 Arvogno Albertini and Fluorite dikes

These two dikes were also grouped because show geochemical and mineralogical affinities and exhibit similar structural and textural characters. Trace elements analysis of Albertini pegmatite was given by samples of bulk rock of the border zone, K-feldspar of intermediate zone and core zone and biotite of core zone. Trace element composition of Fluorite dike was determined with samples from the border and wall zone, K-feldspar, muscovite and albite var cleavelandite of the core pegmatite. Ga average content is 40÷60 ppm, Ba 41÷85 ppm (with Ba consists of 164 ppm in K-feldspar in the border zone of Albertini dike), Cs 80÷103 ppm, Rb 737-1134 ppm. It is important to undeline the Rb content in K-feldspar from the core zone at Albertini dike is 1269 ppm whereas in biotite reaches up 2232 ppm. At the Fluorite dike, K-feldspar of the core zone has Rb equals to 1356 ppm whereas muscovite gives 1605 ppm. Sr averages is 9÷10 ppm, Y 32÷71 ppm (with Y gives 7423 ppm in the fluorite from the Fluorite dike whereas spessartine garnet gives 4208 ppm). LREE ranges is 5÷33 ppm (with LREE gives 395 ppm in the fluorite of the Fluorite dike), HREE range is 8÷11 ppm (with HREE gives 1153 ppm in the fluorite from the Fluorite dikes), U range is 5÷8 ppm, Eu range is 0.08÷0.15 ppm, Sc 14÷72 ppm (with Sc gives 278 ppm in the biotite of the Albertini dike), Hf 1.2÷2.1 ppm and Zr/Hf ratio is 6÷17 ppm. In addition, but not reported in the Tables 6.1 and 6.2, K-feldspar at Fluorite dike has Pb equals to 4.2 ppm whereas muscovite has Pb equals to 8.3 ppm and Zn equals to 73 ppm. In the Albertini dike K-feldspar of the border zone has Pb equals to 2.7 ppm whereas in the core zone equals to 2.6 ppm. Biotite from this latter has Cu 27 ppm, Pb 5 ppm and Zn 1081 ppm.

6.2.5 Emerald and Summit of Pizzo Marcio dikes

Bulk analysis of the albitized intermediate zone of these two dikes gives Ga average content is 13÷18 ppm, Ba 2÷25 ppm, Cs 0÷294 ppm (Cs measured in green beryl of Emerald dike consists of 567 ppm), Rb 3-109 ppm (Rb measured in green beryl of Emerald dike consists of 196 ppm). Sr range is 28÷97 ppm, Y 0 ppm, LREE and HREE 0 ppm, U 2 ppm, Eu range is 0.01÷0.02 ppm, Sc 0÷20 ppm (Sc measured in green beryl of Emerald dike gives 38 ppm), Hf 1.2÷3.3 ppm and Zr/Hf ratio is 2.5÷7 ppm. In addition, but not reported in

the Table 6.1, bulk composition of the albite at Emerald dike gives Pb equals to 13 ppm and green beryl equals to 22 ppm whereas bulk composition of the albite at Summit dike gives Pb equals to 20 ppm.

6.2.6 Summit Pizzo Paglia dike

At the Summit Paglia dike accessory and rock forming minerals are characterized by having large to giants crystals size. Hence trace elements analysis were obtained by samples of the core zone of the pegmatite include K-feldspar, schorl tourmaline, spessartine-almandine garnet and beryl. Ga average content is 40 ppm, Ba 4 ppm, Cs 43 ppm (Cs measured in beryl consists of 167 ppm), Rb 135 ppm (Rb measured in K-feldspar consists of 497 ppm), Sr averages is 0 ppm, Y 20 ppm (Y measured in the almandine-spessartine garnet gives 80 ppm). LREE rangeis 2 ppm, HREE range is 1.3 ppm, U range is 5 ppm, Eu range is 0.01 ppm, Sc 4 ppm, Hf 3.5 ppm and Zr/Hf ratio is 2.2 ppm. In addition, but not reported in the Tables 6.1 and 6.2, K-feldspar has Pb equals to 3.7 ppm whereas almandine-spessartine has Cu equals to 23.5 ppm, Pb equals to 2.2 ppm and Zn equals to 14 ppm.

6.2.7 Colonnello Paglia dike

Trace elements analysis of Colonnello pegmatite is given by samples of bulk rock of the border zone, beryl of the intermediate zone, K-feldspar, beryl, muscovite and schorl tourmaline of the core zone. Ga average content is 160 ppm (Ga measured in muscovite in the core zone consists of 189 ppm), Ba gives 4 ppm (Ba of of the bulk pegmatite in the intermediate zone consists of 117 ppm), Cs (Cs measured in beryl of intermediate zone has 542 ppm; beryl of the core zone has 579 ppm; K-feldspar of the core zone has 771 ppm; muscovite of the core zone has 1492 ppm). Rb average is 1024 ppm (K-feldspar of the core zone has 2433 ppm; muscovite has 3498 ppm), Sr average is 14 ppm (bulk pegmatite of the intermediate zone has 73 ppm), Y 6.3 ppm, LREE range is 5.7 ppm, HREE range is 3.2 ppm, U range is 9 ppm, Eu range is 0.21 ppm, Sc 2.3 ppm, Hf 0.6 ppm and Zr/Hf ratio is 9.3 ppm. In addition, but not reported in the Tables 6.1 and 6.2, K-feldspar core has Pb equals to 1.6 ppm whereas schorl tourmaline has Zn equals to 20 ppm and muscovite has Zn equals to 24 ppm.

6.2.8 Bodengo road cut dike

Bulk composition of this pegmatite has Ga average content of 20 ppm, Ba gives 48 ppm, Cs has 0.5 ppm, Rb average is 46 ppm, Sr average is 148 ppm, Y 2.3 ppm, LREE range is 4.8 ppm, HREE range is 1.9 ppm, U range is 4.4 ppm, Eu range is 0.08 ppm, Sc 3 ppm, Hf 0.3 ppm and Zr/Hf ratio is 24 ppm. In addition, but not reported in the Table 6.1, Cu 2.5 ppm, Pb 6.1 ppm, Zn 3 ppm, As 7.9 ppm and Bi 1.9 ppm.

6.2.9 Garnet Codera dike

Trace elements analysis of Garnet pegmatite was measured on samples of bulk border zone, graphic texture of the border-wall zone, K-feldspar of the core zone and biotite of the border zone. Ga average content is 44 ppm (Ga measured in biotite consists of 111 ppm), Ba gives 65 ppm (Ba of the border zone consists of 204

ppm), Cs has 47 ppm (Cs measured in biotite has 144 ppm). Rb average is 765 ppm (K-feldspar of the core zone has 818 ppm; graphic texture has 485 ppm; biotite has 1583 ppm), Sr average is 38 ppm (bulk pegmatite composition gives 131 ppm). Y measures 79 ppm (biotite has Y equals to 309 ppm), LREE range is 215 ppm (biotite has 839 ppm), HREE range is 50 ppm (biotite equals to 139 ppm), U range is 81 ppm (biotite equals to 323 ppm), Eu range is 0.31 ppm, Sc 49 ppm (biotite equals to 192 ppm), Hf 6 ppm and Zr/Hf ratio is 13.7 ppm. In addition, but not reported in the Tables 6.1 and 6.2, K-feldspar at the core has Pb equals to 2.6 ppm whereas bulk pegmatite has Zn equals to 9 ppm.

6.2.10 Phosphate Codera dike

Trace elements analysis of Phosphate dike was measured on samples of bulk border-intermediate zones with saccharoidal grained albite, albite + K-feldspar + quartz, muscovite+ biotite intergrowths. Ga average content is 73 ppm (Ga measured in biotite-muscovite intergrowth consists of 168 ppm), Ba gives 12 ppm, Cs has 271 ppm (Cs measured in intermediate zone composed of K-feldspar+albite+quartz gives 947 ppm). Rb average is 706 ppm (K-feldspar+albite+quartz of the intermediate zone has 1594 ppm; biotite-muscovite intergrowth has 1093 ppm), Sr average is 5.2 ppm. Y measures 2 ppm, LREE range is 2.7 ppm, HREE range is 1.3 ppm, U range is 3 ppm, Eu range is 0.01 ppm, Sc 43 ppm (biotite-muscovite intergrowth equals to 170 ppm), Hf 2.5 ppm and Zr/Hf ratio is 7.5 ppm. In addition, but not reported in the Table 6.1, feldspar-albite-quartz has Pb equals to 5.4 ppm whereas muscovite-biotite intergrowth has Zn equals to 10 ppm.

Table 6.1 Representative trace elements composition of pegmatites from Central Alps

	Ga	Ba	Cs	Nb/Ta	Ta	Rb	Sr	Th/U	U	Y	Ce	LREE	Eu	HRE	Be	Sc	Hf	Zr/Hf
Arvogno Albert																		
E1 K-feld core	28	72	42	1	1	1269	23	1	1	1	1	2.15	0.13	0.1	14	0	0	0
E3 border	17	51	15	4	5	250	32	6	7	13.8	55	114	0.2	11	7	10	5	24
E6 K-feld	22	164	25	0.7	1	784	57	1	0.5	1.1	0.5	1.5	0.22	0.6	3	0	0	0
E7 biotite	93	51	328	3.4	101	2232	2	0	11	112	3	16.3	0.07	19	7	278	0	0
Average	**40**	**85**	**103**	**2.3**	**27**	**1134**	**29**	**2**	**5**	**32**	**15**	**33**	**0.15**	**8**	**8**	**72**	**1.2**	**6**
Rio Graia																		
C2 border	14	27	8	2.7	3	152	16	0.5	2	7	1	3.4	0.06	2.9	11	2	1	12
C3 muscovite	145	38	274	0.9	225	1862	2	0	0.5	0	0	0.1	0	0	30	3	0.5	3
C4 aplite	14	34	18	2.4	4	138	57	0.5	2	6	3	6.6	0.17	3.3	16	2	0.2	28
C5 K-feld	18	46	20	1	0.2	1339	16	0	0.3	0	0	0.5	0.05	0.1	4	0	0	0
C7 beryl	16	1	1374	0.2	5	38	1	0.4	2	0.7	1.2	2.4	0	0.5		2	0	0
Average	**41**	**29**	**339**	**1.4**	**47**	**706**	**18**	**0.3**	**1**	**2.7**	**1**	**2.6**	**0.16**	**1.4**	***15***	**1.8**	**0.3**	**8.6**
Codera fil gran																		
A1 graphic	17	12	19	1.6	1.6	485	10	0	0.9	0	0	0.5	0	0	2	0	0.2	9
A2 border	18	204	7	3.9	1.7	173	131	1.2	1.5	7	8	18.1	0.5	4	7	3	0.2	33
A3 perthite	30	15	16	0	0	818	7	0	0	0.5	0.6	1.2	0	0.2	3	0	0	0
A7 biotite	111	27	144	8.2	54	1583	3	0.8	323	309	395	839	0.75	194	3	192	24	13
Average	**44**	**65**	**47**	**6.4**	**14**	**765**	**38**	**1.9**	**81**	**79**	**101**	**215**	**0.31**	**50**	**3.7**	**49**	**6**	**13.7**
Bodengo aplite																		
W1 bulk rock	20	48	0.5	8.3	1.5	46	148	0.3	4.4	2.3	2	4.8	0.08	1.9	9	3	0.3	24
Codera fil fosf																		
B1 albite+qz	33	0	34	0.7	25	35	6	0.3	8	4	2.5	6	0.01	2.5	35	1	1	8
B3 feld+ab+qz	69	45	947	0.2	5.6	1594	9	0	0.6	0	0	0	0.01	0	2	0	0	0
B4 bulk rock	20	0	75	1.3	1.5	102	6	1.1	3.3	2.7	1.6	3.2	0.02	1.6	22	1	0.3	9
B5 musc+bio	168	2	28	23	19	1093	0	1	0.7	1.1	0.7	1.6	0.01	0.9	9	170	0.5	13
Average	**73**	**12**	**271**	**6.3**	**13**	**706**	**5.2**	**0.6**	**3**	**2**	**1.2**	**2.7**	**0.01**	**1.3**	**17**	**43**	**0.5**	**7.5**
Paglia Summit																		
P1 tormal	79	8	0	1	1	0	0	0	0	0	0.9	2	0.01	0	6	3	0	0
P2 beryl	15	0	167	0.8	1.3	30	0	0	0	0	0	0	0	0		3	0	0
P3 garnet	49	2	0	0.4	28	11	0	0	18	80	0	6	0.01	61	29	9	10	9
P6 K-feld core	15	4	4	0	0	497	0.7	0	0	0	0	0	0	0	5	0	0	0
Average	**40**	**4**	**43**	**0.3**	**7.6**	**135**	**0.2**	**0**	**5**	**20**	**0.2**	**2**	**0.01**	**15**	**13**	**3.7**	**2.5**	**2.2**
Paglia Colon																		
R1 K-feld core	23	3	671	0	0	2433	10	0	0	0	0	0	0.01	0	6	0	0	0
R2 beryl	23	0	542	0.2	4	35	0	0	2	0.2	0.7	2	0.01	0		4	0.8	8
R3 interm	20	117	18	5	2	139	73	0.4	11	37	13	28	0.31	19	28	5	1	23
R5 tormal	85	2	6	1.1	1.4	5	0	0	0	0	1.5	3	0.01	0	9	2	0.1	15
R6 beryl core	22	0	579	1.7	230	34	0	0.1	41	0.4	0.4	1	0.01	0	*sat*	3	1.2	7
R7 muscovite	189	1	1492	0.4	118	3498	0	0	0	0	0	0	0.01	0	42	0	0.5	3
Average	**60**	**21**	**551**	**1.4**	**59**	**1024**	**14**	**0.1**	**9**	**6.3**	**3.2**	**5.7**	**0.21**	**3.2**	**21**	**2.3**	**0.6**	**9.3**
Pizzo Marc Em																		
H1 albitite	15	11	10	0	13	22	123	0.1	4	0	0	0	0.04	0	0	1	2.4	5.1
H2 beryl alter	11	39	577	0	1	196	70	0	0	0	0	0	0.01	0	*sat*	38	0	0
Average	**13**	**25**	**294**	**0**	**7**	**109**	**97**	**0**	**2**	**0**	**0**	**0**	**0.02**	**0**	**0**	**20**	**1.2**	**2.5**
Pizzo Marc alto																		
L1 albite medio	18	2	0	0.4	15	3	28	0.3	2	0	0.7	1	0.01	0	23	0	3.3	7
Arvogno Fluo																		
D1 border	26	54	54	1.4	48	274	29	1.2	30	77	7	16	0.17	42	11	6	4.8	18
D2 fluorite	0	0	0	0	0	0	28	0	0	7423	123	395	2.94	1153	0	0	0	0
D4 K-feld	30	41	149	0	0	1356	24	0	0	1.3	0	0	0.1	0	6	0	0	0

D5 cleavelandite	39	15	35	0.1	38	197	33	0	5	1	0	0	0.05	0	9	0	0	0
D6 contact	19	93	19	0.8	1.4	251	64	0	0	2	1	1	0.01	0.5	9	2	0	0
D8 muscovite	185	18	143	3	108	1605	1.5	0.5	11	17	2	6	0.06	10	31	52	0.8	8
Spessart Daria		22				0	0	43	1	4208	27					25		
Average	**60**	**41**	**80**	**1.1**	**39**	**737**	**30**	**7.5**	**8**	**71**	**6.2**	**4.6**	**0.08**	**11**	**13**	**14**	**1.1**	**5.2**
Grignaschi																		
F2	20	16	36	2.8	6	394	9	0.6	5	10	6	13	0.04	5	207	0	2.1	17

Table 6.2 Trace elements analysis of quartz form core zone of pegmatites

	Paglia colonnello	**Paglia summit**	**Arvogno Fluorite**	**Arvogno Albertini border**	**Arvogno Albertini core**	**Rio Graia**	**Codera Garnets**
ppm	**R8**	**P5**	**D7**	**E5**	**E2**	**C6**	**A5**
Al	371	265	953	795	106	159	371
K	80	80	85	580	83	166	332
Be	8	2	31	0	1	0	0
Sc	3	2	2	3	3	2	3
Ga	0	3.3	1	0	0	0	0
Rb	1.7	0	0	3.6	0	1	1.3
Cs	1.1	0	0	0	0	0	0
Zr	0	1.2	0	1.6	0	0.6	1.1
Cu	0.6	0.4	0.7	0.4	0.7	1.1	0.7
Zn	1	0.5	0.5	0.5	0.5	0.5	1
Pb	0.1	0	0	0.1	0	0.2	0.2
Ni	1.4	0.9	0.7	0.8	0.6	0.5	1.2
Au ***ppb***	4	12.2	140	55.4	56.1	86.6	932.7

6.3 Geochemical diagrams

6.3.1 REE-HFSE/chondrite

This diagram illustrates the ratios between LILE, HFSE and REE of pegmatites of Central Alps and normalized chondrite data from Taylor and McLennan (1985). The data plotted are related to the trace elements compositions of bulk pegmatites. NYF geochemical signature of Albertini and Fluorite pegmatite dikes (D1 and E3) are clearly distinguishable and characterized by high HREE, U, Th contents. LCT and mixed LCT-NYF pegmatites of Codera valley are less significative and do not evidence REE enrichments as NYF pegmatites of Vigezzo valley (Fig. 6.1).

Fig. 6.1 Spider diagram with trace elements of bulk pegmatites versus chondrite

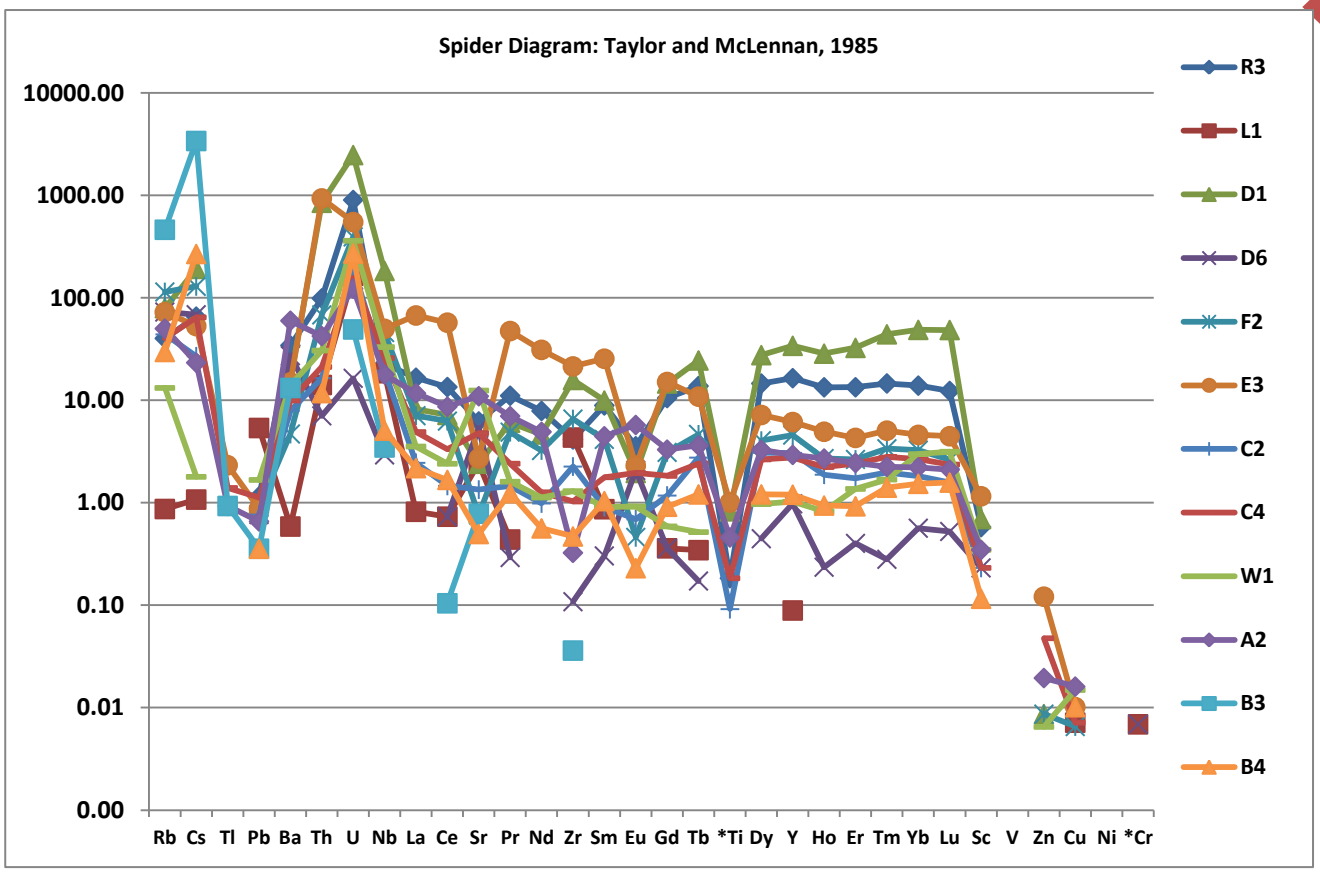

6.3.2 K/Cs versus Cs

Pegmatites which mark LCT geochemical signature are well defined. Cs is incorporated in the crystal structures of beryl, K-feldspar, and muscovite and, as it can be observed, pegmatites display high Cs contents, above 500 ppm, also have the major muscovite, beryl and K-feldspar concentration. Pegmatites from Central Alps which evidence LCT fractionation are Rio Graia (C), Pizzo Marcio-Alpe Rosso (H), Colonnello at Pizzo Paglia (R) and Phosphate Codera (B) dikes (Fig. 6.2).

Fig. 6.2 K/Cs versus Cs diagram

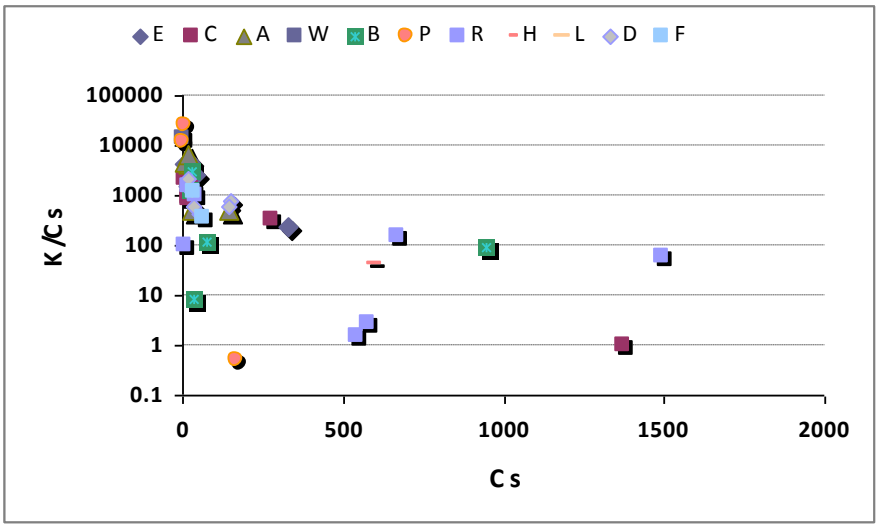

6.3.3 Al/Ga versus Ga

The diagram gives a typical descending curve. As general rule Ga content increases up to nearly 200 ppm in pegmatites with higher contents in albite, muscovite, biotite, tourmaline; these minerals commonly are the primary constituents and the main concentrators of this element in granitic pegmatites (Černý 1982b). In this study pegmatites of Central Alps with the highest Ga content are Rio Graia (C), Arvogno Fluorite (D), Paglia Colonnello (R), Garnet Codera (A), and Phosphate Codera (B) dikes (Fig. 6.3).

Fig 6.3 Al/Ga versus Ga diagram

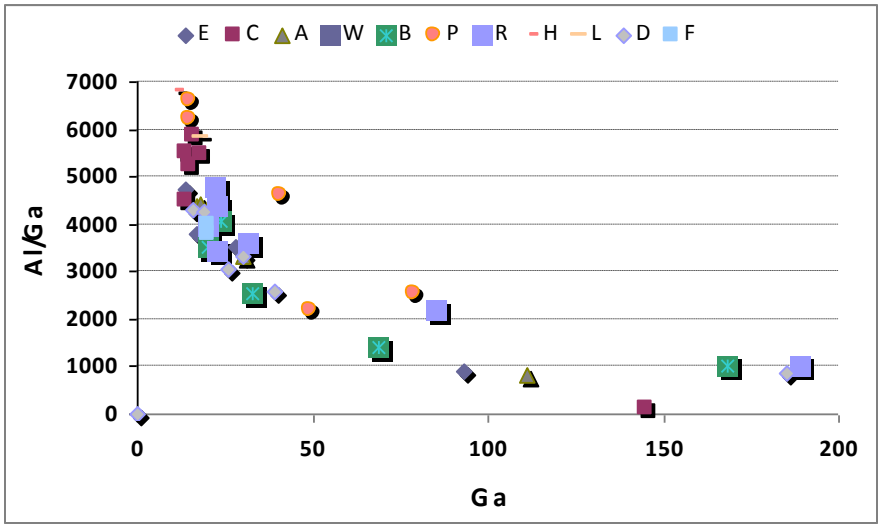

6.3.4 K/Ba versus Ba

The data plotted of K/Ba versus Ba diagram allow to identify those pegmatites which develop a relative primitive geochemical fractionation character as also already reported by Černý (1982b) where steep gradients in Ba are indicators of less geochemical fractionated pegmatites. Pegmatites which show sensible increasing in Ba content, above 100 ppm, and lowering of K/Ba ratio include Albertini Arvogno (E), Fuorite Arvogno (D), Summit Paglia (P) and Garnet Codera (A). These pegmatitee dikes develop NYF or mixed NYF-LCT geochemical character (Fig 6.4).

Fig. 6.4 K/Ba versus Ba diagram

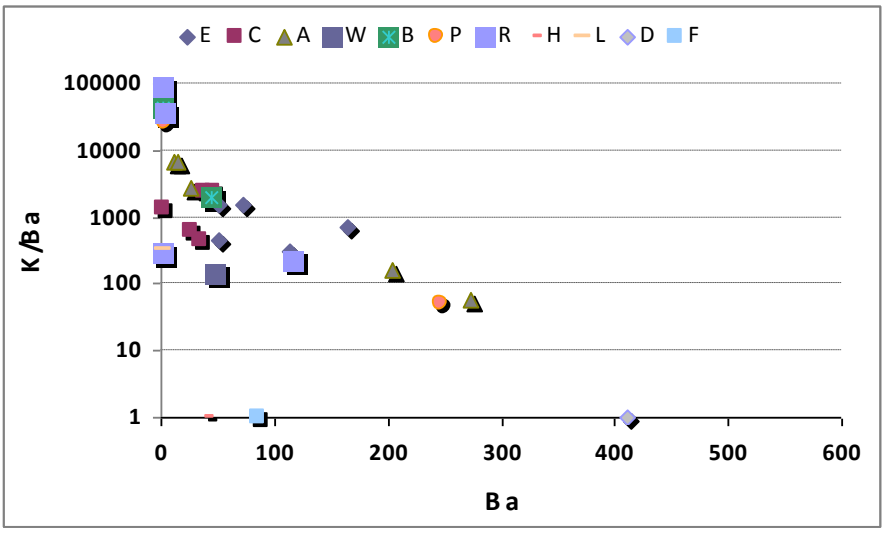

6.3.5 Ba versus Rb

This diagram does not help to discriminate a group or distinct groups of pegmatites which could develop peculiar geochemical trends. This because biotite, muscovite and K-feldspar commonly are the primary constituents and the main concentrators of this element in granitic pegmatites and they are randomly distributed in all pegmatitic zones of the dikes. Arvogno Albertini (E), Arvogno Fluorite (D), Garnet Codera (A) and Paglia Colonnello (R) have the highest Rb contents, generally above 1000 ppm in biotite, K-feldspar muscovite. Muscovite crystallized in the pocket core-zone of the Colonnello pegmatite has the highest Rb content, almost 3500 ppm (Fig. 6.5).

Fig. 6.5 Ba versus Rb diagram

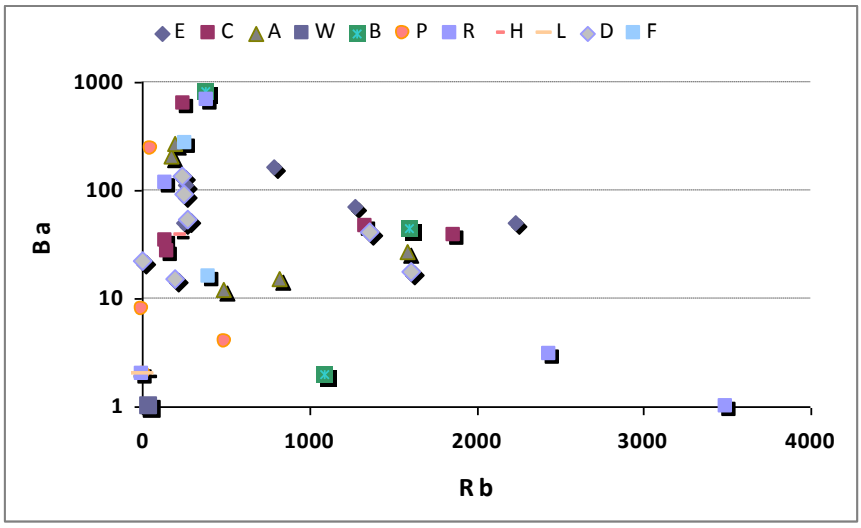

6.3.6 Rb/Sr versus Sr

What the diagram evidences is the high enrichment in Sr content which characterize the border zones of pegmatites and those dikes develop aplitic texture like Bodengo road cut (W). High Sr contents of Rio Graia (C) and Codera Garnet pegmattess are bulk analysis of samples which represent aplite apophysis depart from the main pegmatite body. It is important to observe that samples taken in the intermediate core zone of pegmatites have Sr content abruptly decreases nearly to few tens or less ppm. This strong decreases is caused by the effects of inward crystallization of the pegmatite which consumes all the Sr in the border and less fractionated zones of the pegmatite (Fig. 6.6).

Fig. 6.6 Rb/Sr versus Sr diagram

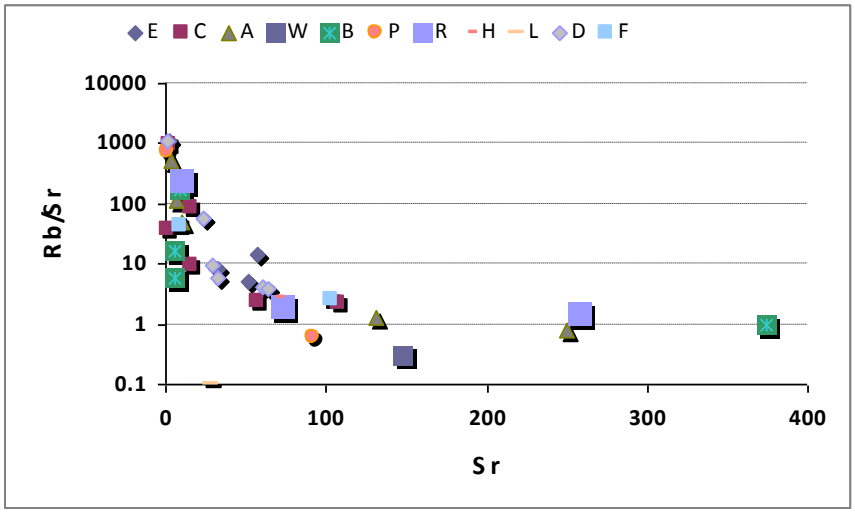

6.3.7 Al/Ga versus K/Rb

Ga and Rb contents are strongly influenced by the mineralogical components of the pegmatite. As it was observed Ga is mainly hosted in albite, muscovite, biotite, tourmaline, whereas Rb is incorporated in biotite, muscovite and K-feldspar. As general rule pegmatites of the Central Alps have Rb content which approaches the highest values in muscovite and K-feldspar which crystallize in the intermediate-core zone of the dike, whereas Ga content is dependant by the crystallization of muscovite, biotite and in less amount by schorl tourmaline (Fig. 6.7).

Fig. 6.7 Al/Ga versus K/Rb diagram

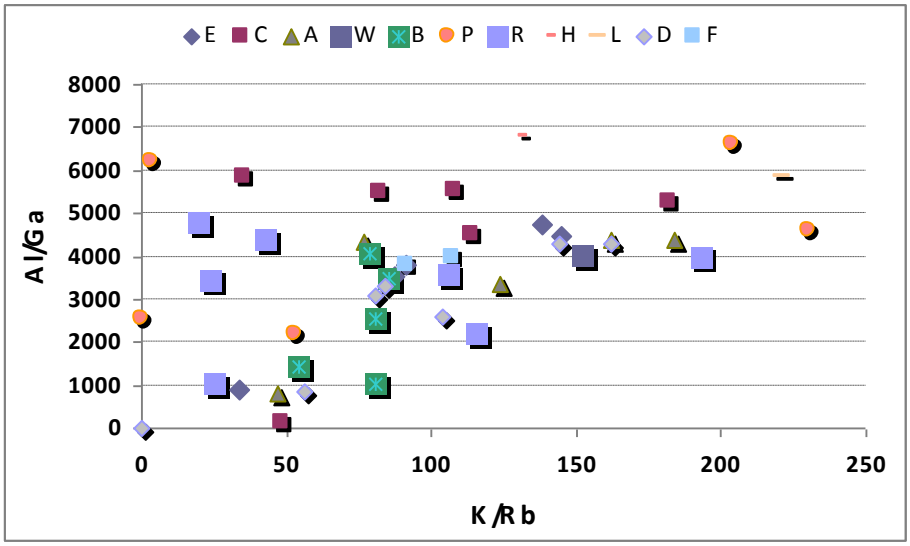

6.4 ICP-OES Bulk rock and ICP-MS trace elements methods to study pegmatites

Inductively Coupled Plasma-Optical Emission Spectrometry (ICP-OES) for bulk rock analysis and Inductively Coupled Plasma-Mass Spectrometry (ICP-MS) for trace elements analysis were performed at the Acme Analytical Laboratories Ltd (Vancouver, Canada), accredited under ISO 9002. The powdered samples (10 grams each) were sent to the laboratory where the samples, mixed with lithium metabo-rate/tetraborate, were fused to glass beads (at 1100 °C) in a furnace. The cooled beads were dissolved in ACS grade nitric acid digestion. The major elements (Si, Al, Fe, Mg, Ca, Na, K, Ti and P) and Ba were analyzed by inductively coupled plasma optical emission spectrometry using Spectro Ciros instrument. Loss on ignition (H_2O and CO_2) was determined by weight difference after ignition at 1000°C. Sulfur was analyzed by combustion, using a LECO CS-200 analyzer. Trace elements were analyzed by inductively coupled plasma-mass spectrometry using a Perkin-Elmer instrument, after lithium metaborate fusion and dilute nitric acid digestion (Cs, Hf, Nb, Rb, Sr, Nb, Ta, Th, U, V, Hf, Zr, Y and REE) or after Aqua Regia digestion at 95 °C for 1 h for heavy metals and metalloids (Mo, Cu, Pb, Zn, Ni, As, Cd, Sb, Bi, Ag, Au, Hg, Tl, Se, Co, Cr, Pd and Pt). The accuracy and precision of the trace element data were about 5%. Analytical conditions and standard utilized are in the Quality Control Report Documents, VAN11002144.1 and VAN 11002145.1, released by Acme Analytical laboratories.

CHAPTER 7

Pegmatite in the Central Alps: classification

The classification of granitic pegmatites of Central Alps chosen for this study is the resume of the structural, textural, petrological data collected in the field and taken from the literature. Geochemical and mineralogical represent new set of data obtained from XRF, ICP, WDS and X-ray diffraction analysis above presented and discussed. The classification scheme is more or less that adopted by Černý (1982b, 1991a) and by Černý and Ercit (2005). Classes, subclasses and types of pegmatites have been maintained in addition to the geochemical concept for the petrogenetic families of pegmatites, respectively NYF and LCT.

The NYF family is marked by Nb>Ta, Ti, Y, Sc, REE, Zr, U, Th, F. The parent granitic rocks may be also pegmatitic in origin; this family of pegmatites often are syngenetic (Garrison et al. 1979; Simmons et al. 1987). Abundances of the REE range commonly enriched at 100 to 800 times chondritic normalized contents. The LCT pegmatite family gets enriched in B, P, Li, Rb, Cs, Be, Sn, and is marked by Ta>Nb. Parent rocks are granitic and most of the time are epigenetic. REE abundances are generally low, with LREE at 100 to 10 times chondritic.

The classification of the Alpine pegmatites which follows has partially been modified by the author respect the original scheme proposed by Černý and Ercit (2005). This modification was derived by the geochemistry and mineralogy character of the pegmatites of Central Alps which in certain cases do not fit with the rigid scheme adopted by the above mentioned authors. The modified scheme include the albitized pegmatites of Pizzo Marcio-Alpe Rosso classified in the beryl type of the rare elements-Li subclass. Černý and Ercit (2005) do not foresee any class or type of pegmatites involved in metasomatic processes of albitization by the hosting rocks. Colonnello Paglia dike has been included within new beryl subtype pegmatite belonging to the miarolitic lithium subclass. Indeed pegmatites of Central Alps show a peraluminous character but the crystallization of topaz in miarolitic cavities as accessory mineral is characteristics of syngenetic miaroltic pegmatites within granitic source rocks. Alpine pegmatites are epigenetic, with the exception of Garnet Codera and Phosphate Codera pegmatites and topaz was never found in any of the pegmatites distributed along the Alpine chain. Arvogno Fluorite and Albertini dikes were unified under a unique new type named allanite-euxenite-gadolinite. Indeed the mineralogical studies of these pegmatites show Be-Nb-Ta-REE-U oxides and silicate groups and series of minerals may occur together in the same dike.

Family: **LCT**

Class: **Rare element (REL)**

Subclass: **Rare elements-Li (REL-Li)**

Type: ***Beryl***

Subtype: ***Beryl-columbite***

Granitic pegmatite: **Grignaschi dike (F)**

Mineralogy: **K-feldspar, albite, quartz, muscovite, biotite, beryl, schorl, spessartine-almandine, tantalite-(Fe), columbite-(Fe), tapiolite-(Fe), microlite, monazite-(Ce), secondary uranium phosphates, uraninite, zircon, bavenite.**

Granitic pegmatite: **Rio Graia dike (C)**

Mineralogy: **K-feldspar, albite, quartz, muscovite, biotite, beryl, spessartine-almandine, schorl (rare), tantalite-(Fe), columbite-(Fe), tapiolite-(Fe), microlite, fersmite, monazite-(Ce), secondary uranium phosphates, uraninite, zircon, bavenite.**

Albitized granitic pegmatite: **Pizzo Marcio-Alpe Rosso dikes (H, L)**

Mineralogy: **albite, tremolite, talc, phlogopite, beryl, beryl var emerald, spessartine (rare), dravite, dravite-schorl, columbite-(Mn), tantalite-(Mn), fersmite, vigezzite, microlite, U-rich microlite, tapiolite-(Fe) (rare), ferrowodginite (rare), allanite-(Ce), beryllium silicates (bavenite, meliphanite, milarite, roggianite) zeolites (chabazite-Ca, gismondine, phillipsite-Ca, thomsonite), cheralite-(Ce), niobian titanite, zircon.**

Granitic pegmatite: **Summit of Pizzo Paglia (P)**

Mineralogy: **K-feldspar, albite, quartz, muscovite, biotite, beryl, schorl, spessartine-almandine, zircon.**

Subclass: **Rare elements-Li (REL-Li)**

Type: ***Beryl***

Subtype: ***Beryl-columbite-phosphate***

Granitic pegmatite: Phosphate Codera **(B)**

Mineralogy: **K-feldspar, albite, quartz, greenish K-feldspar, Rb-rich K-feldspar, muscovite, biotite, colorless to pale pink beryl, spessartine-almandine, Mn-rich elbaite, Mn-rich fluor-elbaite, Mn-rich elbaite-schorl, F-rich triplite, Mn-hydroxides. No niobium-tantalum minerals were observed.**

Family: **LCT**

Class: **Miarolitic**

Subclass: **Miarolitic lithium (Mi-Li)**

Type: ***Beryl-topaz***

Subtype: ***Beryl***

Granitic pegmatite: **Colonnello Pizzo Paglia dike (R)**

Mineralogy: **K-feldspar, albite, albite var. cleavelandite, quartz, muscovite, beryl, schorl, spessartine-almandine, lithiowodginite, zircon.**

Family: **NYF**

Class: **Rare element (REL)**

Subclass: **Rare elements-rare earths (REL-REE)**

Type: ***Allanite-euxenite-gadolinite***

Granitic pegmatite: **Fluorite Arvogno dike (D)**

Mineralogy: **K-feldspar, albite, albite var. cleavelandite, quartz, muscovite, biotite, yttrium-rich fluorite, yttrium-rich spessartine, allanite, gadolinite-(Y), euxenite-(Y), aeschynite-(Y), pyrochlore, xenotime-(Y), monazite-(Ce), beryllium silicates (bavenite, milarite), titanite, uraninite, wulfenite, zircon and sulphides like bismutinite and galena.**

Granitic pegmatite: **Albertini Arvogno dike (E)**

Mineralogy: **K-feldspar, albite, albite var. cleavelandite, quartz, muscovite, biotite, yttrium-rich fluorite, allanite, gadolinite-(Y), aeschynite-(Y), xenotime-(Y), monazite-(Ce), titanite, yttrium-rich fluorapatite, zircon.**

Family: **mixed NYF-LCT**

Class: **Rare element (REL)**

Granitic pegmatite: **Garnet Codera dike (A)**

Mineralogy: **K-feldspar, albite, quartz, muscovite, biotite, spessartine-almandine, beryl, columbite-(Fe), euxenite-(Y), monazite-(Ce), xenotime-(Y), uraninite, zircon, magnetite**

Family: **Barren or ceramics**

Class: **Muscovite**

Granitic pegmatite: **Bodengo road cut (W)**

Mineralogy: **K-feldspar, albite, quartz, muscovite, biotite, almandine-spessartine, apatite.**

CHAPTER 8

Perthites K-feldspar studies: a geothermometry is feasible?

8.1 Prewiev

Thermodynamic studies on binary solvus diagrams od Ab-K-feld systems in granitic rocks establish temperatures at which a single feldspar may contain exsolution lamellae of the minor phase composed of sodium plagioclase with variable Ca content Then binary "solvus" phase diagram (showing the relation of temperature to composition) is typically used to show the phase relations for alkali feldspars. A single homogeneous alkali feldspar occurs at high temperatures, but as the system cools eventually the phase boundary (solvus) is intersected and the exsolution (unmixing) process begins (Fig. 8.1). "Underneath" the solvus a single feldspar is no longer thermodynamically stable, and the system begins to separate into two phases that become increasingly Na-rich or K-rich upon further cooling. (Brown and Parsons, 1983; Parsons, 2010). In granitic pegmatites liquidus, solidus and subsolidus relations among the alkali feldspars in the system Ab-K-feld are ruled by the effects due to undercooling temperatures. Several studies show that intrusion of pegmatite dikes within hosting rocks may promote oriented textures, layered aplitic textures along margins,, anisotropic fabrics (unidirectional solidification) and skeletal mineral structures only if pegmatite melts are forced to undercool (London, 1989). Examples in literature show pegmatite liquidus and host-rock temperatures relationships are ruled by rapid undercooling like Harding pegmatite (20 m thick), New Mexico, would have cooled to its solidus in 3 to 5 months (Chakoumakos and Lumpkin, 1990). Little Three dike (2 m thick), Ramona, CA, in about 25 days (Morgan and London, 1999), Himalaya-San Diego pegmatites (2 mt thick), Mesa Grande, CA, may have cooled to their solidus in just over 1 week (Webber et al., 1999). Mineralogical textures in pegmatites indicate nucleation begins from the margins of pegmatite dikes because these are the areas of greatest undercooling and hence regions of the greatest driving forces to nucleate. The directionality of rapid crystal growth is characterized by comb textures, skeletal crystal branches (e.g. K-feldspars, tourmalines, beryl) so common develop in granitic pegmatite textures.

This preview helps to illustrate the binary Ab-K-feld diagram to be utilized in granitic pegmatites is where hypersolvus crystallization is promoted when a single K-feldspar begins to crystallize at undercooling temperatures when ΔT reaches the solvus curve a new equilibrium process takes place involves splitting of the feldspars into K- and Na-rich lamellae by internal diffusion of ions to form perthitic feldspars

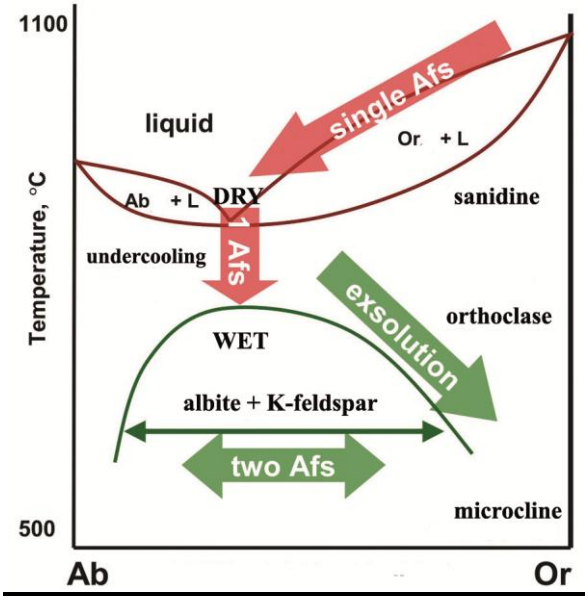

Fig 8.1 Ab-K-feldpar binary diagram.
Redrawn after London 2008

8.2 Studies of perthitic K-feldspar in pegmatites from Central Alps

Six perthitic K-feldspars of different pegmatitic dikes were selected for this study. K-feldspars are from Rio Graia (C5), Fluorite Arvogno (D4), Albertini Arvogno (E1), Colonnello Paglia (R1), Summit of Pizzo Paglia (P6) and Garnet Codera dikes (A3). They all are perthitic in texture and composition and were sampled in the core zones of the pegmatite dikes. Each sample was observed in thin section, analyzed by XRF, EBSD diffraction tecnique and (MICRO-CT) X-ray computed micro-tomography. Perthites observed thin section under polarized light show coherent lenticular film lamellae of albite up to 100 microns in thickness. Additional SEM observations revealed semi-coherent straight film albite lamellae in K-feldspar with misfit dislocations. No microporous or secondary albite vein perthites were observed in all the samples studied.

XRF bulk analysis of albite and K-feldspar molar contents were calculated by pertithes assuming the K/Na ratios were not influenced by low Ca wt% content (which ranges between 0.02-0.06 wt%). Ab molar contents range between 13.1 wt% (E1) to 20.8 wt% (A3) and K-feldspar molar contents range between 79.2 wt% (A3) and 86.9 wt% (D4). MICRO-CT diffraction gave Ab between 1.04 (P6) and 4.18 (R1) mm^3 volume whereas K-feldspar range between 13.34 (R1) and 16.86 (P6) mm^3 volume which correspond to Ab solid fraction between 5.83 and 23.87 % and K-feldspar solid fraction between 76.11 and 94.17 % (Table 8.1 and 8.2).

All K-feldspars were indexed successfully (Phillips and Ribbe, 1973), whereas indexing of the exsolved albite using the constructed low-albite reflector file (Harlow and Brown, 1980) was never possible. Instead albite was indexed successfully when K-feldspar reflector was used. A comparison of the backscatter electron diffraction patterns (EBSPs) of the exsolved albite with those of enclosing K-feldspar showed both

patterns were mostly identical (see Kikuchi Figures 8.1 and 8.2), except that EBSPs of albite is generally a bit blurred. We interpret these observations as twinnings or crystallographic dislocations, also described as misfit dislocations and pull apart by Parsons (2010) which occur in triclinic plagioclase.

Table 8.1 Molar and volume percentages of K-feldspar and perthite albite from Central Alps pegmatites

	C5 Rio Graia	**A3 Codera garnet**	**D4 Arvogno fluorite**	**E1 Arvogno Albertini**	**P6 Paglia filone alto**	**R1 Paglia colonnello**
Ab% molar	15.2	20.8	13.1	13.2	20.2	18.6
Kfeld% molar	84.8	79.2	86.9	86.8	79.8	81.4
Ab % vol. mm^3	2.43	2.94	2.07	1.81	1.04	4.18
Kfeld vol. mm^3	15.46	14.88	15.82	16.02	16.86	13.34
Ab % on solid fraction	13.58	16.52	11.58	10.18	5.83	23.87
Kfeld % on solid fraction	86.42	83.48	88.42	89.82	94.17	76.11
Porosity %	0.06	0.4	0.05	0.35	0.01	2.06

Table 8.2 Bulk composition and trace elements of perthitic K-feldspars

Wt%	**C5 Rio Graia**	**A3 Codera garnet**	**D4 Arvogno fluorite**	**E1 Arvogno Albertini**	**P6 Summit Paglia**	**R1 Colonnello Paglia**
SiO_2	64.99	64.93	64.75	64.60	64.88	64.76
Al_2O_3	18.62	18.90	18.76	18.67	18.72	19.00
Fe_2O_3	0.04	0.06	0.04	0.13	0.05	0.04
MgO	0.00	0.00	0.00	0.00	0.00	0.00
CaO	0.06	0.06	0.02	0.04	0.04	0.02
Na_2O	2.38	3.22	2.08	2.59	3.11	2.87
K_2O	13.18	12.18	13.79	13.33	12.24	12.53
TiO_2	0.01	0.00	0.00	0.00	0.00	0.00
P_2O_5	0.05	0.09	0.02	0.00	0.22	0.35
MnO	0.00	0.00	0.00	0.00	0.00	0.00
LOI	0.50	0.40	0.40	0.50	0.50	0.30
TOT	99.82	99.84	99.86	99.86	99.76	99.87
ppm						
Ba	46	15	41	72	4	3
Cs	120	16	150	42	4	671
Ga	18	30	30	28	15	23
Rb	1339	818	1356	1269	497	2433
Sr	16	7	24	23	1	10

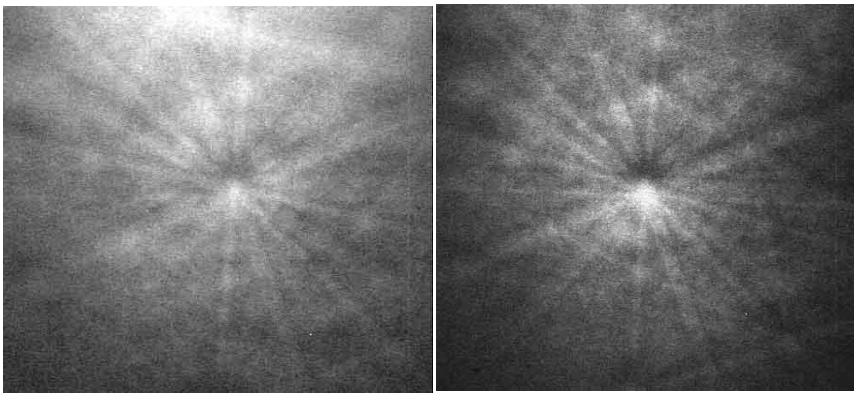

Fig. 8.1 Kikuchi figure in K-feldspar **Fig. 8.2** Kikuchi figure in albite

8.3 Results of perthites study

According to Černý (1994) decreasing in Ab content which occur in pegmatitic dikes is generally quantified from about Ab_{25} in the border zones to Ab_{15} in the innermost zone (intermediate to core zones of the pegmatite). If we consider the molar albite calculated in the pegmatites of Central Alps, composition agree with the data published by Černý (1994) which range between Ab_{13} to Ab_{21} wt%. The observations and the data obtained by EBSD and MICRO-CT diffraction indicate perthititc K-feldspar do not have microporous or secondary albite veins replacement and undoubtedly they are primary exsolved albite. Perthites are exsolved segregated domains of one chemical site by another. They represent a solid state crystallographic rearrangement via Na→K interdiffusion occurs within a continuous Si–Al–O framework and the process occurs at hypersolvus dry conditions without any H_2O participation (Ross Angel personal communication).

Volumetric data of Ab and K-feldspar obtained by MICRO-CT diffraction are useful to form the basis of two-feldspar geothermometry using the binary Ab-K-feldspar diagram (Fig. 8.3) proposed by Parsons (2010). Temperature estimates are strongly dependent on small amounts of An in alkali feldspars but the An content measure in pertithes of Central Alps pegmatites is <0.07 wt % (see Table 8.2) and this does not condition the temperatures at which perthite K-feldspar exsolve at dry conditions in the innermost zones of the pegmatitic dikes. The highest solvus temperature obtained crossing the An-free alkali feldspars binary diagram of figure 8.3 are the perthite K-feldspar of miarolitic pocket at Colonnello Paglia dike. In this pegmatite Ab volume corresponds to 4.18 mm^3 which equals to 23.87 % Ab solid fraction. Estimates exsolving temperature corresponds to 470-480 °C. The lower exsolving temperatures are registred at the Summit Paglia where Ab corresponds to 1.04 mm^3 and equals to 5.83 % Ab solid fraction. Crossing the solvus curve the estimates exsolving temperature is 250-260 °C. At Arvogno Albertini pegmatitic dike Ab volume is 1.81 mm^3 and 10.18 % Ab solid fraction. Estimates exsolving temperature corresponds to 280-290 °C. At Fluorite Arvogno dike Ab volume corresponds to 2.07 mm^3 which equals to 11.58 % Ab solid fraction. Estimates exsolving temperature is at 300-310 °C. At Rio Graia dike Ab volume corresponds to 2.43 mm^3 equals to 13.58 % Ab solid fraction. In this pegmatite estimates temperature corresponds to 310-

320°C. At Garnet Codera dike Ab volume corresponds to 2.94 mm^3 equals to 16.52 % Ab solid fraction and its estimates exsolving Ab-Kfeldspar temperature corresponds to 320-330 °C.

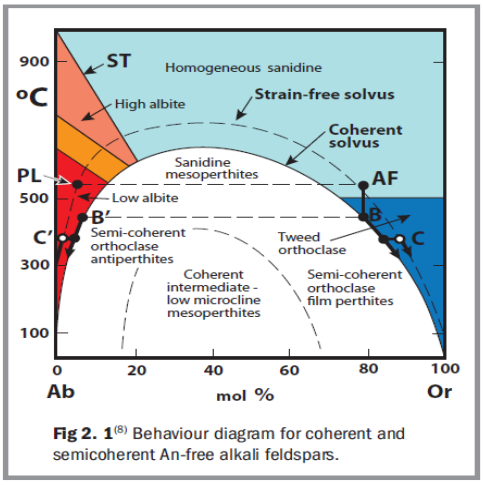

Fig. 8.3 Binary Ab-Or diagram used for estimation of exsolving temperatures of perthitic K-feldspar (from Parsons, 2010)

8.4 X-ray computed micro-tomography (MICRO-CT) method

X-ray tomographic scans were carried out at the Department of Geosciences of the University of Padova on six perthite K-feldspar from different pegmatite dikes (see Table 8.19, using a SkyScan 1172 high resolution micro-CT scanner. The system is equipped with a polychromatic microfocus X-ray tube, characterised by a maximum operating voltage of 100 kV and a maximum output power of 10 W. The anode material is tungsten and the focal spot size is approximately 5 µm. The raw data (radiographs) are collected by a high resolution 12-bit detection system, constituted by a scintillator screen (4000x2672 pixels, ~ 9 µm pixel size) coupled to a CCD chip by a tapered fiber-optic bundle. Owing to the cone-beam geometry of the source, the image resolution can be adjusted according to the size of the specimen by simply varying the source-detector and source-object distances (D_{sd} and D_{so}); the ratio D_{sd}/D_{so} represents the geometrical magnification factor. During data acquisition, the tube voltage and current were set to 48 kV and 204 µA, respectively. 1800 projections were acquired over a 360° rotation (angular step 0.2°), with an exposure time per frame of 950 ms and a frame averaging factor of 10. A 0.5 mm-thick Al filter was placed in the beam path in order to suppress the low-energy portion of the spectrum and minimize undesired artifacts related to the beam-hardening effect (*i.e.*, the preferential attenuation of low-energy X-rays while passing through the sample). For all the experiments, a magnification factor of 4.1, coupled with a 2x2 binning of the detector resulted in a nominal resolution of 4.36 µm. The reconstructions of cross-sectional slices of perthitie K-feldspars (see Figures 8.4 to 8.9) from the acquired 2D projections were carried out using a modified FDK algorithm

(Feldkamp *et al.*, 1984) for cone-beam geometry implemented in the SkyScan NRecon software; corrections for beam hardening effect and ring artefacts were also applied during the reconstruction process.

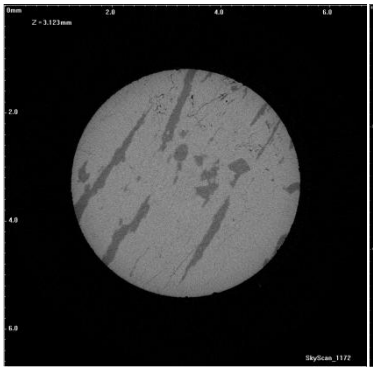

Fig. 8.4 Rio Graia (C5)

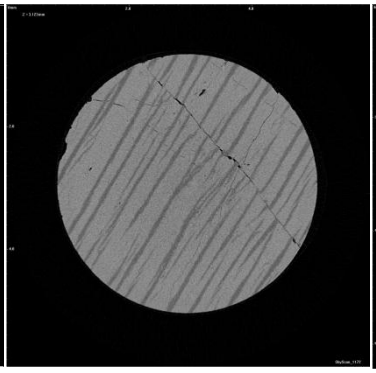

Fig. 8.5 Garnet Codera (A3)

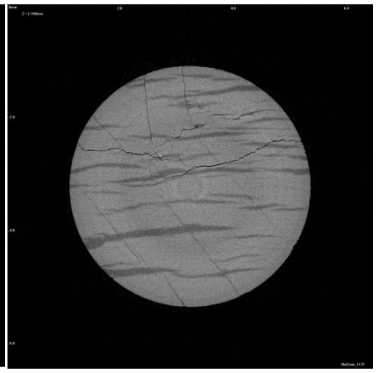

Fig. 8.6 Arvogno Albertini (E1)

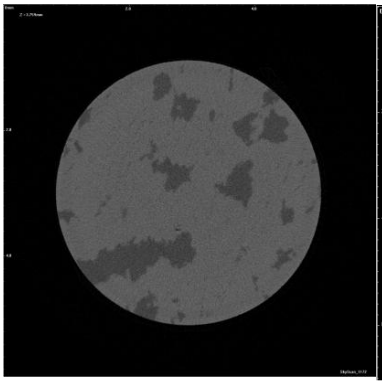

Fig. 8.7 Arvogno Fluorite (D4)

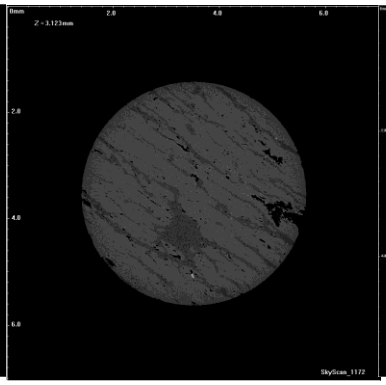

Fig. 8.8 Colonnello Paglia (R1)

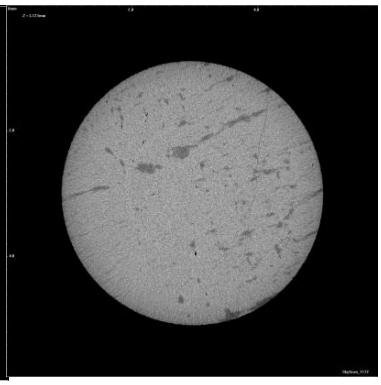

Fig. 8.9 Summit Paglia (P6)

8.5 EBSD diffraction method

Cored perthitic K-feldspars were studied with electron backscatter diffraction (EBSD) carried out at the Department of Geosciences of the University of Padova, using a SEM (CamScan Mx2500) equipped with LaB_6 filament. For EBSD analysis the samples were chemically-mechanically polished (Syton polished) to remove surface damages (Prior et al., 1999) and carbon-coated with a few microns film. Patterns were collected and indexing of EBSD pattern was accepted after at least five Kikuchi bands were identified by the computer simulation. For the construction of the reflector file for K-feldspar crystallographic data from Phillips and Ribbe (1973) were utilized whereas for low albite data crystallographic data from Harlow and Brown (1980) were used for comparison.

CHAPTER 9

Discussion: how pegmatites of Central Alps originated?

9.1 General summary

The pegmatitic field located in the Central-Western Alps Central Alps which extends for more than 90 km from Centovalli Line in the west (nearby Domodossola village), to the Oligocene Masino-Bregaglia intrusive massif to the east, hosts thousand of pegmatites and aplites dikes but only a few percentage (less than 5% of them) have more complex textural, structural characters, contain accessory minerals, and show geochemical enrichments in LILE, HFSE or REE. These pegmatite intrude or cross-cut Alpine Lepontine nappe boundaries along the Southern Steep Belt near the contact with the Insubric Line. SSB represents the root area of Penninic units, in amphibolite-greenschist facies, characterized by steep oriented into subvertical and overturned nappes. Pegmatites also intrude tonalities, granodiorites of Masino-Bregaglia Oligocence two mica granite of San Fedelino stock and migmatitic orthogneisses, and biotite–sillimanite–garnet–(±cordierite)-bearing metapelitic rocks of Gruf Complex which borders the northen-western contact of the Masino-Bregaglia intrusion.

Based on geochemistry and mineralogical characters the pegmatites studied have been classified under the scheme proposed by Černý and Ercit (2005) with some modification made in this study due to the specific characters of Alpine pegmatites. Alpine pegmatites have NYF and LCT geochemical characters. In particular Phosphate Codera dike shows the highest geochemical and mineralogical fractionation and falls within beryl-columbite-phosphate subtype. The remaining dikes have moderate geochemical fractionation and like Garnet Codera dike may also develop mixed LCT-NYF character. Bodengo road cut dike has typical simple mineralogy which characterize most of the barren or ceramics pegmatite and aplites so diffuse in this area of the Alps.

Macrostructural and microstructural characters evidence notable differences between syngenetic dikes hosted within Masino-Bregaglia intrusion and epigenetic pegmatites hosted in the Southern Steep Belt. Syngenetic pegmatites have registered high temperatures (in the range of 400-450 °C) during crystallization clearly evidenced by deformed quartz, K-feldspar and the development of pervasive milonitic recrystallized quartz that also evidences preferred crystallographic orientation. These pegmatites have lobate, anastomized margins, and develop minor aplite apophysis which depart from the main pegmatite body. Epigenetic pegmatites within SSB do not intrude rocks with temperatures as high as the ones registered within Masino-Bregaglia because were emplaced after the peak metamorphism mentioned in the Chapter 2. These pegmatites have straight margins, crosscut the metamorphic foliation and do not evidence ductile deformations. Albitized pegmatites of Pizzo Marcio-Alpe Rosso underwent reactions caused by metamorphic reactions with ultramafic enclosing rocks by intensive circulation of supercritical fluids and successive K-Na metasomatic replacements (Alexandrov et al., 2001; Guastoni et al., 2008). Emerald Pizzo Marcio dike develops pinch and swell structures but the core of the pegmatite was left unaffected by the albitization process and maintain graphic textures, K-feldspar and quartz, to indicate the metasomatic process

was not deeply pervasive. Colonnello pegmatite at Pizzo Paglia has straight contacts, crosscut the enclosing migmatitic rocks and develop large miarolitic pockets, indicating that pressure of fluids was maintained during crystallization of the dike. This pegmatite and Summit Paglia dike were both emplaced after peak metamorphic deformation occurred in this area. Indeed the temperature contour map (see Chapter 2) shows the increase of amphibolites grade metamorphism to 675°C only around Bellinzona within a back-folded root zone of steeply inclined north dipping Peninnic nappes (the Cressim antiform phase).

Niobium- tantalum- yttrium- rare-earths-uranium oxides, tourmalines K-feldspar and other accessory minerals are indicative of the variable geochemical scenario. Rio Graia and Grignaschi dikes have tapiolite-(Fe), tantalite-(Fe) and minor columbite-(Fe). Albertini and Fluorite dikes have aeschynite-(Y) whereas Pizzo Marcio-Alpe Rosso, fersmite, vigezzite, tantalite-(Mn) and columbite-(Mn); Colonnello Paglia dike has lithiwodginite whereas Garnet Codera pegmatite has columbite-(Fe) and euxenite-(Y). In most of the pegmatites tourmaline has schorl composition. In albitized pegmatites of Pizzo Marcio-Alpe Rosso prevail dravite associate with tremolite and talc, indicative of the extensive influx of hypercritical fluids from the ultramafic rocks. At Phosphate Codera pegmatite crystallize Mn-rich fluorelbaite associated with F-rich triplite. In this pegmatite Cs-rich microcline is also present. Cs-rich microcline has been also found in miarolitic pockets at the Colonnello pegmatite. NYF pegmatites of Arvogno (Fluorite and Albertini dikes) carry Y-rich fluorite, Y-rich spessartine, allanite-(Y), xenotime-(Y) and Y-rich fluorapatite as accessory minerals.

Structural data of aplites and pegmatites intruded into Masino Bregaglia pluton and San Fedelino stock indicate these dikes emplaced between 32 to 25 m.y at least (Davidson et al., 1996; Hansmann, 1996; Liati et al., 2000; Oberli et al., 2004). Age determinations of aplites, pegmatites and porphyritic dikes of Central Alps have defined an interval range of age for emplacement and crystallization of pegmatites from 32 to 24.1 m.y. These ages were obtained by geochronological data of zircons, monazite, xenotime, cheralite, titanite, biotite and muscovite (Bürgi and Klötzli, 1990; Gebauer 1996; Romer et al. 1996; Guastoni and Mazzoli 2007; Vignola 2011 personal communication). All these information are utilized to trace the age of emplacement of the pegmatitic field of the Central Alps. The data published were obtained using different mineral phases, different analytical techniques. In some cases the age obtained were of aplites and dikes show strong affinities with a granitic source rock for pegmatites. In other cases have textural and structural characters very close to migmatitic leucosomes rather than pegmatites like in the case of the aplites-pegmatites studied by Romer et al. (1996). It will become crucial in the future to get more homogenous age determination data from NYF and LCT pegmatites, in order to establish more precise ages of pegmatite intrusions within Alpine nappes.

9.2 Granitic pegmatites: magmatic sources

In this Ph.D. thesis geochemical data of bulk rocks from Masino-Bregaglia intrusion, San Fedelino two mica granite, Gruf migmatites, charnokites and granulites were taken from literature to compare with the

analytical data of pegmatites from Central Alps (see Chapter 5). Plots of major elements (Na_2O, K_2O, CaO, P_2O_5, SiO_2) of bulk pegmatite compositions and related potential sources were compared and plotted in several diagrams. The MALI-SiO_2 diagram has showed geochemical affinities among pegmatites with granite-granodiorite, microgranitic dikes of Masino-Bregaglia intrusion, two mica granite of San Fedelino stock, migmatites of Gruf Complex and Permian charnokites. MALI-K_2O diagram revealed geochemical affinities among pegmatites with Gruf migmatites, San Fedelino, and microgranits. FeO/(FeO-MgO) diagram has indicated San Fedelino, microgranits and granite-granodiorites to represent potential sources to generate granitic pegmatites. ASI-P_2O_5 diagram has showed the bulk composition of Phosphate Codera pegmatite to have the highest P_2O_5 content (0.27 wt %). Such trend could be explained assuming Ca-poor anatectic S-type batch of granitic melt derived from metapelites (Nekvasil, 1988) and crystallization of some plagioclase (even with low Ca content) can reduce the Ca/P ratio to ensure that some P will be incorporated in other phosphates (in addition to the phosphorous sequestered by alkali feldspars) such as F-rich triplite.

Trace elements data of Masino-Bregaglia tonalite-granodiorite-granites series, San Fedelino two-mica granite, Gruf migmatites were not compared with the data of pegmatites because the analysis of Ga, Rb, Cs, HFSE and REE elements were lacking or resulted very incomplete (Wenk et al., 1977; von Blanckenburg et al., 1982). In any case London (2005) suggests trace-element fractionation models that attempt to relate such chemically evolved pegmatites to their source granite might be expected to fail, because the available partition coefficients are not calibrated for the experimental petrology of pegmatites.

Plots of the diagrams indicate granite-granodiorite of Masino-Bregaglia, San Fedelino two mica granite and microgranitic dikes within Masino-Bregaglia have geochemical characters to allow them candidate as potential sources of the LCT-NYF pegmatites in the Central Alps. It must be also considered Masino-Bregaglia intrusion extends his tail toward west for more than 50 kilometers. Due to very pronounced easterly axial plunge of up to 25° formed during and after the emplacement, increasingly deeper levels of Masino Bregaglia tonalites (Iorio tonalite) and granodiorite (Melirolo augengneiss) are exposed westwards (Berger and Gierè, 1995). Isotopic measures of Iorio tonalite documents an extended history of crystallization and melt evolution of at least 5 Ma, defining an early interval of 33.0 to 32.0 Ma, followed by crystallization of zoned allanite from 32.0 to 28.0 Ma and formation of magmatic epidote as late as 26 Ma (Oberli et al., 2004). Magmatic mechanism able to generate LCT and NYF pegmatites were invoked by Simmons et al. (1987) and Černý (1991) in which peraluminous, S-type and evolved I-type granitic sources, tend to segregate LCT pegmatites from the roof zones of the plutons, whereas those of the NYF class appear to originate from within the inner geochemical more primitive portions of the plutons. Masino-Bregaglia calc-alkaline pluton has ballooned structure formed by tonalite at the rim of the intrusion and granodiorite with K-feldspar megacrysts in the core. At this point pegmatites could be generated through a filter pressing mechanisms from batches of magma enriched in rare-metals. These observations raise the possibility that pegmatites inherit a vertical chemical zonation from a zoned magmatic source as documented by rhyolite eruptions from large silicic magma chambers (Simmons et al., 1987; Poli and Tommasini, 1990; London, 1992; Bea et al., 1994; Mahood et al., 1996).

If we observe the geographic distribution appears NYF pegmatites concentrate nearby Arvogno, Vigezzo valley, whereas LCT pegmatites have scattered diffusion from Vigezzo valley, to Bellinzona area throughout Codera valley. Pegmatitic dikes within the Southern Steep Belt are epigenetic whereas Codera pegmatites with LCT and NYF characters are syngenetic but always located along the border of the Masino-Bregaglia intrusion or intruded in the immediate surrounding rocks of the Gruf Complex of Chiavenna and Bregaglia valleys (Ghizzoni and Mazzoleni, 2005).

A good question is how to relate pegmatites to their magmatic sources. It may be hypothesized small granitic stocks (similar in composition to San Fedelino two mica granite) buried under metamorphic Lepontine nappes or as indicated by Ciancaleoni and Marquer (2006) outcrop and intrude the Gruf Complex and the Chiavenna ophiolites in Chiavenna valley. Other magmatic sources could be apophysis with composition similar to granodiorite porphyritic dike outcrops at Loana valley, Vigezzo valley, studied by Bürgi and Klötzli, (1990) and Romer et al., (1996) which yielded ages between 29 -31.7 m.y. At this point the possible scenario is represented by pegmatitic liquids in composition were able to escape from satellite granite-or granodiorite bodies and intrude Alpine nappes at different crustal levels.

9.3 Are there anatectic contributions to NYF and LCT Alpine pegmatites?

LCT pegmatites studied contain beryl and Be-bearing minerals as accessory minerals whereas NYF pegmatite have sensible enrichments of niobium- tantalum- yttrium- rare-earths-uranium oxides, phosphates and silicate minerals. Anatectic migmatite melts which could be invoked as potential sources to generate LCT and NYF pegmatites find some unanswered problems and obstacles that can be summarized as follows:

- ✓ Investigators of migmatites in regional metamorphic terranes commonly encounter leucosomes with a pegmatitic texture. Quartz and K-feldspar in particular can reach very coarse grain-sizes, even tens of centimetres across, even though the extent of movement seems to have been very limited in general, to judge from the overall conformity of such domains of granitic pegmatite to the gneissosity of the enclosing metasedimentary package and the common presence of a melanosome developed along the outer contact. Such pegmatites could be expected to be mineralogically very simple, devoid of any zonation from one wall to the other and characterized by the absence of graphic textures.

- ✓ The percentage of partial melting of migmatitic protoliths is too low if compared to generate high concentrations of rare elements in the anatectic magmas (Burry et al., 2005; London, 2005)

- ✓ Migmatitic melts mainly contain quartz, feldspars, and muscovite inherited from the protoliths (i.e. under amphibolites-greenschist facies like the Lepontine Dome in the Southern Stee Belt). Most of the mafic phases enriched in HFSE would remain or, in the case of biotite and cordierite, re-equilibrate in the residuum (Icenhower and London, 1995).

- ✓ Metaevaporites enriched in rare elements are also invoked as sources of pegmatites but they are poor in Be and HFSE at the source and subject to deplete Li and B already at low-grade metamorphism

- ✓ The saturation concentrations of beryl, columbite-group minerals, are highly impossible to be achieved without protracted fractionation of the parent medium (London, 2005). Depending on the temperature at which crystallization takes place, silicic melts may become saturated in beryl with as little as 70-ppm Be (Evensen et al., 1999). Metapelites metamorphic rocks usually arrive at anatectic conditions carrying from 0-5-ppm Be in their whole-rock (Grew, 1998). Cordierite-bearing migmatites which represent a potential reservoir for beryllium, due natural cordierite can accomodate few wt% levels of BeO in its crystal structure (Schreyer et al. 1979), fractionation is evident between Crd-rich restite (melanosomes) and derived liquids (leucosomes). Relative to the Crd-bearing source rocks, crystalline Crd-restites show appreciable enrichments of Be, Mn and Cs and physically separated leucogranite dikes have revealed marked Be depletions (Evensen et al., 1999; London and Evensen, 2001; Morgan and London 2003)

- ✓ Stable and radiogenic isotope signatures of rare-element pegmatites contradict direct anatexis from, or equilibration with, enclosing country rocks (Longstaffe et al., 1981; Taylor and Friedrichsen, 1983; Tomascak et al., 1998). Where studied pegmatite dikes show pronounced isotopic disequilibrium with their host rocks; Sr isotope data, for instance, preclude the derivation of pegmatites from their immediate hosts (Brookins, 1986; Taylor and Friedrichsen, 1983).

9.4 How proximal or distal are the magmatic sources of pegmatites?

The lack of granitoids bodies or dikes outcrop close to pegmatites and the relative distance of LCT-NYF pegmatites from Masino-Bregaglia or San Fedelino intrusive suites make plausible the presence of buried satellite granitic bodied below Lepontine nappes. How far liquid melts can travel through the crust depend by several factors such as rheology of the crust, temperatures of the hosting rocks, the physical-chemical characters of pegmatite liquid melts. London et al. (1989) and Thomas et al. (2000) confirmed experimentally the enormous capacity of F-, B-, P- and Li-rich pegmatite melts to contain up to 18 wt % of dissolved H_2O. Increasing contents of Li, B, P, F, and H_2O reduce polymerization, increase fluidity and mobility, and enhance thermal stability of pegmatite melts to lower temperatures. Thus, pegmatite melts most enriched in volatiles and rare elements can travel the farthest from their source. Thomas and Webster (2000) calculated the viscosity of a very highly fluxed melt containing H_2O + F equals to 17.3 wt % is 4.7 Pas at 600°C, which they equated to the viscosity of castor oil at 20°C. London (1986) estimated the viscosity of highly fluxed melt in the system $Li_2BB_4O_7$-$NaAlSi_3O_8$-SiO_2-H_2O at 500° to 540°C and 200 MPa to be 10 Pas. The transfer of heat in the continental crust, however, is largely by the slow processes of conduction, so the deep parts of the crust are slow to heat up and slow to cool down. Consequently

metamorphic temperatures can remain above solidus (650°C) for times as long as 30 millions years, like in the Himalayan system. Thermal Dome reached its peak temperatures in the SSB at about 32 Ma (Hunziker et al., 1992; Gebauer, 1999). Fission track ages of detrital grains suggest that the core of the Lepontine became exposed at about 14 Ma (Spiegel et al., 2000). This interval of time was enough to maintain crustal elevated temperatures (several hundreds of °C temperatures) and allow pegmatite liquids (aged between 32-25 m.y.) to travel through the crust without freezing. Moreover must be also considered toward west of Central Alps outcrop structurally the deepest Lepontine pile of nappes and the actually erosional surfaces have exposed pegmatites intruded at different crustal levels. For example NYF pegmatites of Vigezzo valley are hosted within Pioda di Crana nappe (Moncucco-Orselina zone) structurally deeper respect LCT miarolitic Colonnello Paglia dike which is hosted within Bellinzona-Dascio zone.

9.5 An anatectic source for barren pegmatites is feasible?

The temperature contour map of Lepontine Dome shows the increase in temperature toward the south of the Dome, where the Insubric line truncates the map. In this area recorded temperatures increase to 675°C (around Bellinzona) where the peak metamorphic temperatures at amphibolite facies at about 32 Ma were reached (Hunziker et al., 1992; Todd and Engi 1997; Gebauer, 1999. Burry et al., (2005) suggest that metamorphic reactions of muscovite dehydration melting observed with leucosome generation at the macroscale, indicative of Alpine age migmatization, occurred around Bellinzona area. Berger et al., (2008) defined metapelitic rocks incorporated into the SSB are not a realistic fluid source, because, at the conditions of partial melting, the released aqueous fluid is too low and it would only lead to in situ partial melting and no fluid would be released into the directly adjacent or overlying rocks to produce large batches of granitic magma. Regardless of the uncertainty about the source of water in such contest (from amphibolite facies metamorphic rocks buried in the southern Alps) leucosome melts were generated in the Southern Steep Belt during the metamorphic peak temperatures and these liquid melts could be represent part of the barren-muscovite class pegmatites promoted in the P-T diagrams by Ginsburg et al. (1979).

Bibliography

ADAM J., GREEN T.H., SIE S.H. (1993) Proton microprobe determined partitioning of Rb, Sr, Ba, Y, Zr, Nb and Ta between experimentally produced amphiboles and silicate melts with variable F content. Chemical Geology, 109, 29-49.

ALBERTINI C., ANDERSEN T. (1989) Non-metamict orthorhombic AB_2O_6 Y-Nb-Ta-Ti oxides from a pegmatite in Arvogno, Crana Valley (Toceno, Vigezzo Valley, Northern Italy).

ALEXANDROV P., GIULIANI G., ZIMMERMANN J.L. (2001) ineralogy, age, and fluid geochemistry of the Rila emerald deposit, Bulgaria. Economic Geology, 96, 1469-1476.

BAYLISS P., KAESZ H., NICKEL E.H. (2005) The use of chemical-element adjectival modifiers in mineral nomenclature. Canadian Mineralogist 43, 1429-1433.

BERGER A., GIERÈ R. (1995) Structural observations at the eastern contact of the Bergell pluton. Schweizerische Mineralogische und Petrographische Mitteilungen, 78, 241- 258.

BERGER A. (1996) Geological-tectonic map of the Bergell pluton. Schweizerische Mineralogische und Petrographische Mitteilungen, Supplement to volume 76/3.

BERGER A., ROSENBERG C., SCHMID S. (1996) Ascent, emplacement and exhumation of the Bergell pluton within the Southern Steep Belt of the Central Alps Schweizerische Mineralogische und Petrographische Mitteilungen, 76, 357- 382.

BERGER A., BURRI T., ALT-EPPING P., ENGI M. (2008) Tectonically controlled fluid flow and water-assisted melting in the middle crust: An example from the Central Alps. Lithos, 102, 598-615.

BIGIOGGERO B., BORIANI A., COLOMBO A., TUNESI A., FERRARA G., TONARINI S. (1981) Età e caratteri petrochimici degli ortogneiss della zona Moncucco-Orselina nell'area ossolana. Rendiconti Società Italiana di Mineralogia e Petrologia, 38, 207-218.

VON BLANCKENBURG F., FRÜH-GREEN G., DIETHELM K., STILLE P. (1992) Nd-,Sr-O-isotopic and chemical evidence for a two-stage contamination history of mantle magma in the Central-Alpine Bergell intrusion. Contribution to Mineralogy and Petrology, 110, 33-45.

BONSIGNORE G., CASATI P., CRESPI R., FAGNANI G., LIBORIO G., MONTRASIO A., MOTTANA A., RAGNI U., SCHIAVINATO G., VENZO S. (1971) Note illustrative della Carta Geologica d'Italia. F. 7-18, Pizzo Bernina e Sondrio, Roma.

BOUSQUET R., GOFFE' B., HENRY P., LE PICHON X., CHOPIN C. (1997) Kinematic, thermal and petrological model of the Central Alps: Lepontine metamorphism in the upper crust and eclogitisation of the lower crust. Tectonophysics, 273, 105-127.

BOWEN N.L. (1928) The Evolution of the Igneous Rocks. Princeton University Press, New Jersey, 332 p.

BRÖGGER W.C. (1890) Die Mineralien der Syenitpegmatitgänge der südnorwegischen Augit-und Nephelinsyenite. Zeitschrift für Kristallographie und Mineralogie, 16, 1-63.

BRONGNIART A. (1813) Essai d'une classification minéralogique des roches mélangées.Journal des Mines, 199, 5-48.

BROOKINS D.G. (1986) Rubidium–strontium geochronologic studies of large granitic pegmatites. Neues Jahrbuch für Mineralogie, Abhandlungen. 156, 81– 97.

BROWN W.L., PARSONS I. (1983) Nucleation on perthite-perthite boundaries and exsolution mechanisms in alkali feldspars. Physics and Chemistry of Minerals, 10, 55-61.

BROWN C. (1999) Mineralogy of NYF granitic pegmatites. Eugene E. Foord Memorial symposium on NYF-type Pegmatites (Denver). Canadian Mineralogist, 37, 848-849 (abstr.).

BUCHER-NURMINEN K., DROOP G. (1983) The metamorphic evolution of garnet-cordierite-sillimanite-gneisses of the Gruf-Complex, Eastern Pennine Alps. Contribution to Mineralogy and Petrology, 84, 215-227.

BUCHER K., FREY M. (1994) Petrogenesis of Metamorphic Rocks (6th ed.). Springer-Verlag, New York, N.Y.

BUCK H.M., ČERNÝ P., HAWTHORNE, F.C. (1999) The Shatford Lake pegmatite group, southeastern Manitoba: NYF or not? Eugene E. Foord Memorial Symposium on NYF-type Pegmatites (Denver). Canadian Mineralogist, 37, 830-831 (abstr.).

BURG J.P., GERYA T.V. (2005) The role of viscous heating in Barrovian metamorphism of collisional orogens: thermomechanical models and application to the Lepontine Dome in the Central Alps. Journal of Metamorphic Geology, 23, 75-95.

BURKE E.A.J. (2008) Tidying up Mineral Names: an IMA-CNMNC Scheme for Suffixes, Hyphens and Diacritical marks Mineralogical Record, 39, 131-135.

BURNHAM C.W. (1975) Water and magmas: A mixing model. Geochimica et Cosmochimica Acta, 39, 1077-1084.

BURRI T., BERGER A., MARTIN E. (2005) Tertiary migmatites in the Central Alps. Schweizerische Mineralogische und Petrographische Mitteilungen, 76, 357-382.

CAMERON E.N., JAHNS R.H., MCNAIR A.H., PAGE L.R. (1949) Internal structure of granitic pegmatites. Economic Geology, Monograph, 2, 115 p.

CANTADORE F., MARCHETTI G. F., MATTIOLI V. (1967) - I minerali della Cava Grignaschi nell'Ossola. Natura, 58, 79.

ČERNÝ P., SILVOLA J. (1980) The Tanco pegmatite at Bernic Lake, Manitoba. XII. Hafnian zircon. Canadian Mineralogist, 18, 313-321

ČERNÝ P., BRISBIN W.C. (1982a): The Osis Lake pegmatitic granite, Winnipeg River district, southeastern Manitoba. Granitic Pegmatites in Science and Industry. Mineralogical Association of Canada, Short Course Handbook 8, 545-555.

ČERNÝ P. (1982b) Petrogenesis of granitic pegmatites In Granitic Pegmatites, Science and Industry . Mineralogical Association of Canada, Short Course Handbook 8, 405-461

ČERNÝ P., SUNN J.V., MASON R.A., DELANEY J.S. (1984) Ceochemistry and petrology of feldspar crystallization in the Věžná pegmatite, Czechoslovakia, Canadian Mineralogist, 22, 631-651.

ČERNÝ P., MEINTZER R. E., ANDERSON A. J. (1985) Extreme fractionation in rare-element granitic pegmatites: selected examples of data and mechanism. Canadian Mineralogist, 23, 381-421.

ČERNÝ P., MEINTZER R.E. (1988) Fertile granites in the Archean and Proterozoic fi elds of rare-element pegmatites: crustal environment, geochemistry and petrogenetic relationships. Geology of Granite-Related Mineral Deposits. Canadian Institute of Mining and Metallurgy, Special Publication, 39, 170-206

ČERNÝ P. (1990) Distribution, affiliation and derivation of rare-element granitic pegmatites in the Canadian Shield. Geologische Rundschau, 79, 183-226.

ČERNÝ P. (1991a) Rare-element granitic pegmatites, Part I: Anatomy and Internal Evolution of Pegmatite Deposits. Geoscience Canada, 18, 29-47.

ČERNÝ P. (1991b) Rare-element granitic pegmatites, Part II: Regional to global environments and petrogenesis Geoscience Canada, 18, 68-81.

ČERNÝ P. (1991c) Fertile granites of Precambrian rare-element pegmatite fields: is geochemistry controlled by tectonic setting or source lithologies? Precambrian Research, 51, 429-468.

ČERNÝ P. (1994) Evolution of feldspars in granitic pegmatites. In Feldspars and their Reactions NATO Advanced Study Institute Series, 421, 501-539.

ČERNÝ P. (2005) The Tanco rare-element pegmatite deposit, Manitoba: regional contaxt, internal anatomy, and global comparisons, In Rare-Element Geochemistry of Ore Deposits. Geological Association of Canada, Short Course Handbook, 17, 127-158.

CHAKOUMAKOS B.C., LUMPKIN G.R. (1990) Pressure-temperature constraints on the crystallization of the Harding pegmatite, Taos County, New Mexico. Canadian Mineralogist, 28, 287-298.

CHORLTON L.B., MARTIN R.F. (1978) The effect of boron on the granite solidus. Canadian Mineralogist, 16, 239-244.

CIANCALEONI L., MARQUER D. (2006) Syn-extension leucogranite deformation during convergence in the Eastern Central Alps: example of the Novate intrusion. Terra Nova, 18, 170-180.

COLLINS W.J., BEAMS S.D., WHITE A.J.R., CHAPPELL B.W. (1982) Nature and origin of A-type granites with particular reference to south-eastern Australia. Contribution to Mineralogy and Petrology, 80, 180-200.

COOK C. W. (1925) Molybdenite deposit near New Ross, Nova Scotia. Economic Geology, 20, 185-188.

CORNELIUS H.P. (1916) Ein alpines Vorkommen von Sapphirin. Centralblatt für Mineralogie, Geologie und Paläontologie, 265–269.

DAVIDSON C., ROSENBERG C., SCHMID S.M. (1996) Synmagmatic folding of the base of the Bergell Pluton, Central Alps. Tectonophysics, 265, 213-238.

DE BEAUMONT E. (1847) Note sur les émanations volcaniques et métallifères. Bulletin de la Société Geologique de France, 2e serie, p. 1249.

DE MICHELE V. (1967) Bavenite nella pegmatite di cava Grignaschi (Val d'Ossola). Atti Società italiana di Scienze naturali. Vol. 106. 171-179.

DE MICHELE V. (1970) Itinerari Mineralogici. Natura, 61, 120 pp., Milano.

DIETHELM K. (1985) Horneblendite und Gabbros im östlichen Bergell (Val Sissone, Sondrio, Italien). Schweizerische Mineralogische und Petrographische Mitteilungen, 65, 223- 246.

ELMER F.L., WHITE R.W., POWELL R. (2006) Devolatilization of metabasic rocks during greenschist-amphibolite facies metamorphism. Journal of Metamorphic Geology, 24, 497-513.

ENGI M., TODD C., SCHMATZ, D. (1995) Tertiary metamorphic conditions in the eastern Lepontine Alps. Schweizerische Mineralogische und Petrographische Mitteilungen, 75, 347– 369.

ENGLAND P.C., THOMPSON A.B. (1984) Pressure-temperature –time paths of regional metamorphism I. Heat transfer during the evolution of regions of thickened continental crust. Journal of Petrology, 25, 894-928.

ERCIT T.S., ČERNÝ P., HAWTHORNE F.C. (1992) The wodginite group III. Classification and new species. Canadian Mineralogist, 30, 633-638

ERCIT T.S., WISE M.A., ČĚRNÝ P (1995) Compositional and structural systematics of the columbite group. American Mineralogist, 80, 613-619.

ERCIT T.S. (2005) REE-enriched granitic pegmatites. In Rare-Element Geochemistry and Mineral Deposits Geological Association of Canada, Short Course Notes 17, 175-199.

ERTL A., HUGHES J.M., PROWATKE S., ROSSMAN G.R., LONDON D., FRITZ E.A. (2003) Mn-rich tourmaline from Austria: structure, chemistry, optical spectra, and relations to synthetic solid solutions. American Mineralogist, 88, 1369-1376.

EVENSEN J. M., LONDON D., WENDLANDT R. F. (1999) Solubility and stability of beryl in granitic melts. American Mineralogist 84, 733–745.

FELDKAMP L.A., DAVIS L.C., KRESS J.W. (1984) Practical cone-beam algorithm, Journal of the Optical Society of America, A1(6), 612-619.

FENN P.M. (1977) The nucleation and growth of alkali feldspars from hydrous melts. Canadian Mineralogist, 15, 135-161.

FENN P.M. (1986) On the origin of graphic granite. American Mineralogist, 71, 325-330.

FERSMAN A.E. (1923) Mineral association in the Khibinsky and Lovozersky tundras. Bulletin of Academy of Science, Russie, 6, 65-80; Regular intergrowths of minerals in the Khibinsky and Lovozersky tundras, 6, 275-290.

FERSMAN A.E. (1931) Über die geochemisch-genetische Klassifikation der Granitpegmatite. Tschemarks Mineralogische und Petrographische Mitteilungen, 41, 64-83.

FLETCHER C.J.N. (1977) The geology, mineralization, and alteration of Ilkwang mine, Republic of Korea, a Cu-W-bearing tourmaline breccia. Economic Geology, 72, 753-768.

FOORD E.E., MROSE M.E. (1978) Rynersonite $Ca(Ta,Nb)_2O_6$, a new mineral from San Diego County, California. American Mineralogist, 63, 709-714.

FOX J.S. (1975) Three-dimensional isograds from the Lukmanier Pass, Switzerland, and their tectonic significance. Geological Magazine, 112, 547-564.

FOWLER A.D., DOIG R. (1983) The age and origin of Grenville Province uraniferous granites and pegmatites. Canadian Journal of Earth Science 20, 92-104.

FREY J. D. (1967) Geologie des Greinagebietes (Val Camadra, Valle Cavalasca, Val di Larciolo, Passo della Greina), Beitr. Geol. Karte Schweiz, 131, 1–112.

FREY M., HUNZIKER J.C., FRANK W., BOCQUET J., DAL PIAZ G.V., JÄGER E., NIGGLI E. (1974) Alpine metamorphism of the Alps: a review. Schweizerische Mineralogische und Petrographische Mitteilungen, 54, 247– 290.

FROITZHEIM N., SCHMID S.M., FREY M. (1996) Mesozoic paleogeography and the timing of eclogite-facies metamorphism in the Alps: a working hypothesis. Eclogae Geologicae Helveticae 89, 81– 110.

FROST B.R., BARNES C.G., COLLINS W.J., ARCULUS R.J., ELLIS D.J., FROST C.D. (2001) A geochemical classification for granitic rocks. Journal of Petrology, 42, 2033-2048.

GALLI A., LE BAYON B., SCHMIDT M.W., BURG J.P., CADDICK M.J., REUSSER E. (2011) Granulites and charnockites of the Gruf Complex: Evidence for Permian ultra-high temperature metamorphism in the Central Alps. Lithos, 124, 17-45.

GALPIN S.L. (1915) A preliminary report on the feldspar and mica deposits of Georgia. Georgia Geological Survey Bulletin, 30, p.27.

GANSSER A., GYR T. (1964) Über Xenolith-schwärme aus demBergeller Massiv und Probleme der Intrusion. Eclogae Geologicae Helveticae, 57, 577-598.

GARRISON J.R., LONG L.E., RICHMANN D.L. (1979) Rb–Sr and K–Ar geochronologic and isotopic studies, Llano Uplift, central Texas. Contribution to Mineralogy and Petrology 69, 361-374.

GEBAUER D. (1996) A P-T-t path (ultra ?) high-pressure ultramafic/mafic rock associations and their felsic country-rock based on SHRIMP dating of magmatic and metamorphic zircon domains. Example: Central Swiss Alps. Earth Processes: Reading the Isotopic Code: American Geophysical Union, Geophysical Monographs, 65, 307-329.

GEBAUER D. (1999) Alpine geochronology of the central and Western Alps: new constraints for a complex geodynamic evolution. Schweizerische Mineralogische und Petrographische Mitteilungen, 79, 191–208

GERYA T. V., STÖCKHERT, B. (2002) Exhumation rates of high pressure metamorphic rocks in subduction channels: the effect of rheology. Geophysical Research Letters, 29, n° 1261.

GHIZZONI S., MAZZOLENI G. (2005) Itinerari mineralogici in Val Codera. Ed. Geologia Insubrica 336 pp.

GINSBURG A.I., TIMOFEYEV I.N., FELDMAN L.G. (1979) Principles of geology of the granitic pegmatites. Nedra, Moscow, 296 p. (In Russian).

GINSBURG A.I. (1984) The geological condition of the location and the formation of granitic pegmatites: 27th International Geological Congress, 15, 245-260.

GIUSEPPETTI G., TADINI C. (1990) The crystal structure of vigezzite, (Ca,Ce)(Nb,Ta,Ti)$_2$O$_6$, intermediate term of the aeschynite series. Neues Jahrbuch fur Mineralogie, Monatshefte, 301-308.

GOFFE´ B., BOUSQUET R., HENRY P., LE PICHON X. (2003) Effect of the chemical composition of the crust on the metamorphic evolution of orogenic wedges. Journal of Metamorphic Geology, 21, 123–141.

GORDIYENKO V.V. (1970) Mineralogy, Geochemistry and Genesis of Spodumene Pegmatites. Nedra, Leningrad (in Russian)

GRAESER S., SCHWANDER H., HÄNNI H., MATTIOLI V. (1979) Vigezzite, (Ca,Ce)(Nb,Ta,Ti)$_2$O$_6$, a new aeschynite-type mineral from the Alps. Mineralogical Magazine, 43, 459-462.

GRAMACCIOLI C.M. (1958) Nuovo ritrovamento di delorenzite a Craveggia. Natura, 49, 110-112.

GRAMACCIOLI C. M., DIELLA V., DEMARTIN F. (2000) The formation of scandium minerals as an example of the role of complexes in the geochemistry of rare earths and HFS elements. European Journal of Mineralogy, **12**, 795-808

GRASEMANN B., MANCKTELOW N. S. (1993) Two-dimensional thermal modelling of normal faulting: the Simplon fault zone, Central Alps, Switzerland. Tectonophysics, 225, 155–165.

GREW E. S. (1998) Boron and beryllium minerals in granulite-facies pegmatites and implications of beryllium pegmatites for the origin and evolution of the Archean Napier Complex of East Antarctica. Memories Natural Institute Polar Researches 53, 74–92.

GREW E.S., YATES M.G., BARBIER J., SHEARER C.K., SHERATON J.W., SHIRAISHI K., MOTOYOSHI Y. (2000) Granulite-facies beryllium pegmatites in the Napier Complex in Khmara and Amundsen bays, western Enderby Land, East Antarctica. Polar Geoscience, 13, 1-40.

GRUJIC D., MANCKTELOW N. S. (1996) Structure of the northern Maggia and Lebendun Nappes, Central Alps, Switzerland. Eclogae Geologicae Helvetiae, 89, 461–504.

GUASTONI A., GRAMMATICA P. (2001) Silicati di berillio della valle Soe. Rivista Mineralogica Italiana, 25, 105-107.

GUASTONI A., DEMARTIN F. (2003) Ferrotapiolite della valle Soe`. Atti della Societa` Italiana di Scienze Naturali, 144, 145-150.

GUASTONI A. MAZZOLI C. (2007) Age determination by µ-PIXE analysis of cheralite-(Ce) from emerald-bearing pegmatites of Vigezzo Valley (Western Alps, Italy). Mitt. Österr. Mineral. Ges. 153, 297-282

GUASTONI A., NESTOLA F., MAZZOLENI G., VIGNOLA P. (2007) Mn-rich graftonite, ferrisicklerite, staněkite and Mn-rich vivianite in a granitic pegmatite at Soe' Valley, central Alps, Italy. Mineralogical Magazine, 71, 579–585.

GUASTONI A., DIELLA V., PEZZOTTA F. (2008) Vigezzite and associated oxides of Nb–Ta from emerald-bearing pegmatites of the Vigezzo valley, Western Alps, Italy. Canadian Mineralogist, 46, 619-633.

GUASTONI A., NESTOLA F., GIARRETTA A. (2009) Mineral chemistry and alteration of rare element (REE) carbonates from alkaline pegmatites of Mount Malosa, Malawi. American Mineralogist, Vol. 94, 1216-1222.

GUASTONI A., NESTOLA F. (2010) Sn-rich thortveitite intergrowth with xenotime-(Y): Y versus Sc fractionation in NYF miarolitic pegmatites at Baveno (Southern Alps, Italy). *Acta Mineralogica-Petrographica*, 20° General Meeting, IMA, Budapest, Ungheria, Abstract Volume **6**, 616.

GUASTONI A., NESTOLA F., FERRARIS C., PARODI G. (2012) Dissolution of xenotime-(Y) and crystallization of Sn-rich thortveitite in miarolitic pegmatites at Baveno (Southern Alps, Italy). Mineralogical Magazine, submitted.

HANDY M.R., BABIST J., ROSENBERG C.L., WAGNER R., KONRAD M. (2005) Decoupling and its relation to strain partitioning in continental lithosphere – insight from the periadriatic fault system (European Alps). In:

Deformation Mechanisms, Rheology and Tectonics. Geological Society of London, Special Publications, 249-276.

HÄNNY R., GRAUERT B., SOPTRAJANOVA G. (1975) Paleozoic migmatites affected by high-grade tertiary metamorphism in the Central Alps (Valle Bodengo, Italy). Contribution to Mineralogy and Petrology, 51, 173-196.

HANSMANN W. (1996) Age determination on the Tertiary Masino-Bregaglia (Bergell) intrusives (Italy, Switzerland): a review. Schweizerische Mineralogische und Petrographische Mitteilungen, 76, 421-451.

HANSON S., SIMMONS JR., FALSTER A. (1999) Proposed nomenclature for samarskite-group minerals: new data on ishikawaite and calciosamarskite. Mineralogical Magagazine, 63, 27-36.

HARLOW G.E., BROWN G.E. (1980) Low albite: an X-ray and neutron diffraction study. American Mineralogist, 65, 986-995.

HARRIS N.B.W., MARRINER G.F. (1980) Geochemistry and petrogenesis of a peralkaline granite complex from the Midian Mountains, Saudi Arabia. Lithos 13, 325-337.

HAÜY R.J. (1801) Traité de minéralogie, 4 volumes and atlas, Paris.

HAWTHORNE F.C., MACDONALD D.J., BURNS P.C. (1993) Reassignment of cation site occupancies in tourmaline: Al–Mg disorder in the crystal structure of dravite. American Mineralogist, 78**,** 265-270.

HAWTHORNE F.C., HENRY D.J. (1999) Classification of the minerals of the tourmaline group. European Journal of Mineralogy, 11, 201-215

HEITZMANN P. (1987) Evidence of late Oligocene early Miocene backthrusting in the Central Alpine "root zone". Geodinamica Acta, 1, 183-192.

HESS F.L., HUNT W.F. (1913) Triplite from Eastern Nevada. American Journal of Sciences., 36, 51-54.

HESS F.L. (1925) The natural history of pegmatites. Engineering & Mining Journal Press, 120, 289-298.

HOLTZ F., JOHANNES W., PICHAVANT M. (1992) Peraluminous granites: the effect of alumina on melt composition and coexisting minerals. Transactions of the Royal Society of Edinburgh, Earth Sciences 83, 409–416.

HUNZIKER J. C., DESMONS J., HURFORD A. J. (1992) Thirty-two years of geochronological work in the Central and Western Alps: a review on seven maps. Mémoires de Géologie (Lausanne), 13, 1–59.

ICENHOWER J.P., LONDON D., LAYNE G.D. (1994) Element partitioning among biotite, muscovite, garnet, cordierite, and peraluminous melt: behavior of Li and Mn. Geological Society of America Abstract Programs, 26, 290.

JACKSON N.J., WALSH J.N., PEGRAM E. (1984) Geology, geochemistry and petrogenesis of late Precambrian granitoids in the central Hijaz Region of the Arabian Shield. Contribution to Mineralogy and Petrology 87, 205-219.

JAHNS R.H. (1953) The genesis of pegmatites. 1. Occurrence and origin of giant crystals. American Mineralogist, 38, 563-598.

JAHNS R.H. (1955) The study of pegmatites. Economic Geology, 50th Anniversary Volume, 1025-1130.

JAHNS R.H., TUTTLE O.F. (1963) Layered pegmatite-aplite intrusives: Mineralogical Society of America, Special Paper 1, 78-92.

JAHNS R.H., BURNHAM C.W. (1969) Experimental studies of pegmatite genesis; 1, A model for the derivation and crystallization of granitic pegmatites. Economic Geology, 64, 843-864.

KALT A., SCHREYER W., LUDWIG T., PROWATKE S., BERNHARDT H.J., ERTL A. (2001) Complete solid solution between magnesian schorl and lithian excess-boron olenite in a pegmatite from Koralpe (eastern Alps, Austria). European Journal of Mineralogy, 13, 1191–1205.

KJELLMAN J., ČERNÝ P., SMEDS S.A. (1999) Diversified NYF pegmatite populations of the Swedish Proterozoic: outline of a comparative study. In The Eugene E. Foord Memorial Symposium on NYF-type Pegmatites (Denver). Canadian Mineralogist 37, 832-833 (abstr.).

KNOBLAUCH P., M. REINHARD, AND E. KÜNDIG (1939) Geologischer Atlas der Schweiz 1:25000, vol. 11 Bl, A. Franke, Bern.

KOGARKO L.N., KRIGMAN L.D., KROT T.V. (1968) The solubility and geochemistry of phosphorous in magmas. Geochemistry International, 25, 1-12.

KÖPPEL V., GÜNTHERT A., GRÜNENFELDER M. (1980) Patterns of U–Pb zircon and monazite ages in polymetamorphic units of the Swiss Central Alps. Schweizerische Mineralogische und Petrographische Mitteilungen 61, 97–119.

KÜNDIG E. (1926) Beiträge zur Geologie und Petrographie der Gebirgskette zwischn Val Calanca und Misox. Schweizerische Mineralogische und Petrographische Mitteilungen, 4, 1-99.

LANDES K.K. (1925) The paragenesis of the granite pegmatites of central Maine. American Mineralogist, 10, 355-411.

LANDES K.K. (1933) Pegmatites and hydrothermal veins. American Mineralogist, 22, 551-560.

LIATI, A., GEBAUER D., FANNING M. (2000) U–Pb SHRIMP dating of zircon from the Novate granite (Bergell, Central Alps): evidence for Oligocene–Miocene magmatism, Jurassic/Cretaceous continental rifting and opening of the Valais trough. Schweizerische Mineralogische und Petrographische Mitteilungen, 80, 305- 316.

LINCIO G. (1905) Sul berillo di Vall'Antoliva e Cosasca. Atti Regia Accademia delle Scienze, vol. 40.

LINDGREN W. (1937) Succession of minerals and temperatures of formation in ore deposits of magmatic affiliations. American Institute of Mining, metallurgical, and Petroleum Engineers, Technical Publication, 126.

LIU X., BYRNE R.H. (1997) Rare earth and yttrium phosphate solubilities in aqueous solution. Geochimica and Cosmochimica Acta, **61**, 1625-1633.

LONDON D., BURT D.M. (1982) Lithium aluminosilicate occurrences in pegmatites and the lithium aluminosilicate phase diagram. American Mineralogist, 67, 483-493.

LONDON D. (1984) Experimental phase equilibria in the system $LiAlSiO_4$-SiO_2-H_2O: a petrogenetic grid for lithium-rich pegmatites. American Mineralogist, 69, 995-1004.

LONDON D. (1986) The magmatic-hydrothermal transition in the Tanco rare-element pegmatite: evidence from fluid inclusions and phase equilibrium experiments. American Mineralogist, 71, 376-395.

LONDON D. (1986a) Liquidus relations of Macusani rhyolite: An analogue to rare-element granite-pegmatite system. Geological Society of America abstract program, 18, 675.

LONDON D. (1986b) Formation of tourmaline-rich gem pockets in miarolitic pegmatites. American Mineralogist, 71, 396-405.

LONDON D. (1987) Internal differentiation of rare-element pegmatites: Effects of boron, phosphorus and fluorine. Geochimica et Cosmochimica Acta, 51, 403-420.

LONDON D., HERVIG R. L., MORGAN G. B. (1988) Melt-vapor solubilities and elemental partitioning in peraluminous granite-pegmatite systems: Experimental results with Macusani glass at 200 MPa. Contribution to Mineralogy and Petrology, 99, 360–373.

LONDON D., MORGAN G. B., HERVIG R. L. (1989) Vapour-undersaturated experiments in the system macusanite-H_2O at 200MPa, and the internal differentiation of granitic pegmatites. Contribution to Mineralogy and Petrology, 102, 1–17.

LONDON D. (1992) The application of experimental petrology to the genesis and evolution of granitic pegmatites. Canadian Mineralogist, 30, 499–540.

LONDON D. (1996) Granitic pegmatites. Transaction of Royal Society of Edinburgh of Earth Science 87, 305–319.

LONDON D. (1997) Estimating abundances of volatile and other mobile componenets in evolved silicic melts through mineral-melt equilibria. Journal of Petrology, 38, 1691-1706.

LONDON D., EVENSEN J. M. (2001) The beryllium cycle from anatexis of metapelites to beryl-bearing pegmatites. In 11th V. M. Goldschmidt Conference, Contribution 1088, Lunar Planetary Institute, Houston, #3367.

LONDON D. (2005) Granitic pegmatites: an assessment of current concepts and directions for the future. Lithos, 80, 281-303.

LONDON D. (2008) Pegmatites. The Canadian Mineralogist, Special Publication 10.

LONDON D. (2009) The origin of primary textures in granitic pegmatites. Canadian Mineralogist, 47, 697-724.

LONGSTAFFE F.J., ČERNÝ P., MUEHLENBACHS K. (1981) Oxygen-isotope geochemistry of the granitoid rocks in the Winnipeg River pegmatite district, southeastern Manitoba. Canadian Mineralogist, 19, 195-204.

LUGEON M. (1901) Les grandes nappes de recouvrement des Alpes du Chablais et de la Suisse. Bulletin de la Société Géologique de France 22, 723– 826.

LUMPKIN G.R., EWING R.C. (1992) Geochemical alteration of pyrochlore group minerals: microlite subgroup. American Mineralogist, **77**, 179-188.

LUTH W.C., JAHN R., TUTTLE O.F. (1964) The granite system at pressures of 4 to 10 kilobars. Journal of Geophysical Research, 69, 759-773.

MÄKINEN E. (1915) Die Granitpegmatite von Tammela in Finnland und ihre Minerale. Commission Géologique de Finlande, Bulletin, 35, p. 22.

MANNING D.A.C., HAMILTON D.L., HENDERSON C.M.B., DEMPSEY M.J. (1980) The probable occurrence of interstitial Al in hydrous F-bearing and F-free aluminosilicate melts. Contribution to Mineralogy and Petrology, 75, 257-262.

MANNING D.A.C. (1981) The effect of fluorine on liquidus phase relationships in the system Qz-Ab-Or with excess water at 1 kb. Contributions to Mineralogy and Petrology, 76, 206-215.

éologique de Finlande, Bulletin, 35, 1-101.

MANNUCCI G., DIELLA V, GRAMACCIOLI C.M., PILATI T. (1986): A comparative study of some pegmatitic and fissure monazite from the Alps. Canadian Mineralogist, 24, 469-474

MARTIN J.S. (1983) An experimental study of the effects of lithium on the granite solidus. Journal of Ussher Society, 5, 417-420.

MARTIN R.F., DE VITO C. (2005) The patterns of enrichment in felsic pegmatites ultimately depend on tectonic setting. Canadian Mineralogist, 43, 2027-2048.

MARTIN-IZARD A., PANIAGUA A., MOREIRAS D., ACEVEDO R.D., MARCOS-PASCUAL C. (1995): Metasomatism at a granitic pegmatite–dunite contact in Galicia; the Franqueira occurrence of chrysoberyl (alexandrite), emerald, and phenakite. Canadian Mineralogist, **33**, 775-792

MATTIOLI V. (1976) Località mineralogiche consigliate: Pegmatite di Rio Graia, Trontano, Valle Vigezzo. Notizie G.M.L., 2, 40-43.

MATTIOLI V. (1986) Una nuova pegmatite in val di Crana. Rivista Mineralogica Italiana, 3, 101.

MATTIOLI V., APPIANI R., CINI, V., GENTILE P., PREITE D. VIGNOLA P. (1995): Val Vigezzo. I Minerali delle Albititi. Edizioni Linea Due, Milan, Italy

MCNEIL, D. (2005) Beryllium. Mining annual review: London, United Kingdom, Mining Communications Ltd. CD-ROM.

MILLER C.F., MITTLEFEHLDT D.W. (1984) Extreme fractionation in felsic magma chambers: a product of liquid-state diffusion or fractional crystallization? Earth Planetary Science Letters, 68, 151-15

MILNES A.G. (1974) Post-nappe folding in the western Lepontine Alps. Eclogae Geologicae Helveticae 67, 333– 348.

MORGAN G.B., LONDON D. (1999) Crystallization of the Little Three layered pegmatite-aplite dike, Ramona District, California. Contributions to Mineralogy and Petrology, 136, 310-330.

MOTICSKA P. (1970) Petrographie und Strukturanalyse des westlichen Bergeller Massivsund seines Rahmens. Schweizerische Mineralogische und Petrographische Mitteilungen, 50**,** 355–444.

MÜLLBAUER F. (1925) Die Phosphatpegmatite von Hagendorf, Bayern. Zeitschrift für Kristallographie und Mineralogie, 61, 318-336.

MÜLLER, S., ANSORGE, J., EGLOFF, R., KISSLING, E. (1980) A crustal cross section along the Swiss Geotraverse from the Rhine Graben to the Po Plain. Eclogae Geologicae Helveticae 73, 463– 483.

MURRAY M.M., ROGERS J.J.W. (1973) Distribution of rubidium and strontium in the potassium feldspars of two granite batholiths. Geochemical Journal, 6, 117-130.

MYSEN B.O., RYERSON F., VIRGO D. (1981) The structural role of phosphorous in silicate melts. American Mineralogist, 66, 106-117.

MYSEN B.O., VIRGO D. (1985) Interaction between fluorine and silica in quenched meltson the points SiO_2-AlF_3 and SiO_2-NaF determined by Raman spectroscopy. Physics and Chemistry of Minerals, 12, 77-85.

NEKVASIL H. (1988) Calculated effect of anorthite component on the crystallization paths of H_2O-undersaturated haplogranitic melts. American Mineralogist 73, 966–981.

NIGGLI E., NIGGLI C.R. (1965) Karten der Verbreitung einiger Mineralien der alpidischen Metamorphose in den Schweizer Alpen (Stilpnomelan, Alkali-Amphibol, Chloritoid, Staurolith, Disthen, Sillimanit) Eclogae Geologicae Helveticae, 58, 335-368.

NIGGLI E. (1970) Alpine metamorphose und alpine Gebirgsbildung Fortschritte der Mineralogie, 47, 16–26.

NOVÁK M., ČERNÝ, P., SELWAY J.B. (1999) The zinnwaldite– masutomilite – elbaite pegmatite at Kracovice from the Třebíč durbachite massif – a complex pegmatite related to the NYF family. In The Eugene E. Foord Memorial symposium on NYF-type Pegmatites (Denver), Canadian Mineralogist, 37, 815-816 (abstr.).

NOVÁK M., UHER P., ČERNÝ, P., SIMAN P. (2000) Compositional variations in ferrotapiolite+tanatalite pairs from the beryl-columbite pegmatite at Moravany nad Váhom, Slovakia. Mineralogy and Petrology, 69, 295-306.

NOVÁK M. (2000a) Compositional pathways of tourmaline evolution during primary (magmatic) crystallization in complex (Li) pegmatites of the Moldanubicum, Czech Republic. Memorie della Società Italiana di Scienze Naturali e del Museo Civico di Storia Naturale, 30, 45-56.

NOVÁK M, POVONDRA P, SELWAY J.B. (2004) Schorl–oxyschorl to dravite–oxy-dravite tourmaline from granitic pegmatites; examples from the Moldanubicum, Czech Republic. European Journal of Mineralogy, 16, 323–333.

NOVÁK M, HENRY D.J., HAWTHORNE F. C., ERTL A., UHER P., DUTROW B. L., PEZZOTTA F. (2009) Nomenclature of the Tourmaline-Group Minerals. Report of the Subcommittee on Tourmaline Nomenclature to the International Mineralogical Association's Commission on New Minerals, Nomenclature and Classification (CNMMN).

OBERLI F., MEIER M., BERGER A., ROSENBERG C.L., GIERÉ R. (2004) U-Th-Pb and $^{230}Th/^{238}U$ disequilibrium isotope systematics: Precise accessory mineral chronology and melt evolution tracing in the Alpine Bergell intrusion. Geochimica et Cosmochimica Acta, 68, 2543-2560.

ORVILLE P.M. (1967) Unit cell parameters of the microcline-low albite and the sanidine-high albite solid solution series. American Mineralogist, 52, 55-86.

OSCHIDARI H., ZIEGLER U.R.F. (1992) Vergleichende Sm-Nd und Rb-Sr Untersuchungen an Bergeller Geröllen aus der Gonfolite Lombarda (Südalpine Molasse) und an Bergeller und Novate-Granitoiden des Ursprungsgebietes. Eclogae Geologicae. Helveticae, 85, 375–384.

PANZA, G.F., MÜLLER, S. (1978) The plate boundary between Eurasia and Africa in the Alpine area. Memorie dell'Istituto di Geologia e Mineralogia, Università di Padova, 33, 45–50.

PARSONS I. (2010) Feldspars 2, phase behaviour. Mineralogical Magazine, 74, 529-551.

PASSAGLIA E. (1969) Roggianite a new silicate mineral. Clay Minerals, 8, 107-111.

PATIÑO DOUCE A. E. (1996) Effects of pressure and H_2O content on the. compositions of primary crustal melts. Transactions of the Royal Society of Edinburgh, Earth Sciences 87, 11–21.

PEACOCK M.A. (1931) Classification of igneous rock series. Journal of Geology, 39, 54-67.

PECO G. (1949) Le pegmatite a berillo di Val Codera (Sondrio). L'industria della ceramica e dei silicati, 10, 7-9, Milano.

PEZZOTTA F., DIELLA V., GUASTONI A. (1999) Sc–Y–REE minerals and evolution of miarolitic cavities in the NYF pegmatites in the western southern Alps, Italy. Eugene E. Foord Memorial symposium. on NYF-type Pegmatites (Denver). Canadian Mineralogist, 37, 805-806 (abstr.).

PEZZOTTA F. (1999a) Madagascar, a mineral and gemstone paradise. Extralapis I.

PEZZOTTA F., DIELLA V., GUASTONI A. (2005) Scandium silicates from Baveno and Cuasso al Monte NYF-granites, Southern Alps (Italy). Mineralogy and genetic inferences. *American Mineralogist*, **90**, 1442-1452.

PHILLIPS M.W., RIBBE P.H. (1973) The structures of monoclinic potassium-rich feldspars. American Mineralogist, 58, 263-270.

PICHAVANT M. (1981) An experimental study of the effect of boron on a water saturated haplogranite at 1kbar vapour pressure. Contribution to Mineralogy and Petrology, 76, 430-439.

PICCOLI G.C., MALETTO G., BOSIO P., LOMBARDO B. (2007) Minerali del Piemonte e della Valle d'Aosta. Associazione Amici del Museo "F. Eusebio" Alba, Ed., Alba (Cuneo) 607 pp.

POLI G., TOMMASINI S. (1990) A geochemical approach to the evolution of granitic plutons: a case study, the acid intrusions of Punta Falcone (northern Sardinia, Italy). Chemical Geology, 92, 87– 105.

PREISWERK H. (1925) Tessinergneis. Eclogae Geologicae Helveticae, 19, 177-187.

PRIOR D.J., BAYLE A.P., BRENKER F. (1999) The application of Electron Backscatter Diffraction and Orientation Contrast Imaging in SEM to textural problems in rocks. American Mineralogist, 84, 1741-1759.

PROBST P. (1980) Die Bündnerschiefer des nördlichen Penninikums zwischen Valser Tal und Passo Di San Giacomo. Beiträge zur Geologischen Karte der Schweiz, vol. 153. Stämpfli and Cie, Bern.

REPOSSI E. (1906) Su alcuni minerali del granito di San Fedelino. Rendiconti Reale Accademia Nazionale dei Lincei, 15, 505-512.

REUSSER C. E. (1987) Phasenbeziehungen im Tonalit der Bergeller Intrusion. Ph.D. thesis, ETH Zürich.

RICHARDSON D., CONDCLIFFE E., MOTTANA A. (1976) Caratteri petrolchimici del Massiccio Val Masino-Val Bregaglia (Alpi Centrali. Rendiconti Società Italiana di Mineralogia e Petrologia, 32, 83-96.

ROGGIANI A.G. (1966) Il filone di feldspato sodico dell'Alpe Rosso a monte di Orcesco (valle Vigezzo). Illustrazione Ossolana, 8, 1, Domodossola.

ROMER R. L., SCHÄRER U., STECK A. (1996) Alpine and pre-Alpin magmatism in the root-zone of the western Central Alps. Contribution to Mineralogy and Petrology. 123, 138-158.

ROSELLE G. T., ENGI M. (2002) Ultra high pressure (UHP) terrains: lessons from thermal modeling. American Journal of Science, 302, 410–441.

ROSENBERG C., BERGER A., DAVIDSON C., SCHMID S.M. (1994) Messa in posto del plutone di Masino-bregaglia, Alpi Centrali. Atti Ticinesi di Scienze della Terra, serie speciale, 1, 31-39.

ROSENBERG C., BERGER A., SCHMID S.M. (1995) Observations from the floor of a granitoid pluton: Inferences on the driving force of final emplacement. Geology, 23, 443-446.

ROSENBLUM S., MOSIER E.L. (1975) Nonmetamict nioboaeschynite-(Ce) from Alaska. American Mineralogist, 60, 309-315.

RYERSON F., HESS P.C. (1980) The role of P_2O_5 in silicate melts. Geochimica et Cosmochimica Acta, 44, 611-624.

SAWYER E.W. (2008) Atlas of Migmatites. The Canadian Mineralogist Special Publication 9, NRC Research Press, Ottawa, Ontario, Canada 371 pp.

SCHALLER W.T. (1925) The genesis of lithium pegmatites of central Maine. American Journal of Science, 10, 269-279.

SCHEERER T. (1847) Discussion sur la nature plutonique du granite et des silicates cristallins qui s'y rallient. Bulletin de la Société Geologique de France, 2e serie, 468.

SCHMID S.M., AEBLI H.R., HELLER F., ZING A. (1989) The role of the periadriatic Line in the tectonic evolution of the Alps. Alpine Tectonics, Geological Society, London, 153-171.

SCHMID S.M., BERGER A., DAVIDSON C., GIERÉ R., HERMANN J., NIEVERGELT P., PUSCHNIG A.R., ROSENBERG C. (1996). The Bergell pluton (Southern Switzerland, Northern Italy): overview accompanying a geological-tectonic map of the intrusion and surrounding country rocks. Schweizerische Mineralogische und Petrographische Mitteilungen, 76**,** 329–355.

SCHREYER W., MARESCH W.V., DANIELS P., WOLSDORFF P. (1990) Potassic cordierites: characteristic minerals for high-temperature, very low pressure environments. Contribution to Mineralogy and Petrology, 105, 162–172.

SHAW H.R. (1965) Comments on viscosity, crystal settling, and convection in granitic magmas. American Journal of Science, 263, 120-152.

SHAW H.R. (1972) Viscosities of magmatic silicate liquids: An empirical method of prediction. American Journal of Science, 272, 870-893.

SHMAKIN B.M. (1976) Muscovite and Rare Metal–Muscovite Pegmatites. Nauka, Novosibirsk, USSR (in Russ.).

SHMAKIN B.M. (1979) Composition and structural state of K-feldspars from some U.S. pegmatites. American Mineralogist, 64, 49-56.

SCHMUTZ H.U. (1976) Der Mafitit-Ultramafitit-Komplex zwischen Chiavenna and Val Bondasca. Beitrage Geoligische Karte Schweiz NF 149, 73.

ŠKODA R., NOVÁK M. (2007) Y,REE,Nb,Ta,Ti-oxide (AB_2O_6) minerals from REL–REE euxenite-subtype pegmatites of the Třebíč Pluton, Czech Republic; substitutions and fractionation trends. Lithos, 95, 43-57.

SIMMONS W.B., LEE M.T., BREWSTER R.H. (1987) Geochemistry and evolution of the South Platte granite–pegmatite system, Jefferson County, Colorado. Geochimica et Cosmochimica Acta 51, 455-471.

SOKOLOV Y.M., KRATZ K.O., GLEBOVITSKYI V.A. (1975) Regularities in the formation and distribution of the muscovite and muscovite–rare metal pegmatite formations in metamorphic belts in muscovite-rare metal pegmatite formations in metamorphic belts. Muscovite pegmatites of the USSR, Nauka, Leningrad, Russia (5-15, in Russian).

SOLODOV N.A. (1962) Internal structure and geochemistry of rare-element granitic pegmatites. Academy Science, USSR, Moscow, (In Russian).

SOLODOV N.A. (1971) scientific principles of perspective evaluation of rare-element pegmatites. Nauka, Moscow, Russia (In Russian).

SPEZIA G. **(**1882) Sul berillo di Craveggia. Atti della Regia Accademia delle Scienze di Torino, 17, 769.

SPIEGEL C., KUHLEMANN J., DUNKL I., FRISCH W., VON EYNATTEN H., BALOGH K. (2000) The erosion history of the Central Alps: evidence from zircon fission track data of the foreland basin sediments. Terra Nova, 12, 163–170.

STECK A., HUNZIKER J. (1994) The Tertiary structural and thermal evolution of the Central Alps – compressional and extensional structures in an orogenic belt. Tectonophysics, 238, 229-254.

STEINMANN M.C. (1994) Die nordpenninischen Bündnerschiefer der Zentralalpen Graubündens: Tektonik, Stratigraphie und Beckenentwicklung. Unpublished PhD thesis, ETH Zürich.

STEWART D.B. (1978) Petrogenesis of lithium-rich pegmatites. American Mineralogist, 63, 970-980.

STRÜVER G. (1885) Sulla columbite di Craveggia in Val Vigezzo. Rendiconti Regia Accademia dei Lincei, 1, 8-9.

TADDEI C. (1940) Pegmatiti della Svizzera Italiana e minerali in esse contenuti. Schweizerische Mineralogische und Petrographische Mitteilungen, 20, 247-252.

TAYLOR S.R. (1963) The application of trace element data to problems in petrology. Physics and Chemistry of the Earth 6, 133-213

TAYLOR B.E., FRIEDRICHSEN H. (1983) Light stable isotope systematics of granitic pegmatites from North America and Norway. Isotope Geoscience, 1, 127–167.

TAYLOR S.R., MCLENNAN S.H. (1985) The Continental Crust: its composition and evolution. Blackwell, Oxford, 312 pp.

TEERSTRA D.K., ČERNÝ P., HAWTHORNE F.C. (1998) Rubidium feldspars in granitic pegmatites. Candian Mineralogist, 36, 483-496.

THOMAS R., WEBSTER J.D., HEINRICH W. (2000) Melt inclusions in pegmatite quartz: complete miscibility between silicate melts and hydrous fluids at low pressure. Contributions to Mineralogy and Petrology, 139, 394-401.

TODD C.S., ENGI M. (1997) Metamorphic field gradients in the Central Alps. Journal of Metamorphic Geology, 15, 513-530.

TOMASCAK P.B., KROGSTAD E.J., WALKER R.J. (1998) Sm-Nd isotope systematics and the derivation of granitic pegmatites in southwestern Maine. Canadian Mineralogist, 36, 327-337.

TROMMSDORFF V. (1966) Progressive metamorphose kieseliger karbonatgesteine in den zentralalpen zwischen Bernina und Simplon. Schweizerische Mineralogische und Petrographische Mitteilungen 46, 431–460.

TROMMSDORFF V., EVANS B.W. (1974) Alpine metamorphism of peridotitic rocks. Schweizerische Mineralogische und Petrographische Mitteilungen 54, 333– 352.

TROMMSDORFF V., AND J. A. D. CONNOLLY (1996) The ultramafic contact aureole about the Bregaglia (Bergell) tonalite: Isograds and a thermal model. Schweizerische Mineralogische und Petrographische Mitteilungen., 76, 537–547.

TRUEMAN D.L., ČERNÝ P. (1982) Exploration for rare-element granitic pegmatites. In granitic Pegmatites in Science and Industry, Mineralogical Association of Canada, Short Course Handbook, 8, 463-494.

TRÜMPY R. (1960) Paleotectonic evolution of the central and western Alps. Geological Society of America, Bulletin, 71, 843-907.

TUTTLE O.F., BOWEN N.L. (1958) Origin of granite in the light of experimental studies in the system $NaAlSi_3O_8$-$KAlSi_3O_8$-SiO_2-H_2O. Geological Society of America, Memoir, 74.

UHER P., ČERNÝ P., NOVÁK M., SIMAN P. (1994) Niobium-tantalum minerals from granitic pegmatites in the Malé Karpaty, Považský Inovec and Žiar Mountains, Western Carpathians, Slovakia. Mineralia Slovaca, 26, 157-164.

U.S. GEOLOGICAL SURVEY (USGS) (2009) Niobium (columbium) and tantalum. Minerals Yearbook, U.S. Department of the Interior 12 p.

U.S. GEOLOGICAL SURVEY (USGS) (2009) Rare earths. Minerals Yearbook, U.S. Department of the Interior 25 p.

VANINI F., CALLEGARI A. (2002) La fersmite della pegmatite di Rio Graia. Rivista Mineralogica Italiana, 4, 212.

VIGNOLA P., GATTA G.D., HATERT F., GUASTONI A., BERSANI D. (2012) On the crystal-chemistry of a near end-member triplite, $Mn^{2+}_2(PO_4)F$, from Codera valley (Sondrio Province, Central Alps, Italy). American Mineralogist (in preparation).

VISSER W., KOSTER VAN GROSS A.F. (1978) Effects of P2O5 and TiO2 on liquid immiscibility in the system K_2O-FeO-Al_2O_3-SiO_2. American Journal of Science, 279, 970-989.

VLASOV K.A. (1961) Principles of classifying granite pegmatites and their textural-paragenetic types. Izvestiya Akademii Nauk SSSR, Seriya Geologischeskaya, 5-20.

WALDROP L. (1969) The crystal structure of triplite, $(Mn,Fe)_2FPO_4$. Zeitschrift für Kristallographie, 130, 1-14.

WALKER R.J., HANSON G.N., PAPIKE J.J., O'NEIL J.R. (1986): Nd, O and Sr isotopic constraints on the origin of Precambrian rocks, southern Black Hills, South Dakota. Geochimica et Cosmochimica Acta **50**, 2833-2846.

WARD R., STEVENS G., KISTERS A. (2008) Fluid and deformation induced partial melting and melt volumes in low-temperature granulite-facies metasediments, Damara Belt, Namibia. Lithos 105, 253-271

WARING G.A. (1905) The pegmatite veins of Pala, San Diego County, California. American Geologist, 35, 366.

WARNER J., EWING R. (1993) Crystal chemistry of samarskite. American Mineralogist, 78, 419-424.

WATSON E.B., CAPOBIANCO C.J. (1981) Phosphorous and the rare earth elements in felsic magmas: An assessment of the role of apatite. Geochimica et Cosmochimica Acta, 45, 2349-2358.

WATSON E.B., GREEN T.H. (1981) Apatite/liquid partition coefficients for the rare earth elements and strontium. Earth and Planetary Science Letter, 56, 405-421.

WEBBER K.L., FALSTER A.U., SIMMONS W.B., FOORD E.E (1997) The Role of diffusion-controlled oscillatory nucleation in the formation of line rock in pegmatite–aplite dikes. Journal of Petrology, 38, 1777-1791.

WEBBER K.L., SIMMONS W.B., FALSTER A.U., FOORD E.E. (1999) Cooling rates and crystallization dynamics of shallow level pegmatite-aplite dikes, San Diego County, California. American Mineralogist, 84, 708-717.

WEBSTER J.D., HOLLOWAY J.R., HERVIG R.L. (1987) Phase equilibria and volatile partitioning in a Be, U and F-enriched vitrophyre from Spor Mountain, Utah. Geochimica et Cosmochimica Acta, 51, 389-402.

WENGER M., ARMBRUSTER T. (1991) Columbite $(Fe,Mn)(Nb,Ta)_2O_6$ in the pegmatites of the calc-alkaline Bergell intrusion (southeast Central Alps). Schweizerische Mineralogische und Petrographische Mitteilungen, 71, 349-369.

WENGER M., KRÄHENBÜHL U., ARMBRUSTER T. (1993). REE characteristics in pegmatites and adjacent wallrocks of the calc-alkaline Bergell intrusion (southeastern Central Alps). Schweizerische Mineralogische und Petrographische Mitteilungen, 73, 383- 389.

WENK E. (1953) Prinzipielles zur geologisch-tektonischen Gliederung des Penninikums im zentralen Tessin. Eclogae Geologicae Helveticae, 46, 9-21.

WENK E. (1970) Zur Regionalmetamorphose und Ultrametamorphose im Lepontin. Fortschrifte der Mineralogie, 47, 34-51.

WENK H.R. (1973) The structure of the Bergell Alps. Eclogae Geologicae Helveticae, 66, 255-291.

WENK E., SCHWANDER H., STERN W. (1974) On calcic amphiboles and amphibolites from the Lepontine Alps. Schweizerische Mineralogische und Petrographische Mitteilungen, 54, 97-150.

WENK H.R., WENK E., WALLACE J.H. (1974a) Metamorphic mineral assemblages in politic rocks of the Bergell Alps. Schweizerische Mineralogische und Petrographische Mitteilungen 54, 507–554

WENK H.R., CORNELIUS S.B. (1977) Geologischer Atlas der Schweiz, 1:25’000. sheet 70 Sciora, Schweizerische Geologische Kommission, Basel.

WHALEN J.B., CURRIE K.L., CHAPPELL B.W. (1987) A-type granites: geochemical characteristics, discrimination and petrogenesis. Contribution to Mineralogy and Petrology, 95, 407-419.

WISE M.A., CĚRNÝ P. (1990) Primary compositional range and alteration trends of microlite from the Yellowknife pegmatite field, Northwest Territories, Canada. Mineralogy and Petrology, 43, 83-98.

WISE M.A., CĚRNÝ P. (1996) The crystal chemistry of the tapiolite series. Canadian Mineralogist, 34, 631,-647.

WISE M.A. (1999), Characterization and classification of NYF-type pegmatites. The Eugene E. Foord Memorial Symposium on NYF-type Pegmatites (Denver). Canadian Mineralogist, 37, 802-803.

WOLF M.B., LONDON D. (1995) Incongruent dissolution of REE and Sr-rich apatite in peraluminous granitic liquids: differential apatite, monazite, and xenotime solubilities during anatexis. American Mineralogist 80, 765–775.

WRIGHT J.E. HAXEL G. (1982) A garnet–two-mica granite, Coyote Mountains, southern Arizona: geologic-setting, uranium–lead isotopic systematics of zircon, and nature of the granite source region. Geological Society of. America, Bulletin, 93, 1176-1188.

WYLLIE P.J., TUTTLE O.F. (1964) Experimental investigation of silicate systems containing two volatile components Part III. The effects of SO_3, P_2O_5, HCl, and Li_2O in addition to H_2O on the melting temperatures of albite and granite. American Journal of Science, 262, 930-939.

WOOD S. A. (1990) The aqueous geochemistry of the rare-earth elements and yttrium 2. Theoretical predictions of speciation in hydrothermal solutions to 350°C at saturation water vapour pressure. Chemical Geology, **88**, 99-125.

WOOLLEY A.R. (1987) Lithosphere metasomatism and the petrogenesis of the Chilwa Province of alkaline igneous rocks and carbonatites, Malawi. Journal of African Earth Science, 6, 891–898.

ZAMBONINI F. (1907) Strüverite, un nuovo minerale. Rendiconto dell'Accademia delle Scienze Fisiche e Matematiche, Sezione della Società Reale di Napoli, 13, 35-51.

ZAMBONINI F. (1908) Delorenzite, un nuovo minerale. Rendiconto dell'Accademia delle Scienze Fisiche e Matematiche, Sezione della Società Reale di Napoli, 13, 35-51.